DEVELOPMENT OF HYDROGEL WOUND DRESSINGS FOR CHRONIC WOUND HEALING

A Dissertation

by

STACY NICOLE CERECERES

Submitted to the Office of Graduate and Professional Studies of
Texas A&M University
in partial fulfillment of the requirements for the degree of

DOCTOR OF PHILOSOPHY

Chair of Committee,	Elizabeth Cosgriff-Hernandez
Co-Chair of Committee,	Daniel Alge
Committee Members,	Melissa Grunlan
	Noah Cohen
Head of Department,	Michael McShane

December 2018

Major Subject: Biomedical Engineering

ABSTRACT

Chronic wounds are a growing healthcare issue afflicting over 40 million people in the United States. Despite the billions of dollars spent each year, complications from diabetic ulcers result in a large number of lower extremity amputations. Current dressings fail to address the complex nature of the wound environment and are often only able to address one aspect of wound healing providing marginal wound closure rates and resulting in treatment failure. To address the limitations of standard treatments, we have developed a biodegradable and bioactive hydrogel dressing that incorporates a novel antimicrobial agent to eliminate and prevent infection. Here, we have developed a wound healing platform that promotes wound fluid maintenance through tunable hydrogel geometries, targeted cellular interactions, and bacterial inhibition.

In this work, a tunable biomaterial platform with integrin-mediated cellular interactions, controlled degradation profiles, and antimicrobial properties was developed to treat a variety of complex wound environments. Engineered Streptococcal collagen-like (Scl2) proteins were optimized with improved stability and promotion of cellular attachment. These poly(ethylene glycol)-based hydrogels were fabricated in hydrogel microspheres and 3D-printed porous hydrogel foams to develop a platform to treat complex wound environments. Swelling ratio and rate were investigated to determine water uptake and equilibrium swelling times. Furthermore, biocompatibility and biodegradation of poly(ethylene glycol)-dithiothreitol hydrogels were modulated and *in vivo* degradation profiles were investigated. The development of a tunable platform with

rapid degradation *in vivo* has potential to be utilized as a resorbable dressing that eliminates inflammatory concerns due to residual dressing fragments. Finally, gallium maltolate (GaM), a novel antimicrobial agent, was incorporated into these hydrogel scaffolds and evaluated *in vitro* and *in vivo* in a splinted wound model. Release profiles, bacterial inhibition, and wound closure was investigated in these GaM loaded hydrogels.

Overall, the development of this wound healing platform with conferred antimicrobial activity and tunable degradation properties resulted in an improved wound dressing system with controlled moisture balance, infection control, and potential for cell mediated wound healing. Furthermore, these technologies can be translated into other regenerative applications and scaffold geometries demonstrating the broader impacts of this wound healing platform.

DEDICATION

To everyone I have met along this journey who has taught me fortitude, strength, and understanding.

ACKNOWLEDGEMENTS

This journey has been the most challenging yet rewarding journey I have embarked on. I have learned a lot about myself personally and professionally because of the great mentorship and friendship that I have received. First, I would like to thank my advisor, Dr. Elizabeth Cosgriff-Hernandez. I have learned what it means to be an independent researcher. I have gained valuable skills that will push me to be the best version of myself. Without your guidance I would have never pursued the path to graduate school and would not be in the position that I am in today.

I would also like to thank my wonderful committee, Dr. Daniel Alge, Dr. Melissa Grunlan, and Dr. Noah Cohen. Dr. Alge's support and mentorship as my LSAMP faculty mentor provided me with the encouragement and tenacity to accomplish my goals. Dr. Grunlan's introductory biomaterials class is what sparked my interest and curiosity in this field. Additionally, her kindness and excellent mentorship has provided me with confidence and determination. Dr. Cohen's unwavering help and thoughtfulness has provided me phenomenal guidance and direction in my project.

I would also like to thank the LSAMP community and leadership, Dr. Karen Butler-Purry, Dr. Karan Watson, Dr. Shannon Walton, Dr. Samuel Merriweather, John Avila, and Shawanee Patrick. This program and their constant support has taught me how to strengthen my academic learning, improve my personal development, and develop my leadership skills. I would also like to thank Dr. Canaan Whitfield-Cargile for his support, commitment, and motivation. I would not have been able to do half of the things I

accomplished without the help of you and your lab and for that I am very appreciative. I would also like to thank Mary Beth Browning-Monroe and Nick Sears for being great mentors, taking a chance on me as an undergrad, and introducing me to research.

I would also like to thank all of the members of my lab that have encouraged, helped, and motivated me to be a better researcher and person. Alysha Kishan, thank you for letting me vent, supporting me, and providing me with an example to live up to. Allison Post, thank you for trying to make my transition to Houston less painful. Your help with the Blender figures at a time when I really needed it, demonstrates your willingness to go above and beyond. Nick Sears, in addition to being my undergraduate mentor, you are also a great friend and I am very grateful for all that I have learned from you professionally and just for fun. Thomas Wilems, thank you for your patience and understanding with everything. Your help with everything from animal studies to being a listening ear has been very much appreciated. Prachi Dhavalikar, thank you for being a genuine and supportive friend. I will definitely miss our Bahama Bucks trips. Ziyang Lan, I knew we would get along great from the first time we met and you had data on your cat's weight. I have enjoyed every moment working with you and you have played an integral part in completing my dissertation. Megan Wancura, thank you for your hard work and time spent teaching me but also for your patience and kindness in having to work with me during a stressful time. I would like to thank all of the other members of our lab, Taneidra Buie, Gabriel Rodriguez-Rivera, and Siliang Wu. Even though I didn't work closely with y'all, the friendship you provided me has been invaluable. Finally, Michael Whitely, your relentless support, unyielding friendship, and passionate discussions have shaped my life

and made me the person that I am today. I would have never made it this far without you and will never forget a single moment of it.

I would also like to thank all of the talented students that I got to work with, Natalia Fabela, Hannah Pearce, Nico Medellin, and Ellen Wang. I would also like to thank all of the wonderful friends that I have made along the way especially, Romi Del Bosque, Sam Holt, Kristen Means, Lindsay Woodard, Candice Sears, Karli Gold, TJ Falohun, and Kyndal Carter. Your friendship, help, compassion, and willingness to listen has made this experience better and easier.

Last but not least, an enormous and indebted thank you to my family. The support, love, and understanding that all of you have shown me has led me this point in my life. You have kept me grounded and reminded me how hard I have worked to get here. I hope to inspire all of you and show you that you can do anything you put your mind to. Most importantly, I want to thank my parents. Despite all of the times I struggled – through anger, sadness, lack of confidence, fear, and panic – you were my biggest support. From the very beginning and to the very end all of this was only possible because of you.

CONTRIBUTORS AND FUNDING SOURCES

This work was supported by a dissertation committee consisting of advisor, Dr. Elizabeth Cosgriff-Hernandez, co-advisor, Dr. Daniel Alge, Dr. Melissa Grunlan, Dr. Michael McShane, Head of the Department of Biomedical Engineering and Dr. Noah Cohen of the Department of Large Animal Clinical Sciences.

The protein engineering and analysis for Chapter II was provided by Dr. Brooke Russel, Dr. Jose Rivera, and Dr. Magnus Hook. Animal studies and histological analysis for Chapters III and IV were completed in collaboration with Dr. Canaan Whitfield-Cargile and Dr. Laura Bryan. Mass spectrometry from Chapter IV was performed and analyzed by Dr. Robert Taylor. All other work conducted for the dissertation was completed by the student independently.

Graduate study was supported by The Texas A&M University LSAMP NSF Bridge to the Doctorate Fellowship and the NSF Graduate Research Fellowship Program.

NOMENCLATURE

^{1}H-NMR	Proton Nuclear Magnetic Resonance Spectroscopy
BSA	Bovine Serum Albumin
CFU	Colony Forming Unit
DCM	Dichloromethane
DMEM	Dulbecco's Modified Eagle Medium
DTT	Dithiothreitol
ECM	Extracellular Matrix
$eCol_{GFPGER}$	Engineered Collagen
EGF	Epidermal Derived Growth Factor
FGF	Fibroblast Growth Factor
FBS	Fetal Bovine Serum
GaM	Gallium Maltolate
H&E	Hematoxylin and Eosin
hDfs	Human Dermal Fibroblasts
LAP	Lithium phenyl-2,4,6-trimethylbenzoylphosphinate
LB	Luria Broth
MIC	Minimum Inhibitory Concentration
MMP	Matrix Metalloproteinase
M_n	Number Average Molecular Weight
M_p	Peak Average Molecular Weight

MRSA	Methicillin-resistant S*taphylococcus aureus*
M_w	Weight Average Molecular Weight
OD	Optical Density
PBS	Phosphate Buffered Saline
PDGF	Platelet-derived Growth Factor
PEG	Poly(ethylene glycol)
PEGDA	Poly(ethylene glycol)-diacrylate
PEGDTT	Poly(ethylene glycol)-dithiothreitol
PGPR	Polyglycerol polyricinoleate
ROS	Reactive Oxygen Species
RPMI	Roswell Park Memorial Institute
S. aureus	*Staphylococcus aureus*
Scl2	Streptococcal Collagen-like Protein 2
TCPS	Tissue Cultured Polystyrene
TEA	Triethylamine
TGF	Transforming Growth Factor
TMPE	Trimethylolpropane ethoxylate triacrylate
VEGF	Vascular Endothelial Growth Factor

TABLE OF CONTENTS

Page

LIST OF FIGURES

Page

LIST OF TABLES

Page

CHAPTER I

INTRODUCTION AND LITERATURE REVIEW

1.1. Clinical Need: Chronic Wounds

Chronic wounds affect approximately 2.4-4.5 million people in the United States and over half of the non-traumatic lower extremity amputations are due to diabetic foot ulcers.[1, 2] Among those with diabetes, over 85% of amputations are due to foot ulceration.[3] These wounds impose not only a large medical burden but also a financial burden on our healthcare system with an estimated cost of $45,000 per patient.[2] The current gold standard is a multidisciplinary approach focusing on compression, infection maintenance, debridement, and appropriate dressing selection.[4] Due to the high recurrence rates and minimal closure rates, low cost treatments to manage chronic wounds are utilized. Unfortunately, these low cost treatments do not provide active wound healing to promote cellular migration to the damaged tissue. Current commercially available active wound healing options such as Alloderm™, Integra Wound Matrix™, and Dermagraft-TC® have concerns and risks relating to infection, potential disease transmission, and high cost.[5, 6] Human skin wounds affect 6.5 million patients per year with an annual financial burden of $25 billion in the United States.[7] These numbers are expected to rise due to increases in the elderly population, obesity, and diabetes.[1, 8, 9] The World Health Organization estimates that over 350 million people globally are affected by Type I and II diabetes with 15% of those patients suffering from diabetic foot ulcers.[3, 10] It is expected that by 2030, a rise in adults with diabetes will reach over 550 million people.[3] In diabetic patients

chronic wounds are prevalent due to underlying health complications and delayed healing times. There have been several advances in wound healing to improve healing capability, reduce amputations, and improve patient comfort and care. Recent wound dressing research has focused on scaffold design, vascularization, regulatory factors, and accurate *in vitro* models.[10]

1.2. Wound Healing Process

Wound healing is the biological process of the repair of tissue damage through growth and neotissue formation. There are four main phases in which consist of hemostasis, inflammation, proliferation, and remodeling. The wound repair process involves several overlapping interactions among cytokines, growth factors, cells, and extracellular matrix (ECM) that restores the wounded tissue.[11]

1.2.1. Hemostasis

The initial phase of wound healing, hemostasis, produces the formation of a clot that provides a temporary matrix for cells to attach and migrate through. This clot is made up of platelets, crosslinked fibrin, fibronectin, vitronectin, and thrombospondin.[12] Aggregation of platelets that form the clot activate the intrinsic part of the coagulation cascade. The formation of the clot initiates the entire healing cascade through the release of cytokines and growth factors. The fibrin clot serves as the scaffolding for the invading inflammatory and proliferative cells.[13] The initial clot plays an important role in the wound healing process due to improved cellular interactions at the wound cite and the release of chemotactic factors (i.e. growth factors and cytokines).[14, 15]

1.2.2. Inflammation

The inflammatory cells such as neutrophils and macrophages are the first cells to arrive at the wound injury which clean out the wound site ridding the wound of bacteria, foreign materials, and damaged tissues.[16] The inflammatory phase is essential to providing chemotaxis of cells through the release of cytokines and growth factors to activate migrating cells.[17] Neutrophils are the first inflammatory cells to the wound site and are the first line of defense to pathogens.[17, 18] Next, macrophages invade the wound site secreting growth factors that stimulate angiogenesis and fibrous tissue formation as well as debridement of surrounding tissue.[17, 19-21]

1.2.3. Proliferation

As the inflammatory stage leads into the proliferative phase, the fibrin clot is remodeled and replaced with ECM to allow for cellular migration and proliferation.[11] Non-activated fibrobalasts become activated so that they can proliferate and provide further matrix and wound support.[17] In the proliferative phase, fibroblasts and endothelial cells proliferate to lay down collagen in order to create a matrix structure and start angiogenesis.[17] Wound contraction begins aided by the formation of ECM to achieve wound closure. The ECM provides a matrix for cells to infiltrate to help return function and integrity to the repaired tissue.[22]

1.2.4. Remodeling

In the final phase of the healing process, remodeling, the collagen fibers become crosslinked and remodeled providing strength for wound tissue. Cellular connective tissue forms strengthening the new epithelium.[23] In the final process of collagen remodeling,

collagen crosslinking and scar maturation occurs.[16] Type III collagen is remodeled into type I collagen primarily through the help of matrix metalloproteinases (MMPs) that are secreted fibroblasts, macrophages, and endothelial cells which help strengthen the repaired tissue.[24]

1.2.5. Chronic Wounds

Chronic wounds fail to progress through the normal phases of wound healing. In chronic wounds, issues with infection, excessive inflammatory responses, biofilm development, and the inability of cells to respond appropriately to reparative chemotactic factors prevent the normal phases of wound healing from occurring.[1, 25] Local and systemic factors impact disease states and impact healing. Some local factors include the presence of foreign bodies, ischemia and infection while systemic factors include age and comorbidities.[26] Additionally, reduction of growth factors, proteinase imbalance, and senescent cells have been shown to complicate wound healing.[27-31] The damage of chemotactic factors impairs the proliferative capacities of target cells (keratinocytes, endothelial cells, and fibroblasts) that prevent the wound from healing. Due to excess inflammation, immune cells produce excess reactive oxygen species (ROS) that damage ECM proteins and cause cell damage.[1] The harmful effects of microbial infection and the control of bacterial balance to prevent wound colonization and biofilm formation has been widely investigated.[32, 33] Typically, biofilm-related infections fail to be resolved by the patients' immune response due to underlying systemic factors.[32] Persistent bacterial infection results in prolonged elevation of proinflammatory cytokines that results in high

levels of MMPs and the decreased production of growth factors, thus suggesting that chronic wounds develop due to bacteria imbalances.[33, 34]

1.3. Current Wound Healing Options

Clinical wound dressings are separated into two different approaches: passive and active wound healing options. In order to provide the patient with appropriate care an assessment of the wound is performed to develop a treatment plan. The wound environment is evaluated on the stage of healing, wound site, wound size, amount of exudate, odor, pain, wound edge, and surrounding skin.[9] Wound types can vary from deep to shallow or necrotic to sloughy. Identification of the wound environment is essential in the selection of the appropriate dressing. The intricate environment of these wounds make selection of one type of treatment difficult to improve overall wound healing. Clinical and experimental evidence has shown that chronic wounds do not follow a progression through normal wound healing.[35] Ideally, wound dressings would initiate and manage wound healing with a focus on the following key design criteria: management of infection and wound fluid maintenance, induction of cellular migration and phenotype to promote healthy tissue formation, and an appropriate degradation profile.

1.3.1. Passive Wound Healing

Passive wound healing options consist of cotton wool, compression bandages, or natural or synthetic gauzes.[23] Although these traditional passive wound healing options are cost effective they lack the ability to provide cellular cues to initiate the wound healing process. Many of these dressings also cause dehydration of the wound bed which is detrimental to healing. These dressings provide a bacterial barrier to the wound; however,

because they are so absorbent they cause further tissue damage during dressing changes. Modern passive wound dressings such as hydrocolloid dressings, hydrogels, and alginates are often applied as gels, foams, or sheets.[23] These dressings are good for absorbing wound exudate and maintaining a moist wound environment; however, if not applied to clean wounds there are concerns with limited oxygen permeability for infected wounds.[6] Hydrocolloid and film dressings are not useful for highly exuding wounds, however; they can adhere to both dry and moist wounds.

1.3.2. Active Wound Healing

Commercially available active wound healing skin substitutes range from decellularized matrices to bioactive cell derived scaffolds.[36] Each of these scaffolds has its own unique benefits and disadvantages but common problems exhibited are reduced vascularization, biocompatibility, low closure rates, and increased product costs.[5, 37-39] Active wound healing options such as Integra®, Dermagraft®, and OrCel® improve wound closure rates; however, there is potential risks of graft rejection due to allogenic cells and they do not address infection.[40] Bioactive dermal substitutes offer the best closure rates but are often expensive since they contain animal-derived extracellular matrix (ECM) materials and often cells that require special handling and preparation.[37, 39, 41] Dermagraft®, a bioresorbable mesh, seeded with cryopreserved neonatal fibroblasts, has marginal wound closure rates at 30% compared to 18% control group treated with gauze.[42] To improve wound closure rates, research has focused on cellular targeting and signaling in order to direct the wound healing process. A summary of clinically available active wound healing dressing advantages and disadvantages is provided in **Table 1.1**.

Table 1.1. Current skin substitutes with their identified advantages and disadvantages.

Skin Substitute	Components	Advantages	Disadvantages
Alloderm®[5]	Decellularized allogenic human skin	Readily available	Potential disease transmission
Integra®[5]	Bovine collagen with chondroitin 6-sulfate	Readily available, reduced scarring	Need to excise wound, risk of infection, high cost
Dermagraft®[5, 37, 39]	Fibroblasts on nylon mesh	Readily available, low recurance of ulcers	Need for multiple applications, high cost, disease risk/rejection
Apligraf®[5, 37, 39]	Bovine collagen, allogenic fibroblasts, and epidermal cells	Readily available, no need for subeseuent autografting	Limited availability, higher costs
OrCel®[37]	Human allogenic fibroblasts, keratinocytes, bovine collagen sponge	Favorable enviornment for host cell migration, provides cytokines and growth factors	Risk of rejection and disease
Epicel®[37, 39]	Cultured epidermal autograft grown from patient skin biopsy	Large area of permanent wound coverage	Long preparation time (>3 weeks), susceptible to blistering, fragile confluent sheets

1.4. Hydrogels as Wound Dressings

Hydrogels are hydrophilic polymer networks that absorb up to a thousand times their dry weight in water.[43, 44] Many hydrogels exhibit tunable properties that can be modulated chemically, physically, and biologically.[45-48] Natural polymers (collagen, gelatin, alginate, and cellulose), synthetic polymers such as poly(ethylene glycol), and hybrid hydrogel systems have all been explored for use in tissue engineering applications.[49-51] Hydrogels are advantageous for tissue engineering and drug delivery

applications due to their similar properties to soft tissue, ability to incorporate water soluble components, and encapsulate human cells and maintain their viability.[52-58]

A primary advantage of hydrogel wound dressings is their ability to influence moisture balance in the wound environment.[38] Maintaining a moist wound environment has been shown to facilitate the wound healing process by preventing tissue dehydration and cell death, enhanced angiogenesis, improved breakdown of nectrotic tissue and fibrin, and initiating the interaction of chemotactic factors with target cells.[59] In order to provide the patient with adequate care an assessment of the patient and the wound is done to develop a systematic approach for treatment. In the patient assessment, factors such as disease, infection, age, medication, and previous wound management are taken into consideration when developing a treatment plan.[9] Additionally, the wound is evaluated on the following conditions: stage of healing, wound site, wound size, amount of exudate, odor, pain, wound edge, and surrounding skin.[9] Identification of these issues are important in selection of the appropriate dressing. The intricate environment of these wounds make selection of one type of treatment difficult to improve overall wound healing.

Hydrogel wound dressings are clinically applied in three ways: amorphous gels, hydrogel sheets, or composite impregnated hydrogels. Amorphous hydrogels are a soft formless gel that becomes less viscous as it absorbs fluid. Sheet hydrogels are firm sheets that swell with fluid but maintain their mechanical integrity. Unlike alginates or hydrocolloids, hydrogels do not require wound secretions to initiate the gel formulation.[60] Hydrogels have been shown to be effective in different wount wound types with

appropritate primary and secondary dressing selection.[60, 61] Many clinically available protducts have have been shown to be sucessful clinically as seen in **Table 1.2**.[60]

Table 1.2. Comparison of clinically available hydrogel wound dressings adapted from Jones et al.

Clincal Hydrogel	Composition	Hydration Donation %	Absorption %
Intrasite™	Propylene glycol, sodium, carboxymethylcellulose	6	14
Aquaform®	Propylene glycol, starch copolymer, glycerol	4	23
Granugel®	Propylene glycol, pectin	6	27
Nugel™	Propylene glycol, carboxymethylcellulose	3	23
Purilon®	Carboxymethylcellulose, calcium alginate	11	18

1.4.1. Hydrogel Degradation

Hydrogels provide good moisture balance which is a critical wound dressing requirement to maintain an appropriate wound environment. Another key requirement is the ability for the dressing to degrade as new tissue is regenerated to eliminate inflammatory responses due to residual dressing fragments left in the wound bed. Slow degrading systems have been shown to reduce nutrient/waste diffusion to cells migrating thorough the network, prevent cellular migration thereby reducing tissue ingrowth and remodeling, and inhibit the healing process.[62-64]

Acrylated and methacrylated poly(ethylene glycol) hydrogels have been shown to degrade slowly demonstrating a need for hydrogel scaffolds with clinically relevant

degradation times.[65] Increasing the rate of degradation in PEG-based hydrogels has been investigated with the inclusion of PLA; however, it has been shown to denature proteins and cause an inflammatory response due to acidic degradation products which would not be beneficial for a bioactive wound dressing.[63] Additionally, the development of poly(β-amino ester)s have been investigated as a system to increase hydrolytic degradation.[66] Studies have shown the ability to tune polymer properties such as degradation rate and modulus through varying concentrations of PEGDA.[67] This system has been widely characterized for its tunable mechanical properties; however, with increasing degradation rate, there was a significant effect on gel fraction, swelling ratio, and resulting compressive and tensile moduli.[68-70]

Another proposed chemical modification to increase the rate of degradation in PEG-based hydrogels is to incorporate thio-β esters into the polymer backbone. The reaction between acrylates and dithoils which occurs rapidly upon mixing creates an easy and efficient synthesis. Additionally, these types of step-growth polymerizations can be tuned using stoichiometric monomer ratios to get desired endgroup functionality.[62, 71] The reaction occurs when PEGDA chains react with a dithiol in a Michael-type addition reaction to form water soluble PEGDTT polymer chains.[72, 73] The increased hydrolytic lability of DTT bridges is due to the presence of a thioether bond proximal to ester bond present in PEGDA.[64, 72] The presence of this thioether creates a more positive atomic charge on the carbonyl carbon of the ester, enhancing the reactivity of nucleophilic attack which is the first step of a base-catalyzed ester hydrolysis.[64] This reaction of DTT with PEGDA allows for degradation to occur within clinically relevant time scales.[73] Bulk

properties of the hydrogel as well as degradation rate can be tuned through variations in molecular weight of the PEGDA and the DTT concentration.[62, 74, 75] Additionally, the system can be tuned by incorporating ratios of PEGDTT:PEGDA before crosslinking to further tune the degradation rate.[67] This biodegradable system has been investigated for the use of protein release, 3D stem cell culture arrays, and to examine ECM cell adhesion on ligand type and concentration.[73, 76, 77]

1.4.2. Hydrogel Fabrication

Maintaining a moist wound environment has been shown to improve wound healing by preventing tissue dehydration and cell death, accelerated angiogenesis, increasing the breakdown of dead tissue, and enhancing the interaction of growth factors with target cells.[59] The high water content in hydrogels as discussed previously makes them ideal for maintaining moist wound environments. The simple fabrication of the hydrogel precursor solutions makes them ideal for fabrication of a wide range of scaffold geometries with varying properties and applications. Hydrogel scaffold geometries that have been utilized include microspheres, porous scaffolds, injectable gel formulations, and various molding and patterning techniques.[78-85] Recently, 3D-printing of hydrogels has been investigated as an enabling technology to generate complex geometries.[86, 87] The characterization of these scaffold fabrication techniques has demonstrated differences in macro- and microstructure, porosity, and mechanical integrity.[88]

Hydrogel microspheres have been shown to improve cellular interactions such as migration and proliferation.[88, 89] Microsphere fabrication gives control over size modulation and morphology for controlled degradation and potential release.[90, 91]

Additionally, microspheres have been used specifically for cell delivery as an injectable platform further demonstrating the versatility of this scaffold design.[92, 93] The ability to deliver hydrogel microspheres via injection allows for adequate space filling of the defect, retention of the dressing at the site of injury, and improves ease of application in a clinical setting.[94, 95] Chitin-based microparticles such as Debrisan™ and Iodosorb™ have been used commercially as a wound dressing to promote favorable cell attachment and proliferation for enhanced wound healing.[96] The use of microparticles in commercial dressings demonstrates the utility of these dressings clinically for easy application.

Porous hydrogel scaffolds have been shown to play a large role in directing tissue formation and function.[97] Superporous hydrogels have been shown to swell rapidly due water uptake via capillary action.[98, 99] Superporous hydrogel fabrication has been accomplished using a gas foaming technique with pore sizes ranging from 5 to 600 μm.[100-102] These porous structures have supported cellular infiltration and vascular ingrowth *in vitro* and *in vivo*.[103] The use of porous hydrogels could be a potential solution in wound environments with heavy wound exudate due their engineered moisture balance control.

1.5. Wound Healing Bioactivity

The extracellular matrix (ECM) is a complex medium consisting of biochemical and biophysical cues such as proteins, growth factors, collagens, laminins, and fibronectin.[104, 105] In normal phases of wound healing inflammatory and proliferative cells release growth factors to begin the active wound healing cascade.[106] However; due to high levels of matrix metalloproteinases and reactive oxygen species, excessive proteolysis and degradation of these cues occur.[25, 107] The destruction of the chemical cues and

surrounding ECM prevents cellular migration and proliferation resulting in lack of wound closure.[25] Thus, incorporation of bioactive cues such as proteins and growth factors are important for therapeutic treatment of chronic wounds to improve active wound healing.

1.5.1. Growth Factors

Hemostasis is the first phase of the normal wound healing process. This phase begins with the formation of a fibrin clot that with surrounding tissue begins to release pro-inflmmatory cytokines and growth factors such as transforming growth factor (TGF)-β, platelet-derived growth factor (PDGF), fibroblast growth factor (FGF), and epidermal growth factor (EGF), **Table 1.3**.[12]

Table 1.3. Growth factor source and primary cell targets. Table adapted from Martin et al.

Growth Factor	Cell Source	Primary Target Cells	References
EGF	Platelets	Keratinocytes	108
TGF-α	Macrophages	Keratinicoytes	108,109
FGF7	Dermal fibroblasts	Keratinocytes	110,111
PDGF	Platelets, macrophages, keratiocytes	Macrophages, fibroblasts	112
HB-EGF	Macrophages	Keratinocytes	113
VEGF	Keratinocytes, macrophages	Endothelial cells	114

These growth factors are polypeptides that control migration, proliferation, and differentiation of cells.[115] Incorporation of growth factors have been investigated to direct cell activity and stimulate migration and proliferation of fibroblasts and keratinocytes.[38]

Many of these growth factors are chemoattractants and stimulate proliferation of cells necessary for wound healing.[116] Encapsulation strategies of growth factors has been investigated to get controlled release from various synthetic and natural polymers. Electrospun meshes and hydrogel scaffolds have been investigated to release multiple growth factors to improve skin tissue regeneration through tunable release and improved cellular interactions.[117-119] Release from these systems is primarily controlled through degradation or heparin incorporation encapsulated into hydrogel scaffolds.[120-122] Unfortunately, to be effective in wound healing there must be sustained and prolonged exposure of growth factors. Release can be modulated from slow releasing polymer networks, however; clinicians will change dressings every 5 to 7 days making this option highly expensive. Additionally, it has been shown that the concentration of some growth factors needs to be 1000 times more concentrated *in vivo* than *in vitro* due to rapid diffusion or proteolytic destruction.[106]

1.5.2. Integrin-Mediated Wound Healing

The extracellular matrix plays a large role in cellular interactions and tissue repair. The cell-matrix interactions take place through cell surface receptors, integrins, which are composed of two α and β subunits. These integrins have control over adhesion, migration and proliferation demonstrating that integrin expression is critical for promoting matrix remodeling.[17] It has been demonstrated that α1β1 and α2β1 integrins are key players in the wound healing process. α1β1 regulates fibroblast proliferation, collagen synthesis, and angiogenesis whereas α2β1 increases fibroblast traction and adhesion, and increases keratinocyte and endothelial cell migration, **Table 1.4**.[5, 123-130]

Table 1.4. Role of integrins in wound healing. *Epithelial cells do not express α1β1.

	α1β1	α2β1
Fibroblast/Myofibroblast	↑ proliferation ↓ COLL synthesis	↑ adhesion ↑ traction
Endothelial	↑ angiogenesis	↑ migration ↑ tubulogenesis
Keratinocytes/Epithelial	*	↑ adhesion ↑ migration

Imparting bioactivity into synthetic hydrogel scaffolds to mimic the natural ECM is typically incorporated through the addition of proteins, peptides, and growth factors. Incorporation of these factors have been investigated to direct cell activity and stimulate migration and proliferation of fibroblasts and keratinocytes.[38] Many chemistries have been investigated to successfully tether bioactive molecules into hydrogels to promote and target cellular interactions. Acrylation of RGD, collagen, and peptides to allow for photopolymerization has been successful utilizing DCC activation and Fmoc protection and various amine-NHS chemistries.[131-133] Additionally, Michael-type additions, thiol-ene and click chemistries, and step-growth derived photoactive macromers have been utilized to modulate cell-material interactions using growth factors and peptides.[134-138] Although peptide-based and mammal-derived proteins have also been investigated as integrin-targets for use in hydrogel scaffolds, there are concerns with infection and possible disease transmission that could further hinder wound healing. Additionally, the reproducibility and cost of these bioactive factors make them difficult to scale-up.

1.5.3. Designer Collagens

PEG-based hydrogels have been shown to resist protein adsorption making them a blank slate to incorporate specific bioactivity. Streptococcal collagen-like (Scl2) proteins can be utilized to impart bioactivity. Scl2 proteins without integrin binding motifs do not provide cellular cues for cell adhesion. Scl2 is a unique protein because it forms a stable triple helix without hydroxyproline and has advantages over mammalian collagens due to the elimination of potential infection or allergic risks.[139, 140] Scl2 is also easily modified to incorporate different binding sequences and is resistant to non-specific enzyme degradation.[139] Using site directed mutagenesis specific binding motifs such as GFPGER can be included to target integrin binding through α1β1 and α2β1 integrins, **Figure 1.1**.[141]

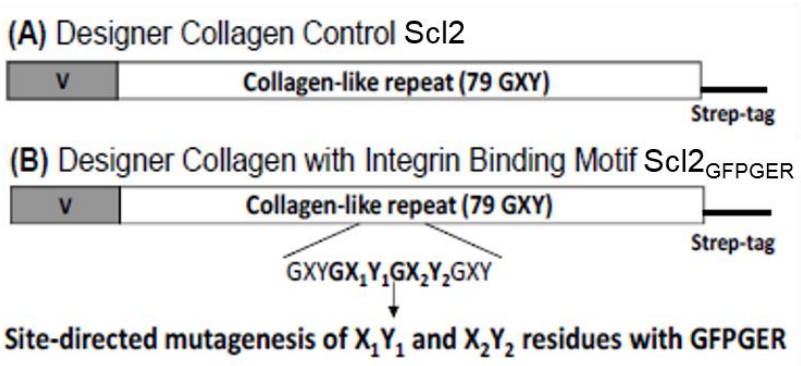

Figure 1.1. Site-directed mutagenesis incorporates specific binding motifs such as GFPGER to target specific integrin binding in Scl2.

Wound healing is a dynamic process in which keratinocytes and fibroblasts encounter a complex environment with ECM molecules, matrix degrading enzymes, and other growth factors.[142, 143] Integrins are the main mediators that promote cell attachment

to the extra cellular matrix especially interactions with collagen.[25, 143] Most integrins are expressed in a wide variety of cells which express several integrins; however, investigation into α1β1 and α2β1 have demonstrated to influence wound healing.[144] Scl2 proteins have been shown to promote cellular interactions through α1β1 and α2β1, such as an increasing angiogenesis, adhesion, and cellular infiltration in keratinocytes and dermal fibroblasts.[145] These recombinantly expressed engineered collagen-mimetic proteins with GFPGER integrin binding sequences, allow us to target cells vital to the wound healing process.[146] Keratinocytes and fibroblasts play a significant role in wound closure and tissue regeneration and Scl2 proteins have potential to recruit these cells through integrin-mediation. Scl2 proteins cannot form stable networks because they are not able to form fibrillary structures so they are limited to coatings and soluble protein delivery.[147, 148] Functionalization of these proteins allows for incorporation into 3D scaffolds that will provide a matrix for them to utilized.

1.6. Antimicrobials for Wound Healing

Infection is one of the most common complications with chronic wounds, increasing healing times and causing damage to surrounding healthy tissue, exacerbating wound damage.[23] Despite extensive research on infection control several controversial issues still exist: critical wound colonization, the role of biofilm, the role of antimicrobials, and the role of antibiotics.[149] Colonization of bacteria is due to proliferation without a noticeable host response with serious issues occurring when there is an excess of 10^5 organisms/g tissue.[150]

1.6.1. Silver

The use of silver is one of the earliest forms of wound care for its use as an antiseptic agent.[38] Silver has been highly investigated as an antimicrobial because it has been shown to be effective against a broad range of micro-organisms.[151, 152] Silver is absorbed by sensitive strains of bacteria impairing cell walls, inhibiting respiration, and inactivating bacterial DNA and RNA.[153] Silver is a bactericidal agent that disrupts bacterial growth by inhibiting the respiratory chain as well as interfering with electron transport, and altering cell membrane permeability. However, it has been suggested that uncontrolled use of silver could result in bacteria developing resistance and reported incidents of allergic response has occurred.[151, 154] One of the main challenges with is maintain high enough concentrations for long enough to provide bactericidal effects without the development of resistance.[152, 155] In order to maintain the effectiveness of silver nitrate, it has been demonstrated that twelve applications per day must be used.[38] Additionally, *in vitro* studies have shown that there have been cytotoxic impacts on fibroblasts and keratinocytes which are target cell types in wound healing necessary for tissue regeneration.[156, 157]

1.6.2. Iodine and Hypochlorous Acid

Iodine products are commonly used in wound care to reduce bacterial growth as it has been shown to prove effective against most miro-organisms.[158] The release of iodine in wound dressings has demonstrated the disruption of mature biofilms *in vitro.*[159] Dressings containg iodine, however; have been contraindicated for patieints suferring from thyroid disorders and Grave's disease.[160] Additionally, patients who are pregnant or

lactating should not be use these products because iodine can be absobed systemically.[161] Hypochlorous acid is another bactericidal compound that can be used as a broach range antimicrobial.[162] However it has been shown that this wound care agent could be potentially neutralized in the wound environment reducing its effectiveness.[163] Although these antimicrobial agents have been sucessful in bacterial inhibiton they have also been shown to significantly decrease wound epithelialization. [164]

1.6.3. Gallium Maltolate

Gallium maltolate is a coordination complex of gallium and maltol, which has an octonal:water partition coefficient of 0.41, illustrating its solubility in both water and lipids.[165, 166] Gallium maltolate has been found to significantly reduce the number of colony forming units (CFUs) of several different bacteria types often causing biofilm formation.[167-170] Gallium functions as a ferric iron mimic that has been used to control various microorganisms by taking advantage of their iron-dependence for growth.[171] This iron-dependent pathway had demonstrated that there are no issues with bacteria developing resistance to GaM as an antimicrobial agent. Literature has shown that *Staphylococcus aureus* has mean inhibitory concentrations (MICs) between 375-2000 µg/ml which are active against biofilm formation.[172] Additionally, GaM has been shown that at low doses can provide nearly complete pain relief with topical applications reducing inflammation.[172, 173] The impact of GaM on cellular actions is unclear but gallium promotes collagen synthesis and cell migration, and favorably modulates integrin expression which are all necessary for wound healing.[174, 175]

1.7. Summary and Approach

Current wound dressings lack a combinatorial approach to address the complex factors needed to improve chronic wound healing. The development of a novel hydrogel wound dressing platform with tunable degradation, bioactivity, and bacterial resistance will provide a system to improve upon the limitations of current dressing options. The novel approach of this engineered PEG-based hydrogel platform exhibits tunable biodegradation, engineered bioactivity incorporation, versatile scaffold geometries, and antibacterial properties. This platform has potential to serve as an ideal wound dressing scaffold to promote active wound healing. The incorporation of thio-β esters via the reaction between d,l-dithiothreitol (DTT) and poly(ethylene glycol)-diacrylate (PEGDA) should accelerate the rate of hydrolysis of PEG-based hydrogels and create for a tunable biodegradable system. Investigation of the *in vivo* degradation rate based on identified compositions from *in vitro* studies will provide a system for identifying hydrogel compositions that degrade in clinically relevant time frames. Using a biodegradable system, hydrogel wound dressings will be fabricated into different scaffold geometries to create a wound dressing platform that can serve to meet the moisture balance requirements of different wound environments. Wound healing is a complex process that can be approached through a platform system of different scaffold geometries and degradation rates to meet specific design requirements necessary for wound moisture balance and appropriate cellular interactions (e.g. attachment, spreading, and infiltration). Hydrogel scaffolds will be fabricated into injectable microspheres and 3D-printed porous hydrogel foams. Each of these hydrogel scaffolds have unique properties necessary for maintaining

wound fluid maintenance, promoting cellular infiltration, and maintaining a resorbable profile. Furthermore, since these scaffolds will be fabricated using PEG-based hydrogels specific bioactivity can be imparted. Engineered Scl2 proteins will be utilized to target specific integrins, α1β1 and α2β1, which have been shown to play an important role in the wound healing process. Protein stability and effect of functionalization density will demonstrate the ability to improve cellular interactions. Finally, the incorporation of GaM into hydrogels will be investigated as a means to control bacterial inhibition to provide immediate infection control. The innovation of the proposed studies is the investigation *in vivo* degradation of engineered bioactive hydrogel scaffolds with the ability to inhibit bacterial growth. Combined, these systems provide fundamental knowledge and tools to address the complex wound environment necessary for improved wound healing.

CHAPTER II

CHRONIC WOUND DRESSINGS BASED ON COLLAGEN-MIMETIC PROTEINS[1]

2.1. Introduction

Skin wounds can have severe consequences such as amputation and infection risk as well as severe quality of life adjustments.[2, 7, 35, 176-178] Treatment for skin wounds varies depending on the severity of the wound and type of healthcare facility. Skin substitutes are often expensive since they contain animal-derived extracellular matrix (ECM) materials and often cells that require special handling and preparation.[179] Collagen is a major component of most skin substitutes due to its structure and bioactive cues.[5] Collagens are abundant extracellular matrix (ECM) proteins, which give structural integrity to many tissues and regulate cell functions through interactions with cellular receptors and additional ECM constituents. There are at least 28 different mammalian collagens, all with a defining left-handed triple helix that is composed of three polypeptide chains. Each polypeptide chain contains continuous GXY motifs, where X is often proline and Y is usually hydroxyproline.[180] Proline hydroxylation and protein glycosylation are important in overall triple helix stability and collagen network formation. Unlike many commercialized recombinant proteins, the required post-translational modifications of collagen have made it difficult to generate viable recombinant collagen products.

[1] Part of the data reported in this chapter is reprinted with permission from Advances in Wound Care "Chronic wound dressings based on collagen-mimetic proteins," by Stacy Cereceres, Tyler Touchet, Mary Beth Browning, Clayton Smith, Jose Rivera, Magnus Hook, Canaan Whitfield-Cargile, Brooke Russell, and Elizabeth Cosgriff-Hernandez, Advances in Wound Care, 2015, Volume 4, Issue 8, pp. 444-456, published by Mary Ann Liebert, Inc., New Rochelle, NY.

Synthetic collagen peptides have limited quantities and are cost prohibitive, which has limited collagen products to animal sources.[181] These animal-derived materials have inherent disease risk, batch variability, and are often milled with heterogeneous results.[182]

In contrast, bacterial-based collagen mimics have been characterized as triple helical proteins despite a lack of hydroxyproline which circumvents the need for post-translational modifications and enables facile recombinant expression. Several researchers are currently investigating these proteins as potentially useful biomaterials.[141, 148, 181, 183-192] Their production and purification from bacterial expression systems allows for batch conformity and scale-up.[188] One bacterial collagen isolated from *Streptococcus pyogenes*, Scl2, has shown particular promise as a biomaterial for wound care. Scl2 contains an N-terminal globular domain followed by a collagen-like region composed of GXX repeats, where X is often proline or a charged residue to provide helix stability.[141,193] Since bacterial protein engineering is possible in reasonable timeframes, Scl2 possesses an additional advantage in that it can be optimized to possess specific properties.[194] Ligands for Scl2 have not been identified and therefore selective introduction of mammalian collagen sequences can be used to control and tune cell-material interactions. This is a feature unavailable with current animal collagens which offer a broad array of signals to cells. We previously used site directed mutagenesis to introduce the GFPGER motif into the Scl2 sequence (termed $Scl2_{GFPGER}$) and provided evidence that human integrin binding sites function within $Scl2_{GFPGER}$ to bind and activate $\alpha1\beta1$ and $\alpha2\beta1$. Integrins are cell surface heterodimers that enable outside in and inside out signaling which regulate numerous processes such as migration, proliferation, and phenotype, which are key

processes in wound healing.[130, 194-204] The $Scl2_{GFPGER}$ platform provides a unique opportunity to investigate the contribution of collagen binding integrins to wound healing. Although integrin signaling is not the only event leading to wound closure, our scouting studies in a rodent excisional model demonstrated that soluble $Scl2_{GFPGER}$ application increased wound closure rates. Since soluble protein is not a therapeutically viable option, we have incorporated the $Scl2_{GFPGER}$ into microspheres that should retain the same bioactivity.

The collagen-mimetic protein, $Scl2_{GFPGER}$, was incorporated into hydrogels utilizing conjugation chemistry developed in our lab to generate a robust wound dressing.[148] Specifically, the Lys residues of $Scl2_{GFPGER}$ were conjugated to a photo-crosslinkable poly(ethylene glycol) (PEG) linker for incorporation into the hydrogels. We have previously demonstrated that the degree of functionalization has an effect on cell-material interactions where a higher degree of functionalization imparted steric hindrance of the integrin binding site.[205] Sufficient functionalization is required to anchor proteins within the hydrogel and too little functionalization results in protein loss and reduction of cell adhesion. Here, we present a redesigned Scl2 backbone to address these issues, Engineered Collagen ($eCol_{GFPGER}$). The $eCol_{GFPGER}$ was designed to have functionalization sites further away from the integrin-binding motif to decrease steric hindrance.

Although hydrogel dressings are common in wound care management, slabs or sheets of hydrogels may be difficult to fit to deep or irregularly shaped wounds. Cellular migration is also hampered in these geometries and limited to the rate of hydrogel

degradation. In contrast, hydrogel microspheres provide a gel-like dressing that is able to conform to wound shape offering immediate hydration balance and infection protection to the wound. Cellular infiltration into the microsphere network is facilitated by the gaps between each particle. Moisture control is also expected to be enhanced due to the increased surface area allowing for more rapid water uptake and diffusion. Typical fabrication of hydrogel microspheres involving water-in-oil emulsions; however, these methods suffer from size heterogeneity and decreased yields.[206] Droplet formation using passive co-flowing streams can provide greater control over droplet size and uniformity.[207] Fluidic methods have shown improved fabrication processes with the potential to photopolymerize hydrogel microspheres.[208]

In this study, integrin affinity and cell adhesion to $Scl2_{GFPGER}$, $eCol_{GFPGER,}$ or an animal-derived collagen control were determined as an initial assessment of potential for wound care applications. Two microsphere fabrication systems were investigated to fabricate monodisperse hydrogel microspheres or to increase fabrication throughput achieving smaller average particle sizes for injectable delivery. Finally, hydrogel microspheres were fabricated using a co-fluidics setup and the water uptake properties of both hydrogel slabs and microspheres were quantified. The potential of this dressing to conform to an irregular wound was then demonstrated in a rat model. Overall, this strategy harnesses biological dressing advantages while providing wound coverage and hydration through the presence of a tunable hydrogel network.

2.2. Materials and Methods

2.2.1. Materials

All chemicals were purchased from Sigma Aldrich (Milwaukee, WI) and used as received unless otherwise noted.

2.2.2. Protein Engineering

Recombinant $eCol_{GFPGER}$ protein was derived from Scl2 containing integrin-binding motif GFPGER at positions 118-123. The C-terminus of Scl2 contains regions where triple helix is predicted to be less stable and contributes to a lower melting temperature (algorithm used to predict collagen stability is described in Persikov et al.[193]). Using this algorithm GXY triplets were identified that may contribute to protein stability and selected triplets were mutated to more stable triplets. To generate a more thermally stable collagen, two triplets GKDGKD were mutated to GDRGER (Lys314→Asp314, Asp315 →Arg315, Lys317→Glu317, Asp318→ Arg318) where D and E at X position and R in Y position of GXY triplet are predicted to be more stable and are more frequent in eukaryotic collagens. To stabilize functionalization of $Scl2_{GFPGER}$ single Lys residues were replaced by Arg residues in GKD triplets at Lys positions 182, 236, 248, 263, 269, 275, 278, 284, 290, 293, 299, 305, 308, and 323 (the Arg at the X position of a GXY triplet exist at same frequency in eukaryotic collagens as replaced Lys residues and are similarly thermally stable). The mutations were introduced by gene synthesis (Genewiz). Histidine-tagged recombinant proteins were expressed from a pCold vector in E. *coli* Top3 cells and purified by Ni++ affinity chromatography on a 5 ml column (GE Healthcare). Protein purity was determined by SDS-PAGE followed by Coomassie blue staining and western

blot analysis. SDS-PAGE analysis was used to determine multimer formation as described. Briefly, proteins were denatured by incubation at 95°C for 5 minutes in the presence of 0.1% SDS and 2% β-mercaptoethanol. Non-denatured samples were incubated in 5% glycerol and kept on ice prior to electrophoresis on 12% SDS gels. Gels were stained with Coomassie blue, and protein migration as it corresponds to size was determined using protein standard.

2.2.3. Circular Dichroism

Circular dichroism spectra of protein samples in 50 mM Acetic acid were recorded on a Jasco J720 spectropolarimeter in a thermostatically controlled cuvette with a 0.5 mm path length. Data were collected at ambient temperature in a wavelength range from 250 nm to 190 nm, and integrated for 1 s at 0.2 nm intervals with a bandwidth of 1 nm. For each spectrum, ten scans were averaged and the contribution from the buffer was subtracted. For thermal transition experiments, the ellipticity at 220 nm in a cuvette with a 0.5-mm path length was monitored as the sample temperature was increased from 25 to 50°C, with an average temperature slope of 10°C/h.

2.2.4. Protein Functionalization

$Scl2_{GFPGER,}$ $eCol_{GFPGER,}$ and rat tail collagen type I were functionalized with Aam-PEG-I. Briefly, Aam-PEG-I was dissolved in anhydrous dimethylformamide and added dropwise to a collagen solution in phosphate buffered saline (PBS) and $Scl2_{GFPGER}$ and $eCol_{GFPGER}$ in 50 mM acetic acid at room temperature (acetic acid for $Scl2_{GFPGER}$ and $eCol_{GFPGER}$). The molar ratio of Aam-PEG-I:NH2 was 0.1:1 for collagen and $Scl2_{GFPGER,}$ and 0.5:1 for $ECol_{GFPGER}$. After 2 h of stirring, dialysis against RO water for 24 h (MWCO

= 20,000 Da) was used to purify functionalized proteins. FTIR spectroscopy confirmed functionalization of proteins with Aam-PEG-I.

2.2.5. Solid Phase Binding Assays

Microtiter wells were coated with 2 μg per well of recombinant alpha 1 integrin I-domain. The samples were blocked with TBS containing 2% bovine serum albumin (BSA) for 1 hr. Solutions of 1 μM $Scl2_{GFPGER}$, $eCol_{GFPGER}$, functionalized $Scl2_{GFPGER}$ or functionalized $eCol_{GFPGER}$ were added to the wells and incubated for 1 hr at room temperature. Rabbit polyclonal antibodies raised against $Scl2_{GFPGER}$ followed by donkey anti-rabbit-HRP and SigmaFast OPD were used to detect bound proteins. The absorbance at 450 nm was measured using a Thermomax plate reader.

2.2.6. Cell Adhesion Study

All cell culture supplies were purchased from Life Technologies (Carlsbad, CA) and used as received unless otherwise noted. To assess adhesion and spreading of HT1080 fibroblasts, 48 well tissue culture polystyrene (TCPS) plates were coated with 10 μg of $Scl2_{GFPGER,}$ $eCol_{GFPGER,}$ rat tail collagen type I or Scl2 overnight at 4°C. Protein solutions (0.1 mg ml^{-1} 20 mM acetic acid) were filtered through 0.22 μm PVDF syringe filters prior to coating (4 wells per protein type). Wells were blocked with 4 vol% BSA in PBS for 1 hr at room temperature and rinsed with sterile PBS three times. HT1080s were cultured in DMEM with 10% fetal bovine serum and 1% penicillin-streptomycin. Cells were adapted to serum-free media for 12 hr prior to seeding at 5,000 cells cm^{-1} in protein-coated TCPS well plates. After 3 hr of exposure, wells were rinsed three times with warm PBS to remove unadhered cells, and the remaining cells were fixed with 3.7% glutaraldehyde for

20 min at room temperature. Cells were stained with rhodamine phalloidin (actin/cytoplasm, Sigma-Aldrich) and SybrGreen (DNA/nucleus) and imaged (3 images per sample, 4 samples per protein) on a DeltaVision Elite microscope (GE Healthcare). Fluorescent images of SybrGreen- and rhodamine phallodin-stained cells were utilized to quantify cell adhesion and spreading. Manual counts of SybrGreen-stained cell nuclei in each image provided adhesion density measurements. Spreading, or cell area, was quantified by applying the Photoshop "magic wand" tool to image backgrounds until all extracellular regions were selected. The histogram function was utilized to determine the number of extracellular pixels (P_{EX}), and the average number of pixels per cell (A_{CELL}) for a given image was quantified as:

$$A_{CELL} = \frac{P_T - P_{EX}}{N} \qquad [1]$$

where P_T is total image pixels and N is total number of cell nuclei. Pixels were then converted to microns using known objective scaling.

2.2.7. Synthesis of Poly(ethylene glycol) diacrylate (PEGDA)

PEGDA was synthesized according to a method adapted from Hahn, et al.[56] Briefly, acryloyl chloride was added dropwise to a solution of PEG 2 kDa or 6 kDa diol and triethylamine in dichloromethane (DCM) under nitrogen. The molar ratio of PEG, acryloyl chloride, and triethylamine was 1:2:4, respectively. After the addition of acryloyl chloride, the reaction was stirred for an additional 24 hours at room temperature. The resulting solution was then washed with 8 molar equivalents of 2 M potassium bicarbonate to remove acidic byproducts. The product was then precipitated in cold diethyl ether, filtered, and dried under vacuum.

2.2.8. Synthesis of Poly(ethylene glycol) diacrylate with thio-β esters (PEGDTT)

PEGDTT was synthesized by adding d,l-dithiolthreitol (DTT) and triethylamine (TEA) dropwise to a solution of PEGDA (2 kDa) in DCM. The molar ratio of DTT, PEG and triethylamine was 2:3:0.9, respectively. After the addition of the DTT and triethylamine, the reaction was stirred for 24 hours at room temperature. The resulting solution was then precipitated in cold diethyl ether, washed, filtered, dried under ambient conditions for 24 hours then placed under vacuum to remove any excess solvent.

Characterization of PEGDA and PEGDTT was confirmed using Fourier transform infrared spectra (FTIR) and proton nuclear magnetic resonance (^{1}H-NMR) spectroscopy. Transmission FTIR spectra of control and functionalized polymers were acquired on a Bruker ALPHA spectrometer by solution casting directly onto KBr pellets with 32 scans and a resolution of 2 cm^{-1}. Proton NMR spectra of control and functionalized polymers were recorded on a Mercury 300 MHz spectrometer using a TMS/solvent signal as an internal reference. Percent conversions of PEG diol to acrylate endgroups was greater than 85%. ^{1}H-NMR ($CDCl_3$): δ 3.6 ppm (m, -OCH_2CH_2), 5.8 ppm (dd, -CH=CH_2), 6.1 (dd, -CH=CH_2) and 6.4 ppm (dd, -CH=CH_2). PEGDTT number average molecular weight (Mn) was determined by normalizing to the PEG backbone and calculating the number of DTT macromers bound to PEG.

2.2.9. Hydrogel Characterization

Hydrogels were fabricated by making (10 wt%) precursor solutions in RO water to demonstrate a tunable degradation rate. A photoinitiator solution (1 mg Irgacure 2959 per 0.01 ml 70% ethanol) was added at 1 vol% of precursor solution. Solutions were

pipetted between 1.5 mm spaced plates and crosslinked by 6 min exposure to long wave UV light (Intelli Ray Shuttered UV Flood Light, Integrated Dispensing Solutions, Inc., 365 nm, 4 mW/cm^2). To measure water uptake, eight 8-mm discs were punched from hydrogel sheets. Samples were swollen in RO water for 24 hours and weighed to determine the equilibrium swelling mass (W_s). Then specimens were dried under vacuum overnight to determine dry mass (W_d). The equilibrium swelling ratio (Q) was calculated from the mass swelling ratio:

$$Q = \frac{W_s}{W_d} \qquad [2]$$

The water uptake (U) was calculated from the equilibrium mass swelling ratio:

$$U = \frac{W_s - W_d}{W_d} \qquad [3]$$

2.2.10. Hydrogel Microsphere Co-flow Fluidics Fabrication

A 30% hydrogel precursor solution was prepared by dissolving PEGDA (6 kDa) in water. The solution was mixed, and a photoinitator solution (1 mg Irgacure 2950 per 10 µL 70% ethanol) was added at 1 vol % of precursor solution. Microspheres were then fabricated via a fluidics water in oil emulsion technique adapted from Gokmen et al.[209] The hydrogel precursor solution was injected dropwise (KD Scientific-100 Infusion Pump) into an external mineral oil phase (Harvard PHD 2000 Infusion Pump) and passed through UV excitation (UVP High Performance Transilluminator 365 nm) for 2 min to initiate radical crosslinking. Needle gauge, aqueous flow rate, and hydrogel injection rate were varied to modulate particle size. Collected microspheres were filtered using vacuum aspiration. Microspheres were imaged using a 4X objective on a stereoscope (National

Optical) with 3.0 mega pixel built in camera using Motic Image Plus 2.0. A total of 10 particles were analyzed for 4 different batches (n =40).

2.2.11. Bulk Microsphere Fabrication

To increase fabrication throughput, a bulk microsphere technique was established and variables were modulated to control average particle size. A 20% hydrogel precursor solution was prepared by dissolving a ratio of 75% PEGDTT to 25% PEGDA (6 kDa) in water. The solution was mixed, and a photoinitator solution (1 mg Irgacure 2950 per 10 µL 70% ethanol) was added at 3 vol% of precursor solution. The external continuous phase consisted of light mineral oil, oil soluble photointiator, and a surfactant. An oil soluble initiator, phenylbis(2,4,6-trimethylbenzoyl)phospine oxide, solution (15% w/v in acetone) was added at 1-10 µL/ml of mineral oil. The surfactant, polyglycerol polyricenoleate (PGPR 4125 – donated by Palsgaard), was added at 1-10 wt% of the mineral oil. Microspheres were then fabricated via water in oil emulsion technique using a FlackTek Speedmixer DAC 150 FVZ-K. The external continuous phase was mixed at 100 rpm for 2.5 minutes prior to emulsification. Once, thoroughly mixed, the hydrogel precursor solution was added in one addition (1 ml precursor solution per 6 ml mineral oil) and mixed between 750-2000 rpm for 5 minutes. The emulsion was then transferred to petri dishes and exposed to UV light (UVP High Performance Transilluminator 365 nm) for 12 minutes to initiate radical crosslinking. Collected microspheres were then filtered and purified through a series of ethanol ramps and vacuum aspiration. Hydrated hydrogel microspheres were flash frozen and lyophilized in 3 ml syringes.

Bulk microparticles were imaged using a 10X objective with phase contrast on a Motic AE3 using a Moticam 1SP 1.0 MP camera connected to the microscope with Motic Image Plus 3.0. Particle size was then determined utilizing Motic Images Plus 3.0 software scale and measurement tools. A total of 10 particles were analyzed for 4 different batches (n =40). Lyophilized hydrogel microspheres were rehydrated in 1.5 mL of PBS in two solution mixes. First, 750 µL of PBS was drawn into the syringes using a 16G needed and mixed 10 times by drawing the plunger up and down. After 2 minutes of rehydration, the remaining 750 µL of PBS was drawn into the syringes and the same procedure for mixing was followed. After full hydration of hydrogel microspheres delivery was investigated through controlled injection volumes.

2.2.12. Rat Excisional Wound Model

A 3 month old male Sprague Dawley rat that had been euthanized less than an hour previously was obtained through the Comparative Medicine Program at Texas A&M University. This was done under AUP IACUC 2014-010 "Maintenance & Utilization of Animals for Animal Care & Use Training" which allows for excess animals and animals euthanized under other AUP's to be utilized in a tissue share program to maximize use of all research animals. A ~1.5 x 2.0 cm full-thickness irregularly shaped defect was created on the dorso-lateral aspect of the rat and extended into the underlying muscle layers.

2.2.13. Statistical Analysis

All statistical analyses were expressed as the mean ± standard derivation of the mean. Statistical analysis was performed by an unpaired two-tailed student's t-test. Statistical significance was accepted at $p < 0.05$.

2.3. Results and Discussion

2.3.1. Protein Engineering

First, we modified the Scl2 protein to enhance its use as bioactive component of our hydrogel wound dressing. Efforts were taken to improve $Scl2_{GFPGER}$'s thermal stability and reduce steric hindrance of the PEG linkers around the integrin binding site. 14 single Lys in the collagen-like region of the protein were mutated to Arg residues in GKD triplets, which was predicted to have similar thermal stability, but not support PEG-linker attachment. The resulting protein, $eCol_{GFPGER}$, was then evaluated for retention of a triple helix, thermal stability, and integrin interactions. After recombinant production and purification of $eCol_{GFPGER}$, circular dichroism was used to assess the protein's triple helix. **Figure 2.1A and 2.1B**, showed a typical triple helical spectra with a peak at 220 nm indicating our protein engineering did not disrupt the triple helix. In addition, SDS-PAGE analysis revealed the presence of multimers (data not shown). A marked increase in melting temperature from 37°C to 45°C was observed in thermal transition studies, **Figure 2.1C**.

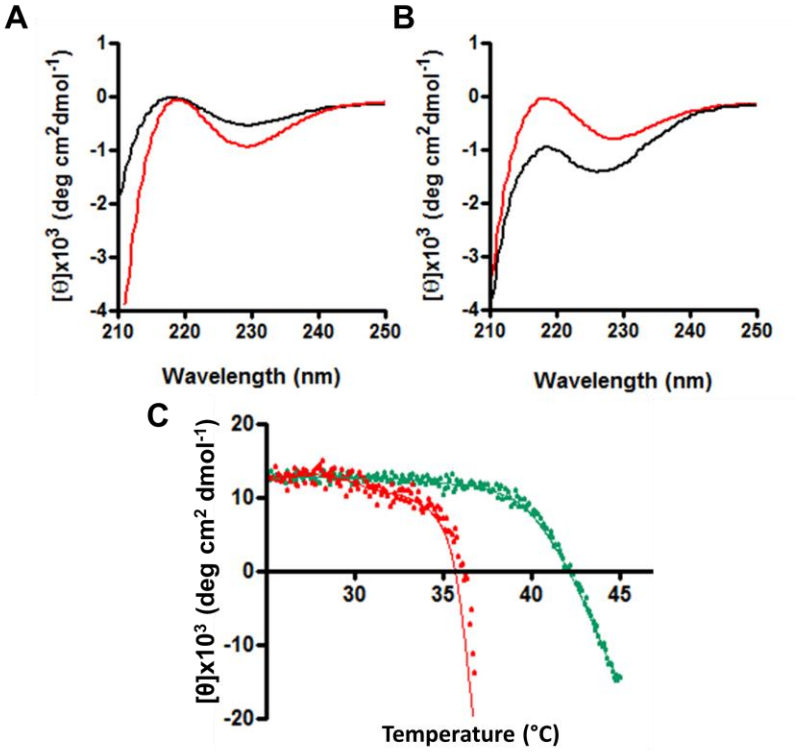

Figure 2.1. CD analysis indicates that functionalization does not significantly affect triple helix formation. CD wavelength scans of (A) $Scl2_{GFPGER}$ (black) and F-$Scl2_{GFPGER}$ (red) and (B) $eCol_{GFPGER}$ (black) and F-$eCol_{GFPGER}$ (red) demonstrate the presence of a peak at 220 nm, indicative of a triple helical structure. CD thermal transition of (C) $Scl2_{GFPGER}$ (red) and $eCol_{GFPGER}$ (green). Reprinted from Cereceres *et al.*[67]

The collagen-mimetic proteins were then functionalized with PEG linkers to determine whether $eCol_{GFPGER}$ had improved integrin binding site availability. FTIR spectroscopy was first used to confirm successful functionalization of $Scl2_{GFPGER}$ and $eCol_{GFPGER}$ with PEG linkers to formulate F- $Scl2_{GFPGER}$ and F-$eCol_{GFPGER}$, respectively. The functionalized protein spectra contained absorption peaks corresponding to the carbonyl of the amides (~1650 cm^{-1}) in the protein backbone and ether (~1110 cm^{-1}) of the PEG linker (data not shown). An ELISA-type assay was then used to measure the

effect of protein functionalization on recombinant α1 I-domain binding. We consistently observed a decreased in integrin affinity regardless of which collagen-mimetic was analyzed; however, the observed decreased was less pronounced with $eCol_{GFPGER}$, **Figure 2.2**. Protein binding was measured using polyclonal antibodies raised against $Scl2_{GFPGER}$ in rabbits; however, these polyclonal antibodies displayed similar titers against all collagen-mimetics tested (data not shown).

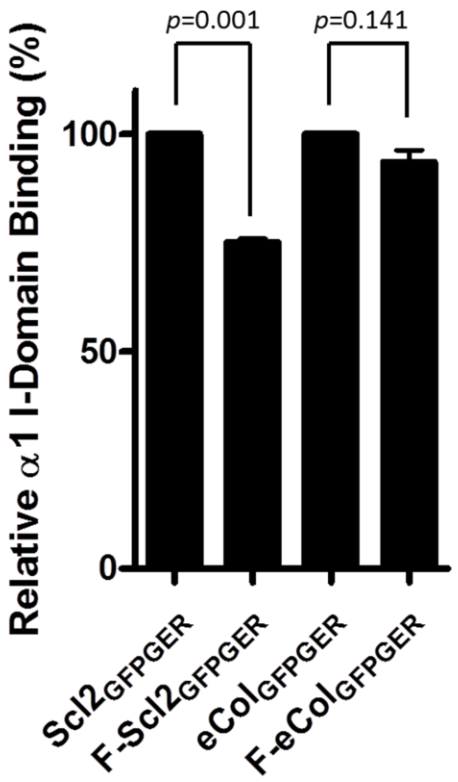

Figure 2.2. $eCol_{GFPGER}$ exhibits reduced steric hindrance of PEG linkers. 1 μM collagen-mimetic, $Scl2_{GFPGER}$, F-$Scl2_{GFPGER}$, $eCol_{GFPGER}$, and F-$eCol_{GFPGER}$, were incubated with immobilized recombinant human α1 I-domains (1 μg/well) with 1 mM Mg2+. Collagen-mimetic binding was detected as described in Experimental Procedures. Data shown are representative of at least three replicates and normalized to the nonfunctionalized control protein. Reprinted from Cereceres *et al.*[67]

The Scl2 backbone has been characterized as a potentially useful recombinant biomaterial and can support the introduction of human integrin sequences to facilitate cell adhesion, migration, and proliferation.[141, 148, 181, 184-188, 190-192, 194, 210] Our results demonstrate that selective triplet substitutions may be used to further optimize the backbone helix to achieve certain properties. Given that it has been established that a triple helical conformation is required for integrin binding and activation[197, 198, 200, 211], our demonstrated ability to stabilize triple helices is expected to affect ligand interactions and potentially cellular behavior.[124] To anchor these proteins into the hydrogel, it is necessary to first functionalize the protein with PEG linkers that can photocrosslink with the PEG matrix. The placement of these PEG-linkers along the triple helical backbone can have significant implications regarding integrin binding site availability to cells due to steric hindrance.[205] Our targeted modification of the Scl2 protein to limit the steric hindrance of these PEG linkers during integrin binding was successful. In addition, stability predictions were used to mitigate any changes in the backbone that might result in disrupted interchain interactions. These efforts resulted in a protein construct with an increase in melting temperature of ~7°C. The studies here show an increase in cell adhesion on $eCol_{GFPGER}$ compared to $Scl2_{GFPGER}$ indicating that these substitutions had some effect on cell-material interactions.

2.3.2. Cell-Material Interactions

To assess the functionality of the integrin binding site in $eCol_{GFPGER}$, HT1080 fibroblast adhesion and spreading on protein coats was assessed at 3 hours, **Figure 2.3**. Although cell spreading was similar between the three collagen-mimetic proteins, a

significant increase in adhesion was observed on $Scl2_{GFPGER}$ with the introduction of the integrin binding site into Scl2, as shown previously.[148] A further increase in adhesion was observed on $eCol_{GFPGER}$ relative to $Scl2_{GFPGER}$, to a level that is comparable to that on collagen I.

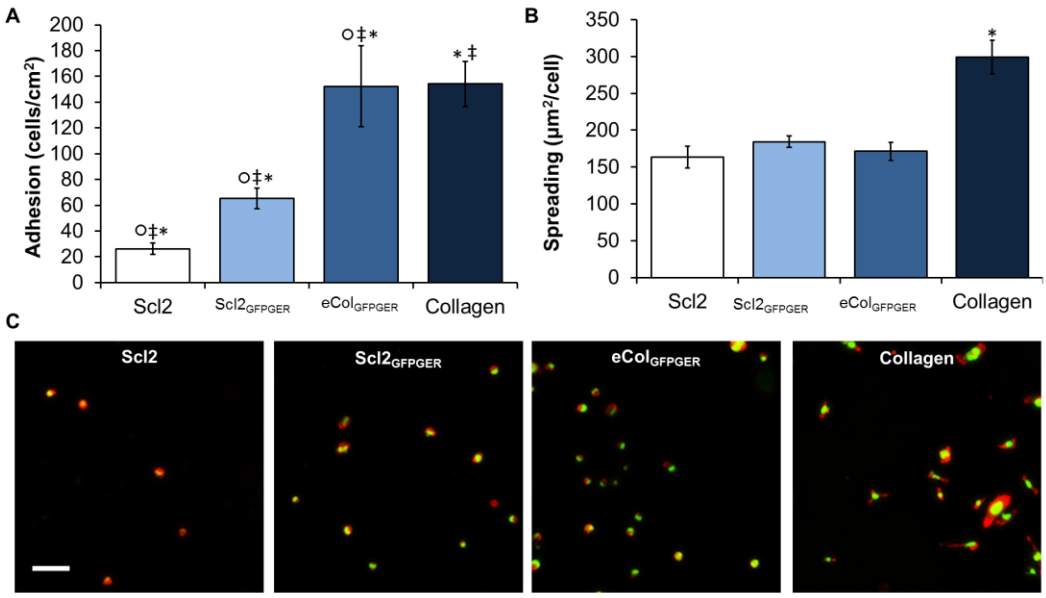

Figure 2.3. HT1080 fibroblast adhesion and spreading on collagen-mimetic protein-coated wells. (A) Adhesion numbers on protein coats after a 3-h incubation period. (B) Average cell spreading (area) at 3 h. (C) Rhodamine phalloidin and SYBR Green-stained HT1080 fibroblasts. n=4 wells per protein, 3 images per well for a total of 12 images per sample; mean±standard deviation displayed; °‡* indicate statistically significant differences between respective samples $p<0.05$. Reprinted from Cereceres *et al.*[67]

Analysis of HT1080 fibroblast interactions demonstrated that $eCol_{GFPGER}$ induced comparable cell adhesion to that of collagen I. Considering the presence of only one integrin binding site in $eCol_{GFPGER}$ compared with collagen's multitude of integrin binding

sites, this result demonstrates a notable increase in protein functionality. Furthermore, when compared with $Scl2_{GFPGER}$, significantly higher cell adhesion was induced on $eCol_{GFPGER}$. These two proteins have the same integrin binding motif; thus, the increased integrin interactions with $eCol_{GFPGER}$ are either due to its increased thermal stability or an overall triple helical change resulting in altered integrin interactions. A stable triple helix is required for integrin α1β1 and α2β1 binding to the GFPGER site. Cells were incubated on protein-coated plates at 37°C, which is the approximate melting temperature of both collagen I and $Scl2_{GFPGER}$.[212] Therefore, it is possible that both collagen and $Scl2_{GFPGER}$ experienced some denaturation during this experiment, rendering their integrin binding sites inactive. $eCol_{GFPGER}$ was well below its thermal transition temperature of ~45°C in this experiment, indicating that it was intact with active integrin binding sites. However, we cannot rule out the possibility that these changes did not have an effect on the interaction with the integrin itself and studies are underway to characterize the binding mechanism.

2.3.3. Hydrogel Characterization

The final purified polymer structure of PEGDA and PEGDTT was confirmed with both FTIR and ^{1}H-NMR spectroscopy. For PEGDA, the presence of ester peaks at 1730 cm^{-1} and loss of hydroxyl peaks at 3300 cm^{-1} in the IR spectra confirmed successful acrylation. For PEGDTT, the loss of the thiol stretch at 2600 cm^{-1}, the presence of the hydroxyl peaks at 3300 cm^{-1} and decrease in the 842 cm^{-1} peak correlating to the carbon carbon double bond confirmed successful coupling, **Figure 2.4**. The ratio of integrated protons of acryloyl to backbone methyl groups in the ^{1}H NMR spectra confirmed the

structure of PEGDA. Percent conversions of PEG-diol to acrylate endgroups was greater than 90%. The PEGDTT structure and number average molecular weight (Mn) was determined by the ratio protons of the methyl groups in the PEGDA backbone to the number of protons from DTT backbone. The Mn was found to be 6.4 kDa with an acrylation of greater than 90%, **Figure 2.5**.

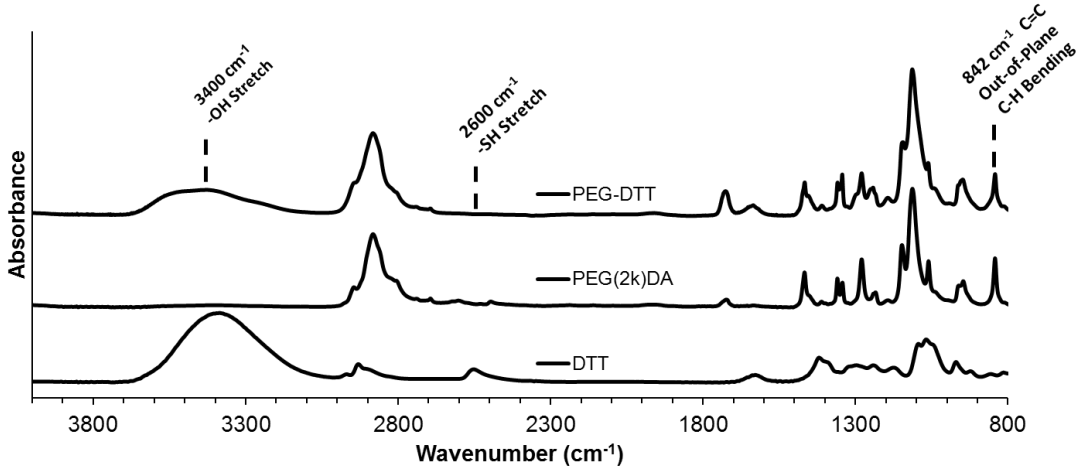

Figure 2.4. Transmission FTIR spectrum of the PEGDTT (Top), PEG(2k)DA (Middle), and DTT (Bottom). Transmission FTIR spectra of control and functionalized polymer neat films were acquired on a Bruker ALPHA spectrometer by solution casting directly onto KBr pellets with 32 scans and a resolution of 2 cm^{-1}. Reprinted from Cereceres *et al.*[67]

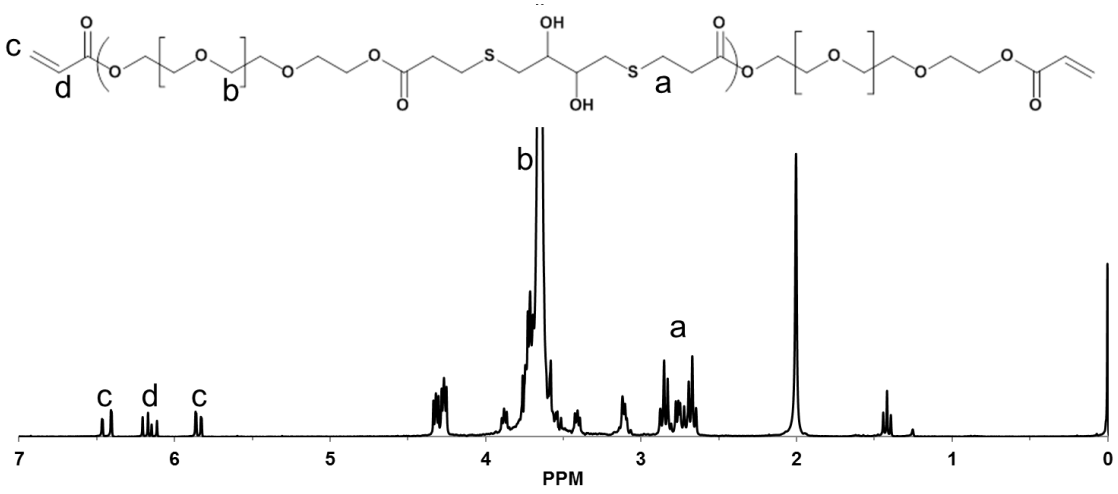

Figure 2.5. H[1]NMR spectra of the PEGDTT in CDCl3. Proton NMR spectra of control and functionalized polymer solutions were recorded on a Mercury 300 MHz spectrometer using a TMS/solvent signal as an internal reference. 1H NMR (CDCl3): δ 3.6 ppm (m, -OCH2CH2), 5.8 ppm (dd, CH=CH2), 6.1 (dd, CH=CH2), and 6.4 ppm (dd, -CH=CH2). Reprinted from Cereceres *et al.*[67]

Finally, its fabrication into hydrogel microspheres provides a bioactive dressing that can readily conform to irregular wounds. Future studies will determine if the observed enhancement in cell interaction is conferred to the bioactive gels and due to reduced steric hindrance around the integrin binding site, increased stability of the triple helix, or a combinatory effect. Overall, this new $eCol_{GFPGER}$ shows strong promise in the generation of bioactive hydrogels for wound healing as well as a variety of tissue scaffolds.

2.3.4. Hydrogel Microsphere Properties

Microspheres fabricated using the water-in-oil emulsion technique described above were filtered using vacuum aspiration and then characterized, **Figure 2.6**. Fully swollen fabricated microspheres had an average diameter of 878 ± 45 μm. Particles of this size were achieved with an 800 μL min^{-1} continuous phase flow rate, 0.5 μL hr^{-1} dispersed

hydrogel phase flow rate, and 1.6 mm inner diameter PVC tubing (McMaster-Carr). A blunted 30-gauge needle was used to inject the hydrogel precursor solution into the continuous mineral oil phase. Particle size can be tuned by changing the flow rates of the continuous and dispersed phases. Decreasing the flow rate of the continuous phase or increasing the flow rate of the dispersed phase decreases the particle size. The flow rate of the continuous phase has the most impact on particle size and shape.

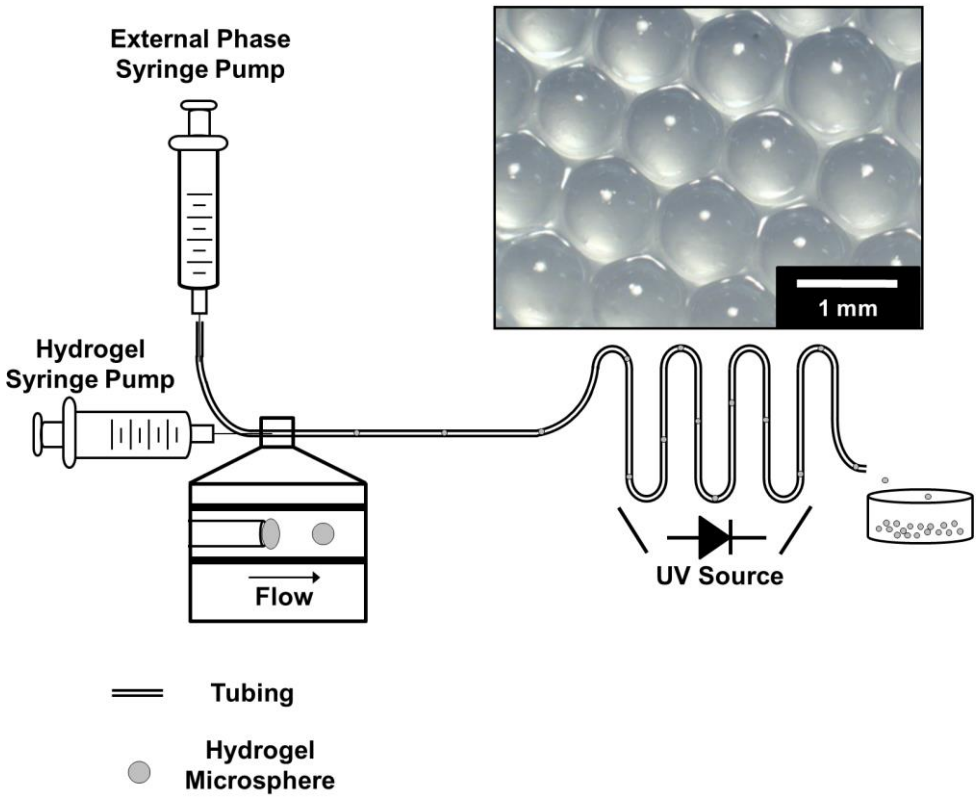

Figure 2.6. Schematic of microsphere fabrication. Using co-flow fluidics, hydrogel microspheres were fabricated by injecting dropwise a hydrogel precursor solution into a continuous mineral oil phase, creating a water-in-oil emulsion. Hydrogel microspheres were then cross-linked using UV light while traveling along the tubing. Reprinted from Cereceres *et al.*[67]

Swelling ratio and water uptake of 10% PEGDA (6 kDa) and PEGDTT (5.8 kDa) hydrogel slabs were measured to compare to 30% PEGDA (6 kDa) microspheres, **Table 2.1**. Both the 1.0 PEGDTT and PEGDA hydrogel slabs had similar swelling and water uptake values. The microspheres had a slightly lower but comparable swelling ratio and water uptake values compared to the hydrogel slabs which demonstrate the ability of the hydrogel microspheres to absorb wound exudate. Finally, we demonstrated that this tunable microsphere design allows for improved wound filling when applied to irregularly shaped wounds in a rat model, **Figure 2.7**. The defect was packed with hydrated microspheres such that the defect was completely filled to the level of the surrounding, undamaged tissue.

Table 2.1. Swelling and water uptake comparisons of PEGDTT and PEGDA slabs and microspheres. [a,b]Indicate statistically significant differences between respective samples $p<0.05$. PEGDA, poly(ethylene glycol) diacrylate; PEGDTT, poly(ethylene glycol) d,l-dithiothreitol. Reprinted from Cereceres *et al.*[67]

	Swelling Ratio (Q)	Water Uptake (mL H_2O / g polymer)
PEGDTT Slab[a]	15.31 ± 0.49	14.32 ± 0.49
PEGDA Slab[b]	16.41 ± 0.94	15.41 ± 0.94
PEGDA Microspheres[a,b]	11.41 ± 2.35	8.06 ± 2.35

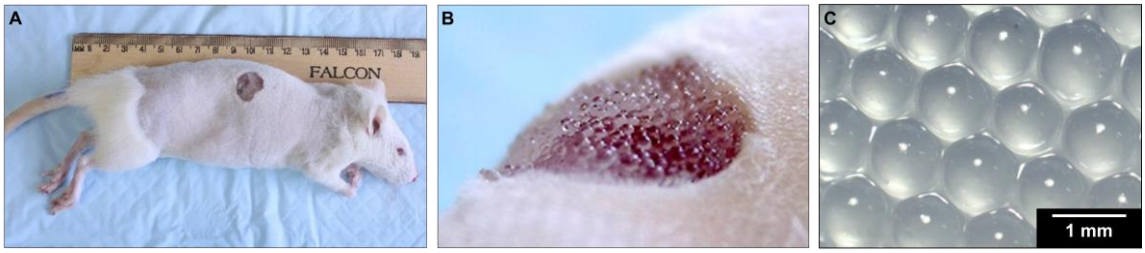

Figure 2.7. Hydrogel microspheres filling the wound defect in rat model. (A) Irregularly shaped wound on the dorsolateral aspect of the rat (B) Wound packed with hydrated microspheres, 5 mm scale bar (C) Swollen hydrogel microspheres, 1 mm scale bar. Reprinted from Cereceres *et al.*[67]

Although the fabrication of these co-fluidic hydrogel microspheres resulted in uniform particle size, batch size and throughput was limited by the fabrication technique. Additionally, co-flow microsphere sizes were tuned between 499.6 ± 84.9 µm and 1064.9 ± 42.5 µm based on external oil flow rate of 600 µL/min and 2000 µL/min, respectively. To further decrease particle size an external flow rate of 3000 µL/min was used, however; there was no statistical difference in particle size at the 2000 uL/min flow rate. Although it was demonstrated that particle size could be tuned using this system we were limited to sizes 500 µm and above. To address these limitations, we investigated the use of a FlackTek Speedmixer to improve up-scale techniques and fabrication time utilizing an oil-in-water emulsion, **Figure 2.8**.

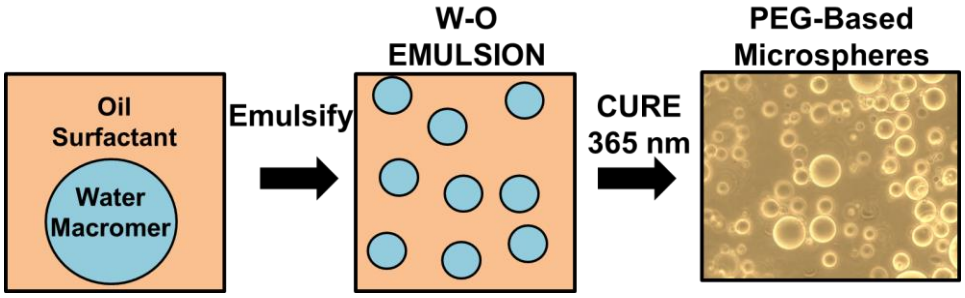

Figure 2.8. Schematic of bulk microsphere fabrication. Using emulsion fluidics, hydrogel microspheres were fabricated by creating a water-in-oil emulsion. Hydrogel microspheres were then cross-linked using UV light after emulsification.

Average particle size was tuned through control of emulsion fluidic parameters such as mixing speed, surfactant concentration, and concentration and use of a dual initiator system, **Figure 2.9**. Modulation of mixing speeds resulted in average particle sizes between 30 ± 14 µm and 94 ± 78 µm with smaller particle sizes observed at higher mixing speeds due. Additionally, concentration of surfactant was investigated to modulate average particle size with average particle sizes ranging from 40 to 70 µm. Franco et al. demonstrated the use of a dual-photoinitiator technique to improve microparticle yield and crosslinking at the surface.[206] To further modulate our system, an oil soluble and water soluble initiator were used to investigate effect on particle size ranging between 30-70 µm. Another limitation of the co-fluidics system was the inability to make smaller particle size despite modulation of system parameters but we demonstrate the ability to tune particle size with this bulk system between 95 and 30 µm through controlled emulsion variables. Although this system did not result in uniform particle size distribution, the delivery and space-filling capability of this system was maintained, **Figure 2.10A**. Additionally, the ability to control particle size allowed for injectable delivery utilizing the bulk fabrication

technique, **Figure 2.10B**. After lyophilization and rehydration of the microspheres in a syringe, controlled injections of 100 µL were weighed to determine delivery reproducibility. Five injections per syringe were analyzed with an average delivery of 78.68 ± 4.05 mg demonstrating delivery of controlled doses. This injectable delivery system can reproducibly and accurately deliver a targeted dose of microspheres. This important fabrication modification, demonstrates the capability to incorporate therapeutic agents into these hydrogel microspheres for controlled delivery of proteins or antimicrobial agents to modulate the wound healing environment.

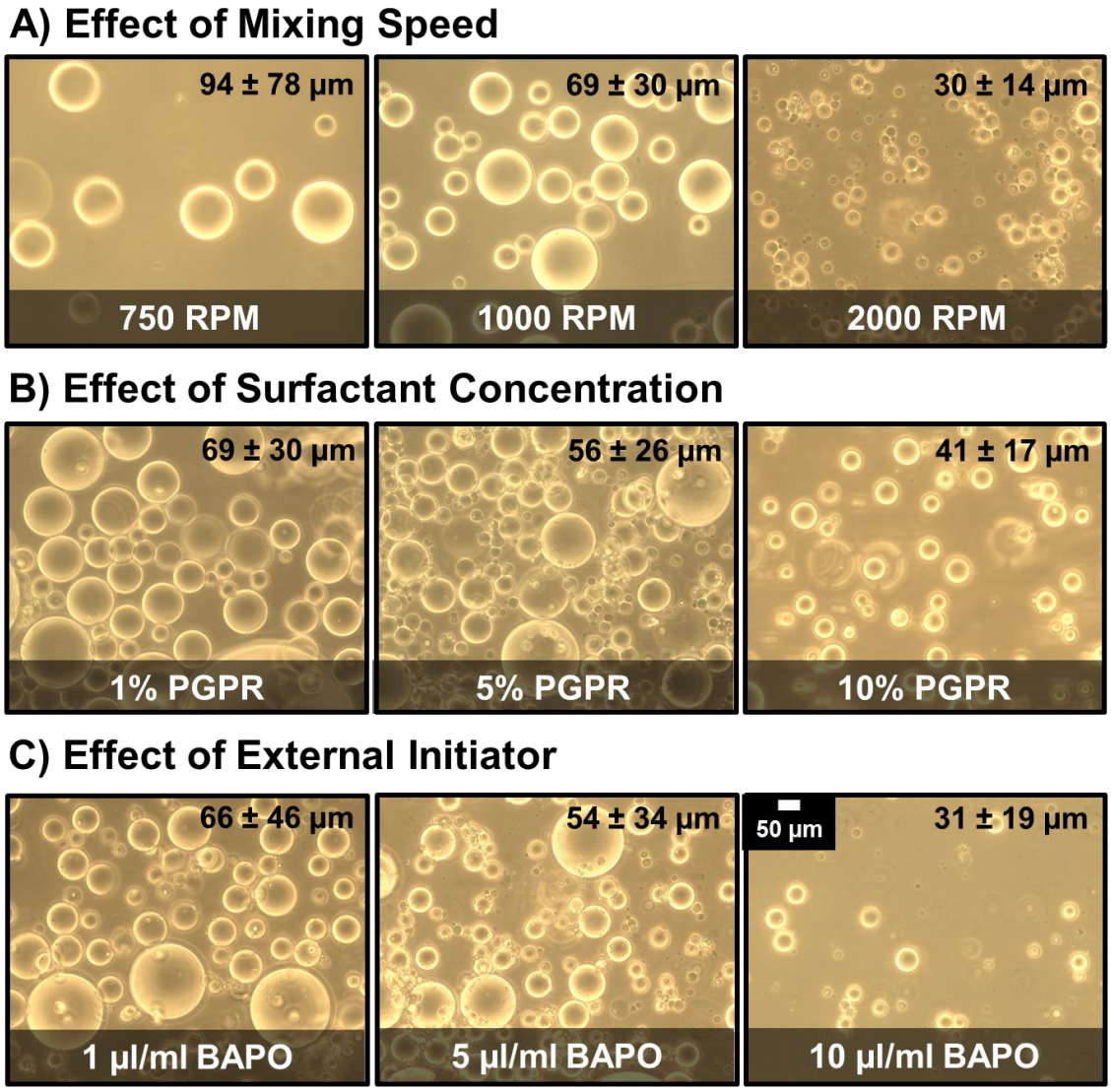

Figure 2.9. Average microsphere particle size was tuned through controlled emulsion parameters to create a tunable system for injectable delivery. Scale bar represents 50 µm and is representative for all images.

A) Bulk Microsphere Wound Packing

B) Microsphere Delivery

Injection Sample	Weight
Injection 1	74.39 mg
Injection 2	84.97 mg
Injection 3	76.59 mg
Injection 4	80.00 mg
Injection 5	77.47 mg
Average	**78.68 ± 4.05 mg**

Figure 2.10. A) Wound packed with hydrated microspheres demonstrating space-filling capability. B) Microsphere rehydration and delivery protocol developed to accurately deliver consistent controlled doses.

2.4. Conclusions

Although hydrogel sheets are popular wound dressings, these passive dressings do not promote regeneration, require frequent changing, and cannot conform to irregularly shaped wounds. Previously, we fabricated bioactive hydrogels through the addition of collagen-mimetic proteins that can regulate key processes in wound healing. Here, we present a novel collagen-mimetic protein with reduced steric hindrance, reduced melting properties, and increased cell-material interactions. A collagen mimetic, $eCol_{GFPGER}$, was developed that has improved stability and functionalization profile while maintaining integrin and cell interactions. A degradable hydrogel matrix was utilized to permit

controlled modulation of degradation rate without impact on other physical properties. Hydrogel microspheres were then fabricated to provide a dressing that can readily conform to irregular wounds and facilitate cell infiltration. Finally, the microsphere fabrication system was tuned to allow for a high throughput, injectable system to allow for controlled dose delivery.

CHAPTER III

CHARACTERIZATION OF THE *IN VIVO* DEGRADATION PROFILE OF TUNABLE POLY(ETHYLENE GLYCOL) HYDROGELS WITH THIO-B ESTERS

3.1. Introduction

Hydrogels are widely used for biomedical applications due to their soft tissue properties, high water content, and biocompatibility.[43, 44, 47, 213] The versatility and control over hydrogel properties make them ideal for a range of scaffold geometries such as bulk slabs, microspheres, foams, and 3D-printed constructs.[85, 214, 215] Many hydrogels exhibit tunable properties that can be modulated chemically, physically, and biologically making them ideal for tissue engineering.[45-47, 148, 216-218] Degradable hydrogels have been increasingly investigated for their use in a variety of applications ranging from drug delivery to cell matrices. Control over degradation properties is important to promote functional tissue growth, controlled drug release, and controlled cell behavior.[50, 219] Slow degrading systems have been shown to limit cellular migration, tissue ingrowth, and remodeling.[62-64] Additionally, non-degradable, woven gauzes used in wound treatment are prone to linting fibers and adhering to wound tissue during removal.[65] The development of hydrolytically degradable wound dressings serve to improve tissue ingrowth and reduce inflammatory responses due to residual dressing debris.

Acrylated and methacrylated poly(ethylene glycol) (PEG) hydrogels have been shown to degrade slowly *in vivo* demonstrating a need for hydrogel scaffolds with clinically relevant degradation times.[65, 216, 220] Enzymatically labile peptide sequences in

polymers have been investigated to increase degradation profiles; however, they rely solely on cell mediated degradation.[50, 221-223] Additionally, increasing hydrolytic degradation has investigated through the use of poly(β-amino ester)s (PBAEs). A library of linear macromers was synthesized and resulting degradation and mechanical behavior was analyzed.[66] Studies have shown the ability to tune properties of the PBAEs such as degradation rate and modulus through varying concentrations of PEGDA.[68] This use of PBAEs to develop a tunable degradation system has been widely characterized for its tunable mechanical properties; however, with increasing degradation rate there was a significant effect on gel fraction; thus effecting resulting hydrogel properties such as swelling ratio, compressive modulus, and tensile modulus.[68-70] Another method to increase hydrolytic degradation of PEG hydrogels is the use of thiol-acrylate chemistries. These step-growth polymerizations can be tuned using stoichiometric monomer ratios to get desired endgroup functionality.[62, 71] The reaction occurs when PEG-diacrylate (PEGDA) chains react with a dithiol in a Michael-type addition reaction to form water soluble PEGDTT polymer chains.[72, 73] The increased hydrolytic lability of dithiothreitol (DTT) bridges is due to the presence of a thioether bond proximal to the ester bonds present in PEGDA.[64, 72] The presence of this thioether creates a more positive atomic charge on the carbonyl carbon of the ester, enhancing the reactivity of nucleophilic attack which is the first step of a base-catalyzed ester hydrolysis.[64] This reaction of DTT with PEGDA allows for degradation to occur within clinically relevant time scales.[73] Bulk properties of the hydrogel as well as degradation rate can be tuned through variations in molecular weight of the PEGDA and the DTT concentration.[62, 74, 75] Although the addition of DTT

concentration increases degradation rate, these systems lack the control over matrix swelling and modulus which has been shown to play a role in cell-material interactions.[224-227] Another method of that has been investigated to control degradation includes the modulation of ratios of PEGDTT:PEGDA.[67] This biodegradable system has been investigated for the use of protein release, 3D stem cell culture arrays, and to examine ECM cell adhesion on ligand type and concentration.[73, 76, 77] Although extensive *in vitro* analysis on mechanical properties and cell compatibility has been completed to characterize these hydrogels the *in vivo* degradation and host response has yet to be investigated to demonstrate clinically relevant degradation and cytocompatibility.

In this study, the *in vivo* degradation profile of PEGDTT hydrogels were investigated to understand the correlation between *in vivo* and *in vitro* degradation profiles. PEGDA and PEGDTT of similar molecular weights were synthesized and swelling ratio was analyzed to demonstrate initial hydrogel properties. Different ratios of PEGDTT:PEGDA were investigated to determine degradation profile over 4 weeks. First, *in vitro* degradation profiles in PBS were characterized at 37°C, measuring changes in swelling ratio over time until complete dissolution. Samples were also implanted subcutaneously using a standard rat model for up to 4 weeks. Swelling ratio and sample recovery were used as an indicator of the *in vivo* degradation over time. Additionally, cell attachment of bioactive compositions and cell viability of the degradation products was evaluated to determine cytocompatibility and cell-material interactions. Collectively, this work provides an evaluation of the *in vivo* degradation profile and cellular response to a

biodegradable PEG-based hydrogel system to support neotissue formation and reduce inflammatory response due to residual wound dressing particulate.

3.2. Materials and Methods

3.2.1. Materials

All chemicals were purchased from Sigma Aldrich (Milwaukee, WI) and used as received unless otherwise noted.

3.2.2. Synthesis of Poly(ethylene glycol) diacrylate (PEGDA)

PEGDA was synthesized according to a method adapted from Hahn, et al.[56] Briefly, acryloyl chloride was added dropwise to a solution of PEG 2 kDa, 3.4 kDa, 6 kDa, or 10 kDa diol and triethylamine (TEA) in dichloromethane (DCM) under nitrogen. The molar ratio of PEG, acryloyl chloride, and triethylamine was 1:2:4, respectively. After the addition of acryloyl chloride, the reaction was stirred for an additional 24 hours at room temperature. The resulting solution was then washed with 8 molar equivalents of 2 M potassium bicarbonate to remove acidic byproducts. The product was then precipitated in cold diethyl ether, filtered, and dried under vacuum.

3.2.3. Synthesis of Poly(ethylene glycol) diacrylate with thio-β esters (PEGDTT)

PEGDTT was synthesized by adding d,l-dithiolthreitol (DTT) and TEA dropwise to a solution of PEGDA (2 kDa or 3.4 kDa) in DCM, **Figure 3.1**. PEGDTT-L and PEGDTT-H were synthesized from PEGDA 2kDa or 3.4 kDa, respectively to develop low and high molecular weight macromers. The molar ratio of PEGDA, DTT and triethylamine was 3:2:0.9, respectively. After the addition of the DTT and triethylamine, the reaction was stirred for 24 hours at room temperature. The resulting solution was then

precipitated in cold diethyl ether, washed, filtered, dried under ambient conditions for 24 hours then placed under vacuum to remove any excess solvent.

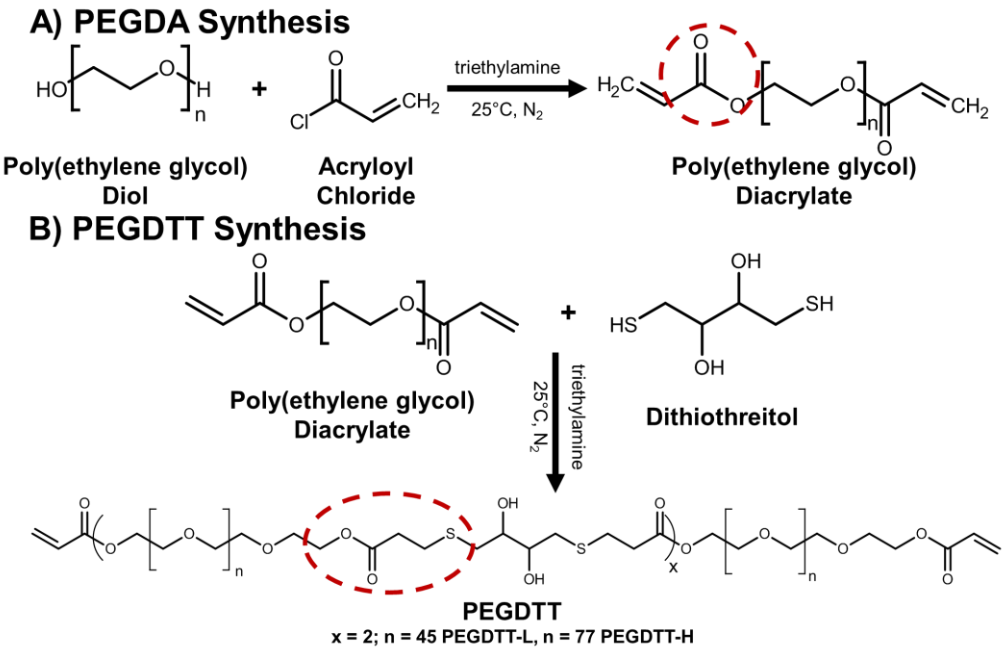

Figure 3.1. (A) Synthesis of poly(ethylene glycol) diacrylate with ester linkages indicated. (B) Synthesis of PEGDTT with thio-β esters indicated.

Characterization of PEGDA and PEGDTT was confirmed using proton nuclear magnetic resonance (^{1}H-NMR) spectroscopy and gel permeation chromatography (GPC). Proton NMR spectra of control and functionalized polymers were recorded on a Mercury 300 MHz spectrometer using a TMS/solvent signal as an internal reference. Percent conversions of PEG diol to acrylate end groups was greater than 85%. Percent acrylation of both macromers were confirmed as greater than 90% by NMR. **PEGDA**: ^{1}H-NMR

($CDCl_3$): 3.6 ppm (m, -OCH_2CH_2-), 4.3 ppm (t, -CH_2OCO-) 6.1 ppm (dd, -CH=CH_2), 5.8 and 6.4 ppm (dd, -CH=CH_2). **PEGDTT**: ^{1}H NMR (CDCl3): δ 2.6 ppm (t, -CH_2CH_2S-), 2.7 ppm (dd, -SCH_2COH-), 2.8 ppm (t, -OCOCH_2-), 3.0 ppm (two overlapping s, -CHOH), 3.6 ppm (m, -OCH_2CH_2), 4.2 and 4.3 ppm (t, -CH_2OCO-), 6.1 ppm (dd, -CH=CH_2), 5.8 and 6.4 ppm (dd, -CH=CH_2).

Molecular weights of the PEGDA and PEGDTT macromers were also determined with an Agilent Technologies 1260 Infinity II GPC system. Approximately 5 mg specimens were dissolved in 0.1 M lithium bromide in dimethylformamide at a concentration of 5 mg/mL at room temperature and syringe filtered. Samples were prepared just prior to injection into the GPC system to limit degradation of PEGDTT samples. Injections of 100 μL of DMF were passed through 2 Phenogel columns with molecular weight ranges of 1k – 75k Da at a flow rate of 1.0 mL/min and temperature of 25ºC. The separated components were passed through an Agilent Multi Detector system at 30 ºC, and the molecular weight distribution was determined using the Agilent GPC/SEC software using RI detection. Molecular weight averages were reported relative to polyethylene glycol standards. Averages were obtained for each polymer by dissolving 3 separate specimens and running the specimens in duplicate.

3.2.4. Hydrogel Swelling Ratio

Hydrogels of varying composition were fabricated by making (10 wt%) precursor solutions in RO water to demonstrate a tunable degradation rate. A photoinitiator solution (1 mg Irgacure 2959 per 0.01 ml 70% ethanol) was added at 1 vol% of precursor solution. Solutions were pipetted between 1.5 mm spaced plates and crosslinked by 6 min exposure

to long wave UV light (Intelli Ray Shuttered UV Flood Light, Integrated Dispensing Solutions, Inc., 365 nm, 4 mW/cm^2). The compositions varied the concentration of PEGDTT and PEGDA (100:0, 85:15, 75:25, and 0:100 wt%) while keeping the total polymer fraction constant at 10 wt%. To measure swelling ratio, six 10-mm discs were punched from hydrogel sheets. Samples were swollen in PBS for 3 hours to reach equilibrium swelling ratio and weighed to determine the equilibrium swelling mass (W_s). Then specimens were dried under vacuum overnight to determine dry mass (W_d). The swelling ratio (Q) was calculated from the equilibrium mass swelling ratio:

$$Q = \frac{W_s}{W_d} \qquad [1]$$

3.2.5. Gel Fraction

Gel fraction of hydrogel compositions was also evaluated to determine extent of network formation of starting macromers and mixed compositions. To measure gel fraction, six 10-mm dics were punched from hydrogel sheets after crosslinking and dried under vacuum over night to determine dry mass (W_d). The samples were then soaked in 2 ml of DCM for 24 hours to remove uncrosslinked polymer and dried under vacuum overnight. Then specimens were weighed to determine the redried mass (W_{rd}). The gel fraction (GF) percentage was then calculated:

$$GF = \frac{W_{rd}}{W_d} \times 100 \qquad [2]$$

3.2.6. Compressive Modulus

For modulus measurements, 6 specimens (D = 10 mm, T = 1.5 mm) were punched from crosslinked sheets and swelled in PBS for 3 hours to reach equilibrium swelling. Specimens were subjected to mechanical testing using a dynamic mechanical analyzer

(RSAIII, TA Instruments) equipped with a parallel-plate compression clamp. Testing was performed under unconstrained compression at room temperature. The linear viscoelastic range was determined for each composition using dynamic strain sweeps. Then a strain within the upper end of the linear viscoelastic range was used on a constant strain frequency sweep between 0.79 and 79 Hz. The compressive storage modulus was taken at 1.25 Hz.

3.2.7. In Vitro *Degradation*

The 10 mm hydrogel discs were also evaluated to determine hydrolytic degradation by incubation in 7.4 pH PBS supplemented with 1% Penicillin Streptomycin at 37°C for 28 days with biweekly solution changes. The swollen masses were recorded at discrete time points for 28 days or until complete dissolution. The swelling ratio (Q) was then calculated and used to characterize the network degradation.

3.2.8. Human Dermal Fibroblast (hDF) Activity

All studies were performed with human dermal fibroblasts (hDFs, Gibco) cultured in Dulbecco's Modified Eagle Medium (DMEM; Gibco) supplemented with 10% fetal bovine serum (FBS) and 1% Penicillin Streptomycin. All cells were harvested for use at passage P2-P4 and seeded at 10,000 cells per well.

3.2.9. hDF Viability of Degradation Products

10 wt% hydrogels of PEGDTT-L and PEGDTT-H and were fabricated and dried to obtain 10 mg/ml concentration of polymer in supplemented DMEM. Polymer solutions were then incubated at 37°C for 1 week until complete dissolution. Solutions were then serially diluted to 1 and 0.1 mg/ml in supplemented DMEM. hDFs were seeded in 48 well

plates and grown for 3 days to reach a confluent monolayer. hDFs were then exposed to the degradation products for 24 and 72 hours and viability was analyzed utilizing a LIVE/DEAD assay kit (Molecular Probes). Cells were washed with PBS, stained with 2 µM calcein-AM (live) and 2 µM ethidium homodimer-1 (dead) for 30 minutes at 37°C, and washed with PBS for imaging. Imaging (5 images per specimen) was conducted on four specimens with a fluorescence microscope (Nikon Eclipse TE2000-S).

3.2.10. hDF Proliferation

A Quant-iT™ PicoGreen® dsDNA Assay Kit (Molecular Probes) was utilized to quantify cell proliferation and density after exposure to degradation products for 24 and 72 hours. At selected time points, hDFs were thermally lysed and the assay was performed according to manufacturer instructions. Fluorescence intensity was assessed using a plate reader (Tecan Infinite M200Pro) with excitation/emission wavelengths of 480/520 nm, respectively. Average cell number was determined by converting dsDNA values to individual cell number using 6.9 pg DNA/cell (n = 4 per composition).

3.2.11. hDF Adhesion and Spreading

Bioactivity was conferred to the hydrogels by adding 4 mg/ml of 0.1X functionalized collagen to hydrogel precursor solutions as previously reported by Browning et al.[205] Briefly, collagen type I was functionalized with an acrylate-PEG-NHS linker (JenKem) to incorporate photoreactive crosslinking sites at a molar ratio of 0.1:1 (Acr-PEG-NHS:NH_2). Cylindrical slabs (D = 10 mm) were punched from PEGDTT-L and PEGDTT-H hydrogel compositions and placed into a 48 well plate. Cells were seeded and attached for 3 hours, then washed twice with warm phosphate buffered saline (PBS;

Gibco). hMSCs were washed with PBS, fixed in 3.7% glutaraldehyde, stained for F-actin and nuclei with ActinGreen 488 and NucBlue ReadyProbes Reagents (Molecular Probes), and imaged via fluorescence microscopy (Nikon Eclipse TE2000-S). Cell adhesion was quantified using ImageJ software (n = 4).

3.2.12. In Vivo *Analysis*

All procedures were approved by the Texas A&M University Institutional Animal Care and Use Committee. Hydrogel specimens (D = 10 mm, T = 1.5 mm) were obtained from the same slabs used in the *in vitro* degradation studies to ensure consistency between studies and sterilized via sterile filtration, electron beam, or ethylene oxide sterilization for sterilization studies. The chosen formulations were determined via scouting studies with gels fabricated from a range of compositions of PEGDTT:PEGDA to ensure that compositions would degrade within the time points of the study and sterilized via ethylene oxide sterilization. Three month old female Sprague Dawley rats were anesthetized with 3% isoflurane, their backs were shaved, and incision sites were scrubbed with povidone-iodine and isopropyl alcohol. Two 15 mm incisions were made on the dorsal side of the rats and blunt dissection was used to prepare implant pockets (2 per side). Specimens were introduced through the incision and positioned within the pocket away from the incision site. The incisions were then closed with stainless steel surgical staples and were removed 7 days post-implantation. After 2, 3, 7, 14, and 28 days, rats were euthanized via carbon dioxide inhalation with subsequent bilateral thoracotomy performed as a secondary form of euthanasia. The hydrogel specimens were carefully removed from the rats and placed

in PBS for 3 hours prior to analysis. Swelling ratio was then measured as described above to measure the extent of degradation.

3.2.13. Statistical Analysis

All statistical analyses were expressed as the mean ± standard derivation of the mean unless stated otherwise. Statistical analysis was performed by a paired two-tailed student's t-test. Statistical analysis for comparison between multiple groups was conducted with one-way analysis of variance (ANOVA) with Tukey's post-hoc analysis. Statistical significance was accepted at $p < 0.05$.

3.3. Results and Discussion

3.3.1. Hydrogel Characterization

Macromer synthesis of PEGDA and PEGDTT was confirmed using ^{1}H-NMR, **Figure 3.2**. End-group analysis yielded an average number average molecular weight (M_n) of ~6.4 kDa and ~11.1 kDa for PEGDTT-L and PEGDTT-H, respectively. GPC was used to further characterize the molecular weight and polydispersity of the resulting macromers, **Figure 3.3**. Although average M_n was similar between PEGDTT-L and PEGDA 6K macromers (5220 vs 5590 Da) and PEGDTT-H and PEGDA 10K macromers (8160 vs 9090 Da), there was a large increase in molecular weight distribution with the synthesized PEGDTT macromers. This analysis demonstrated the synthesis of the PEGDTT macromers resulted in a heterogeneous population of macromers with molecular weight distributions between 1.9-64 kDa and 3.2-57.5 kDa for PEGDTT-L and PEGDTT-H, respectively. The observed peak average molecular weight (M_p) values for PEGDTT-L start at 2 kDa PEGDA blocks and build sequentially to 4, 6, and 10 kDa molecular weights.

A similar trend was also observed in PEGDTT-H with molecular weight values starting at 3 kDa PEGDA blocks building to molecular weights of 6, 9, and 12 kDa. Maximum M_p observed were 64 and 57.5 kDa for PEGDTT-L and PEGDTT-H, respectively. These results indicate that there was a portion of the PEGDA macromer that remains unreacted, a portion that forms the desired triblock, and a portion that undergoes subsequent coupling to form higher molecular weight species. Future work will investigate improved control of stoichiometric ratios and reaction times to yield a more homogeneous molecular weight macromer. It is hypothesized that the observed variation in molecular weight distribution will have an effect on resulting hydrogel mesh size thus affecting material properties.[228] Namely, that the variable chain length will increase the heterogeneity of the network structure with localized regions of higher and lower crosslink density. A similar result was previously achieved through the addition of a 4-arm PEGDA.[217]

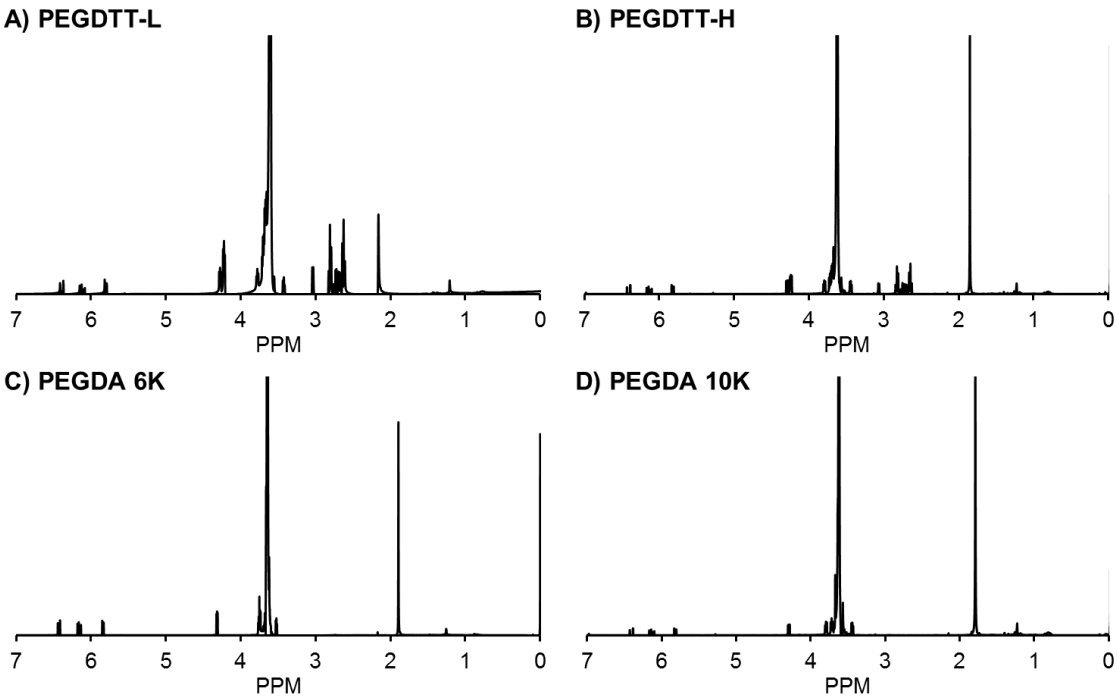

Figure 3.2. Proton NMR spectra of (A) PEGDTT-L, (B) PEGDTT-H, (C) PEGDA 6K, and (D) PEGDA 10K in $CdCl_3$.

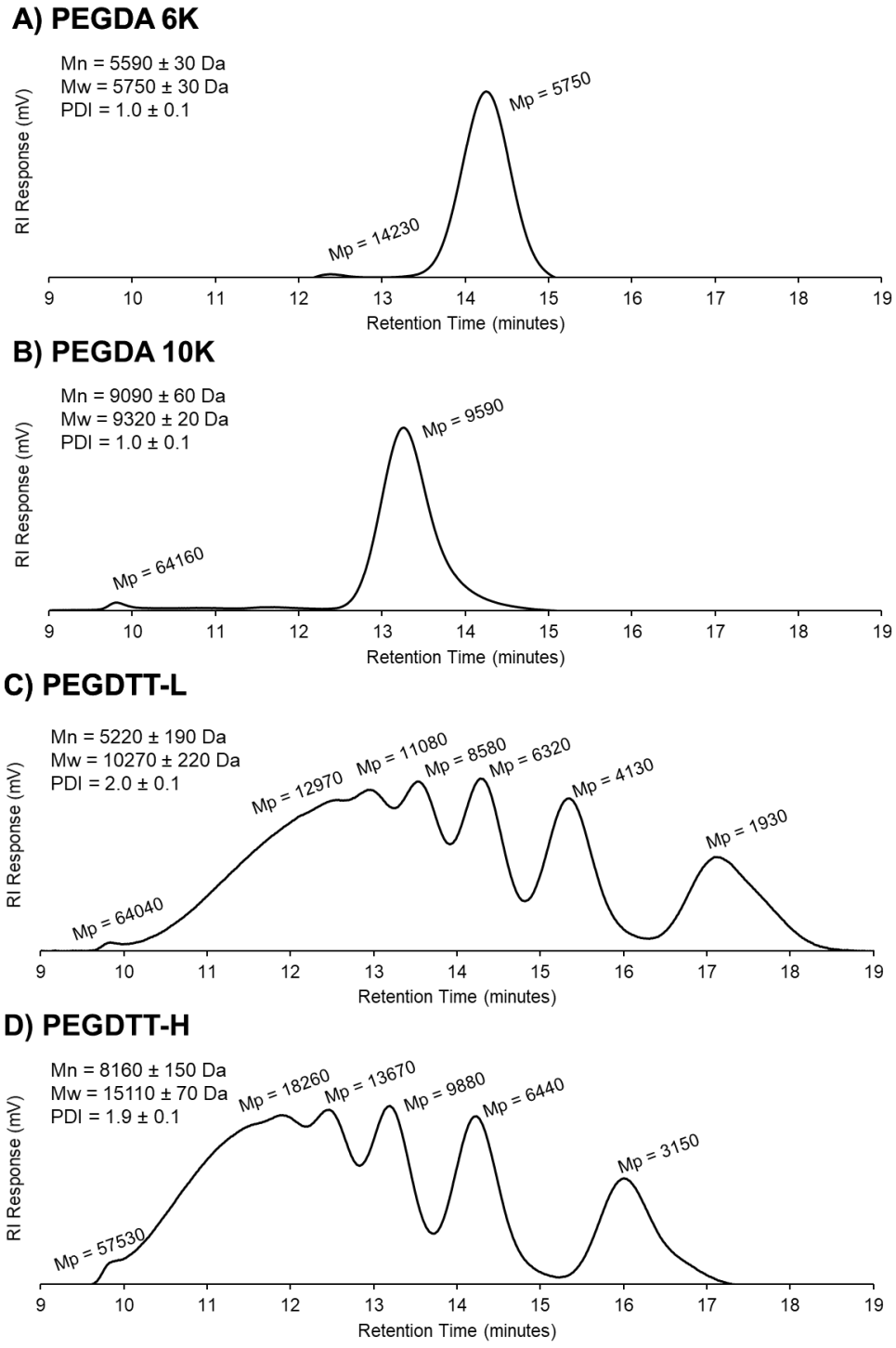

Figure 3.3. GPC chromatagrams of PEGDA 6K (A), PEGDA 10K (B), PEGDTT-L (C), and PEGDTT-H (D). Average M_n, M_w, and PDI of each composition (n = 3) are indicated on the representative chromatograms.

Initial gel fraction and swelling ratio of degradable macromers were measured to characterize the properties of each macromer, **Figure 3.4**. Comparable gel fraction was observed for all compositions containing PEGDTT-L (~93%), with the PEGDA 6K control having a 97% gel fraction. Similarly, comparable gel fraction was observed in the PEGDTT-H compositions and the PEGDA 10K (>94%). These high gel fractions demonstrate good network formation in the original macromers and with their resulting compositions. Following a similar trend, observed swelling ratios for the PEGDTT-L compositions were statistically similar between 16.6-17.1, and the PEGDA 6K swelling ratio was 15.0. Additionally, PEGDTT-H and PEGDA 10K compositions exhibited swelling ratios between 17.7-18.8. Here, we demonstrate the capability of creating PEGDTT-based degradable macromers with comparable swelling ratio independent of the number of incorporated thio-β esters. Although all PEGDTT-H compositions exhibited similar properties to that of the non-degradable PEGDA 10K control, it was observed that the PEGDTT-L compositions had slightly different properties to that of the non-degradable PEGDA 6K control. We hypothesize that slightly different changes in initial starting properties can be attributed to initial macromer acrylation and the distribution of molecular weight as demonstrated by PDI, **Table 3.1**. Table 1 summarizes the hydrogel physical properties for all initial starting compositions.

Tables 3.2 and 3.3 summarize the complete property evaluation of all compositions of PEGDTT-L and PEGDTT-H (0/100, 60/40, 75/25, 85/15, and 100/0 PEGDTT/PEGDA), respectively. Compressive moduli for compositions containing PEGDTT-L were statistically similar and ranged from 232-255 kPa; whereas, the PEGDA

6K control displayed an average compressive modulus of 355 kPa. Similarly, compositions containing PEGDTT-H and its non-degradable PEGDA 10K control exhibited statistically similar compressive moduli ranging from 158 to 195 kPa. In addition to maintaining hydrogel swelling ratio, these results demonstrate that the number of degradable linkages can be modulated while maintaining a relatively constant initial matrix modulus. In contrast, other systems that have utilized the introduction of β-thioesters to increase rates of hydrolysis have demonstrated reduction in compressive modulus and increases in swelling ratio with increased concentration of the labile group.[62, 64]

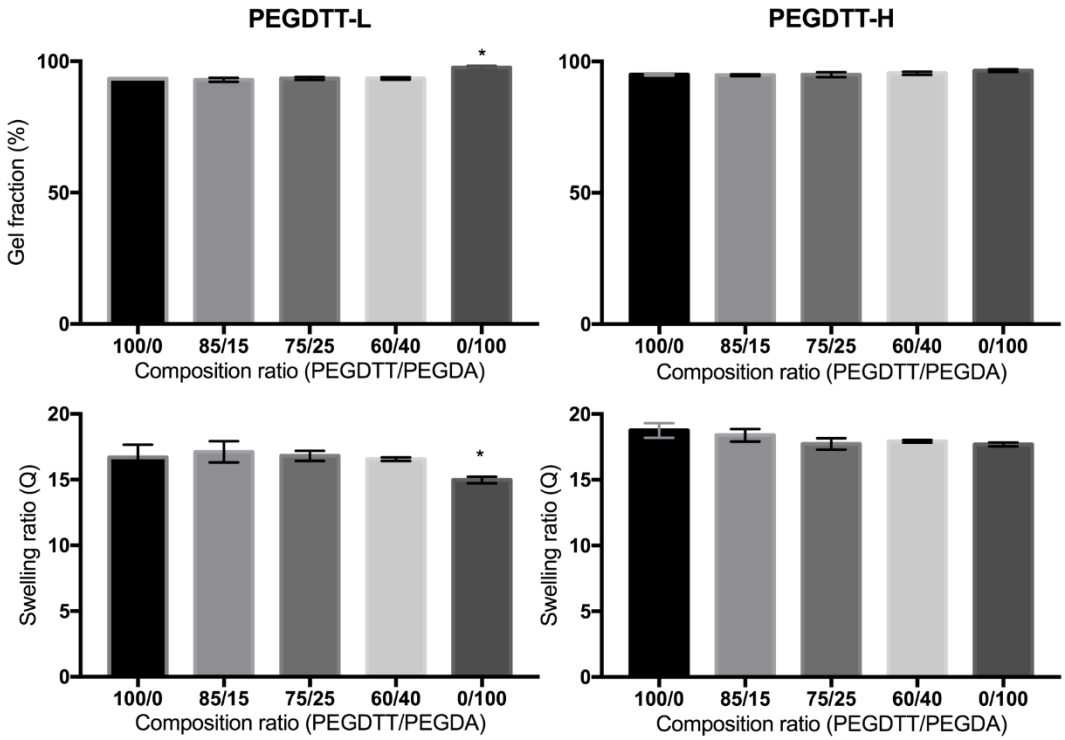

Figure 3.4. Swelling ratio and gel fraction of PEGDTT-L (A) and PEGDTT-H (B) of varying PEGDTT/PEGDA compositional ratios (100/0, 85/15, 75/25, 60/40, 0/100). * denotes statistical significance with $p \leq 0.05$.

Table 3.1. Summary of hydrogel physical properties: swelling ratio, gel fraction, compressive modulus, and molecular weight analysis.

	Swelling Ratio (Q)	**Gel Fraction (%)**	**Compressive Modulus (kPa)**	**M_n (Da)**	**PDI**
PEGDA 6K	15.0 ± 0.3*	97.6 ± 1.5	355.3 ± 46.5	5590 ± 30	1.0 ± 0.1
PEGDTT-L	16.7 ± 1.0	93.4 ± 0.0	233.2 ± 20.2	5220 ± 190	2.0 ± 0.1
PEGDA 10K	17.7 ± 0.4	96.6 ± 1.0	240.2 ± 24.8	9090 ± 60	1.0 ± 0.1
PEGDTT-H	18.8 ± 1.4	95.1 ± 0.8	197.4 ± 23.1	8160 ± 150	1.9 ± 0.1

Table 3.2. Summary of hydrogel physical properties of PEGDTT-L with varying concentrations of PEGDA 6K (PEGDTT/PEGDA: 100/0, 85/15, 75/25, 60/40, 0/100).

PEGDTT/PEGDA	Swelling Ratio (Q)	Gel Fraction (%)	Compressive Modulus (kPa)
0/100	15.0 ± 0.3*	97.6 ± 1.5*	355.3 ± 46.5*
60/40	16.6 ± 0.1	93.5 ± 0.9	255.4 ± 30.6
75/25	16.8 ± 0.4	93.5 ± 1.0	243.1 ± 42.3
85/15	17.1 ± 0.8	93.0 ± 1.5	232.7 ± 15.8
100/0	16.7 ± 1.0	93.4 ± 0.0	233.2 ± 20.2

Table 3.3. Summary of hydrogel physical properties of PEGDTT-H with varying concentrations of PEGDA 10K (PEGDTT/PEGDA: 100/0, 85/15, 75/25, 60/40, 0/100).

PEGDTT/PEGDA	Swelling Ratio (Q)	Gel Fraction (%)	Compressive Modulus (kPa)
0/100	17.7 ± 0.4	96.6 ± 1.0	195.6 ± 44.4
60/40	17.9 ± 0.2	95.6 ± 1.2	185.2 ± 34.5
75/25	17.7 ± 1.0	95.0 ± 1.9	175.9 ± 28.0
85/15	18.4 ± 1.2	94.8 ± 0.7	158.0 ± 7.0
100/0	18.8 ± 1.4	95.1 ± 0.8	184.2 ± 23.1

3.3.2. In Vitro *Degradation*

Swelling ratio was utilized to assess extent of hydrogel degradation due to cleaved network groups resulting in reduced crosslink density.[216] *In vitro* degradation of PEGDTT hydrogels was investigated in PBS at physiological temperatures to mimic physiologic conditions, **Figure 3.5**. The ratio of PEGDTT:PEGDA was varied to achieve a range of degradation rates. As expected, control PEGDA hydrogels of both molecular weights did

not exhibit any significant degradation over the 28-day period. 100% PEGDTT compositions demonstrated a loss of mechanical integrity by day 14 for PEGDTT-L and day 17 for PEGDTT-H. Compositions containing 75% or less PEGDTT demonstrated increased swelling ratio but did not undergo complete dissolution over the 28-day time frame. 100 and 85/15 compositions of PEGDTT-H exhibited slower degradation profiles with complete dissolution occurring at 14 and 21 days, as compared to 17 and 28 days for PEGDTT-L. As expected, a concentration dependent effect was observed with compositions with increasing amounts of PEGDTT experiencing more rapid degradation than control PEGDA hydrogels, as demonstrated previously.[67] Here, we demonstrate the modulation of PEGDTT:PEGDA ratio results in a tunable degradation system that exhibits complete degradation between 14 and >28 days with minimal effect on initial matrix modulus.

Macromer molecular weight had an unexpected effect on degradation rate with the PEGDTT-H of lower crosslink density displaying a similar degradation rate to that of the PEGDTT-L. Previously, Metters et al. demonstrated poly(ethylene glycol)-based hydrogel swelling ratio and degradation predictions utilizing experimental measurements and theoretical models with increased with molecular weights. Additionally, they demonstrate that structural imperfections can lower crosslink density and network architecture can result in different hydrolysis kinetics.[229] Browning et al. has also demonstrated increases in accelerated hydrolytic degradation of 10 kDA PEGDA hydrogel compared to 3.4 kDa hydrogels due to changes in crosslink density.[230] We hypothesize the differences in degradation profiles can be supported by the broad distributions of molecular weight

affecting crosslink density and the number of thio-β esters incorporated. Although PEGDTT-H had higher initial swelling ratio, it is hypothesized that the increased number of thio-β ester linkages (1.5X) in PEGDTT-L compared to PEGDTT-H resulted in more rapid hydrolytic degradation. For the PEGDTT-H hydrogels, the total number of thio-β ester bonds within the crosslinked network was relatively lower compared to the PEGDTT-L. The number of incorporated thio-β ester linkages could be primarily dictating degradation rate over crosslink density attributed to initial swelling ratio.

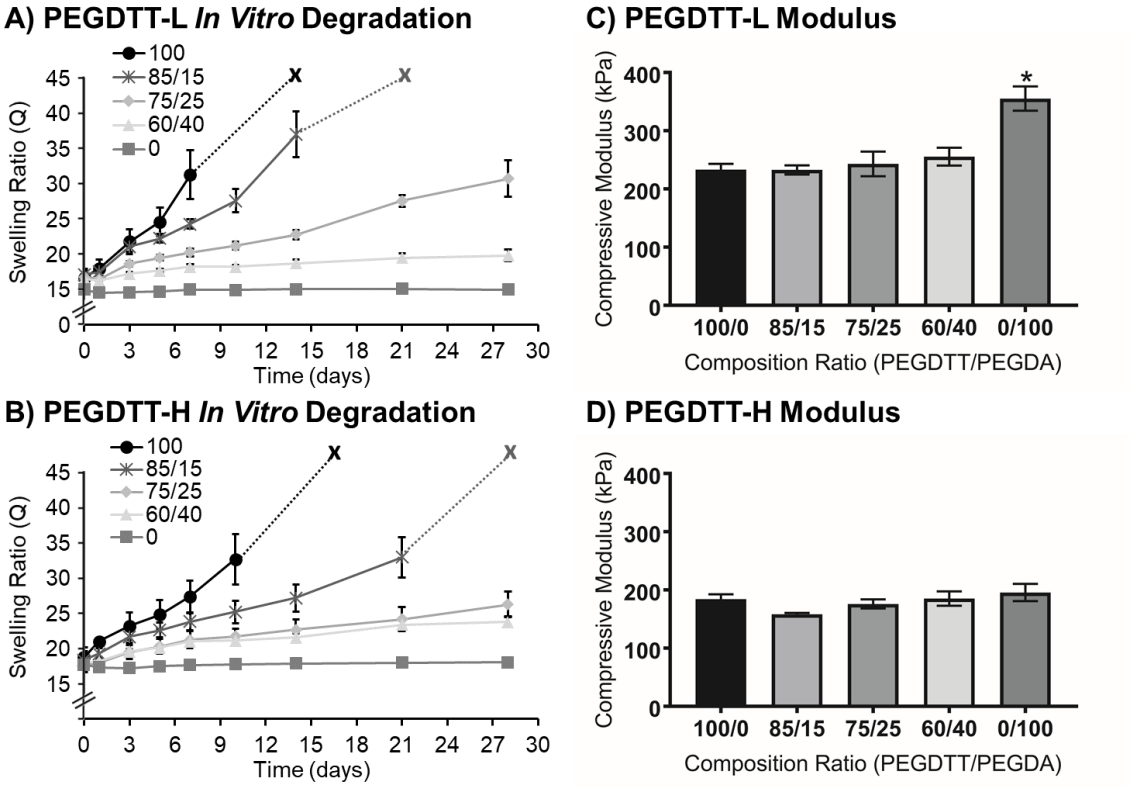

Figure 3.5. *In vitro* hydrolytic degradation profile as monitored by changes in swelling ratio of PEGDTT-L (A) and PEGDTT-H (B) with varying PEGDTT/PEGDA compositional ratios (100/0, 85/15, 75/25, 60/40, 0/100) over 28 days at 37°C. ^{X}Denotes complete dissolution, (- - -) dotted lines denote loss of mechanical integrity. Corresponding compressive moduli of PEGDTT-L (C) and PEGDTT-H (D) of varying PEGDTT/PEGDA compositional ratios. *denotes statistical significance with $p \leq 0.05$.

3.3.3. Cellular Interactions

In vitro cellular viability of hydrogel degradation products was investigated to ensure no cytotoxic effects would be observed as a result of hydrogel degradation, **Figure 3.6**. As PEGDTT has been used previously as a vehicle for stem cell encapsulation and delivery, no negative effects on cytocompatibility were expected.[72, 75, 77] Li et al. previously demonstrated a cytotoxicity study testing concentrations between 0.01 and 10

mg/ml in a macromer dilution assay to test cell viability for biodegradable hydrogel compositions.[231] Based on this reported data, human dermal fibroblast (hDf) viability was determined after 24 and 72 hours of exposure to increasing concentrations of PEGDTT-L and PEGDTT-H degradation products. Negative effects were not observed as all tested concentrations for both PEGDTT macromers exhibited viability greater than 90% after 24 and 72 hours. Furthermore, cell density quantification confirmed that cells retained their ability to proliferate and maintain high cell densities following exposure to degradation products demonstrating no significant difference in cell behavior to degradation byproducts.

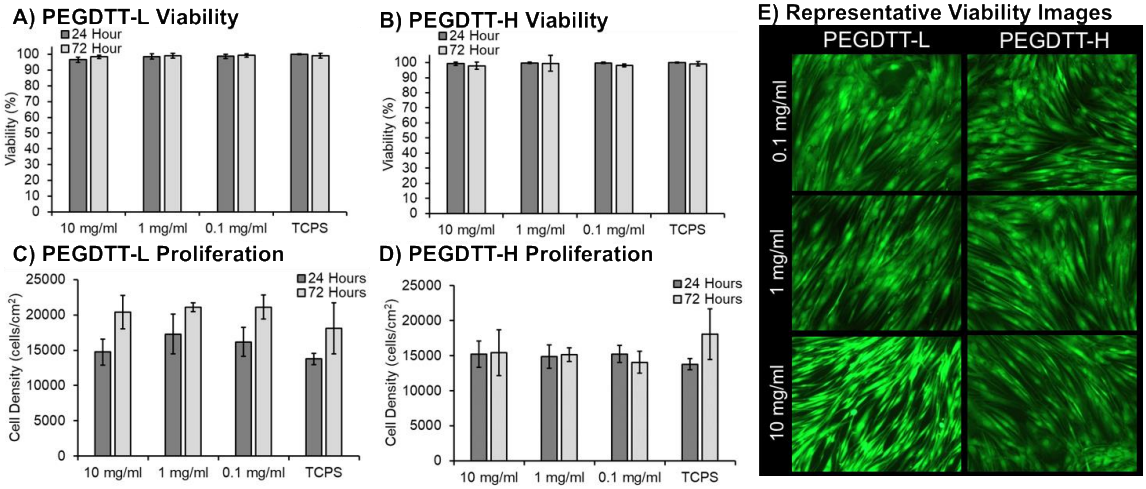

Figure 3.6. *In vitro* cellular viability of human dermal fibroblasts seeded onto tissue culture polystyrene (TCPS) after 24 and 72 hour exposure to the degradation products of PEGDTT-L (A) and PEGDTT-H (B) at 0.1, 1, and 10 mg/ml. *In vitro* cellular density of human dermal fibroblasts seeded onto tissue culture polystyrene (TCPS) after 24 and 72 hour exposure to the degradation products of PEGDTT-L (C) and PEGDTT-H (D) at 0.1, 1, and 10 mg/ml. (E) Representative images of live cells stained with Calcein AM.

To demonstrate the utility of PEGDTT hydrogels in regenerative medicine, bioactivity was conferred to the biodegradable hydrogels by incorporating acrylate-functionalized collagen (4 mg/ml). Incorporation of functionalized collagen has been utilized to improve cell attachment and activity on hydrogel scaffolds.[205] Here, we demonstrate that both PEGDTT-Coll scaffolds support high cell attachment and spreading compared to a PEGDA 6K-Coll control, **Figure 3.7**. Cell morphology and adhesion density was found to be statistically similar ($p > 0.05$) for all bioactive hydrogels and the tissue culture polystyrene (TCPS) control. PEG-based hydrogels are generally considered bioinert and incorporation of bioactive cues into these synthetic hydrogel scaffolds makes them ideal for controlled cellular interactions. Acrylation of RGD, collagen, and peptide sequences has been utilized to incorporate bioactivity into hydrogel scaffolds through various chemistries to target specific cellular interactions.[131-133] In addition to biological cues, mechanical signals such as substrate stiffness has been shown to influence cell adhesion, migration, and differentiation.[224, 225, 232, 233] This work demonstrates a biocompatible system that can incorporate targeted bioactivity independent of matrix modulus to guide cellular interactions.

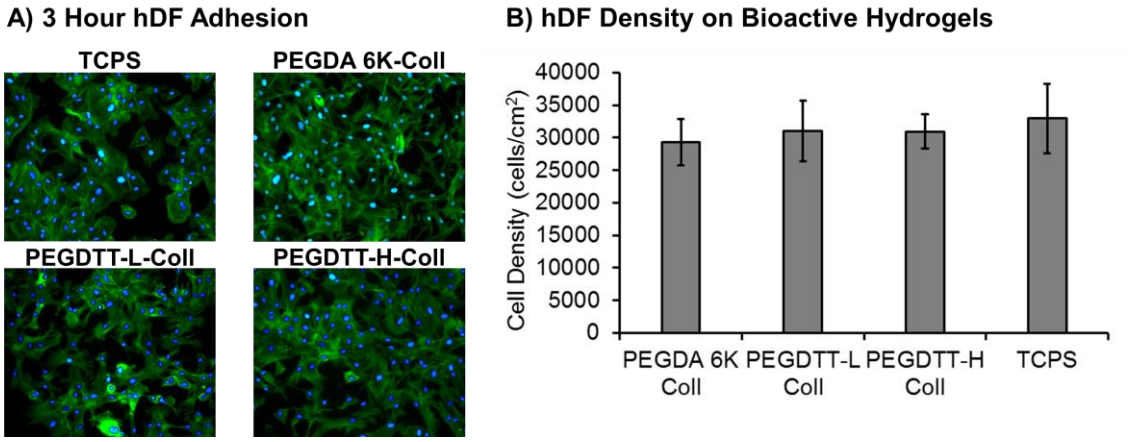

Figure 3.7. Representative *in vitro* 3 hour cellular attachment of human dermal fibroblasts seeded onto PGEDA and PEGDTT-collagen hydrogels (4 mg/ml) and tissue culture polystyrene (TCPS) Representative images of cells stained with NucBlue (nucleus) and ActinGreen (cytoplasm). (B). *In vitro* cellular density of human dermal fibroblasts quantified by nuclear staining per well area.

3.3.4. In Vivo *Degradation*

Prior to implantation, the effect of sterilization method on hydrogel swelling ratio and degradation ratio was investigated, **Figure 3.8**. There were no statistical differences ($p < 0.05$) in swelling ratio or degradation profiles for any of the sterilization techniques tested. Subcutaneous rat models were utilized to assess degradation of PEGDTT compositions relative to a PEGDA control, **Figure 3.9**. All compositions containing PEGDTT exhibited significant increases in degradation in the *in vivo* model compared to PEGDA controls. 100% PEGDTT compositions exhibited complete dissolution after 2 days and no residual sample could be collected. 85/15 and 75/25 PEGDTT-L compositions exhibited loss of mechanical integrity after three and 14 days, respectively for PEGDTT-L. Slower degradation profiles were observed for PEGDTT-H with 85/25 compositions losing mechanical integrity after seven days. Although loss of mechanical integrity for the

75/25 PEGDTT-H composition, the swelling ratio was approaching the limit for loss of mechanical integrity and likely would have reached complete dissolution shortly after 14 days. The *in vivo* trends correlated with the results observed *in vitro* with varying concentrations of PEGDTT/PEGDA. However, significantly faster rates of hydrolysis were observed *in vivo* compared to *in vitro* profiles. The increased rate of degradation *in vivo* has been seen in other systems and attributed to decreases in local pH due to acidic degradation products or contribution of inflammatory cells.[234]

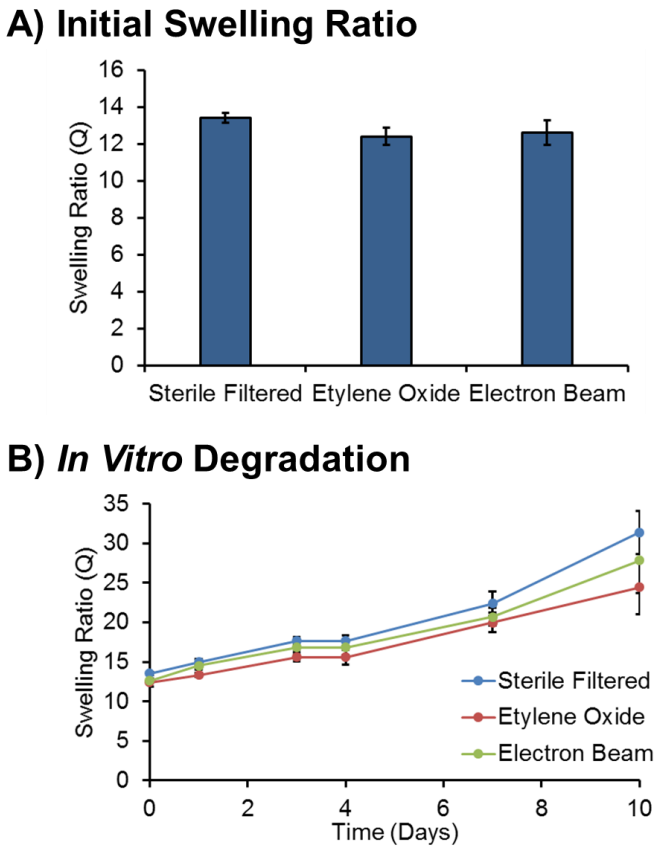

Figure 3.8. A) Effect of sterilization method on swelling ratio for degradable PEGDTT-L hydrogels. B) Effect of sterilization method on PEGDTT-L hydrogel degradation profile.

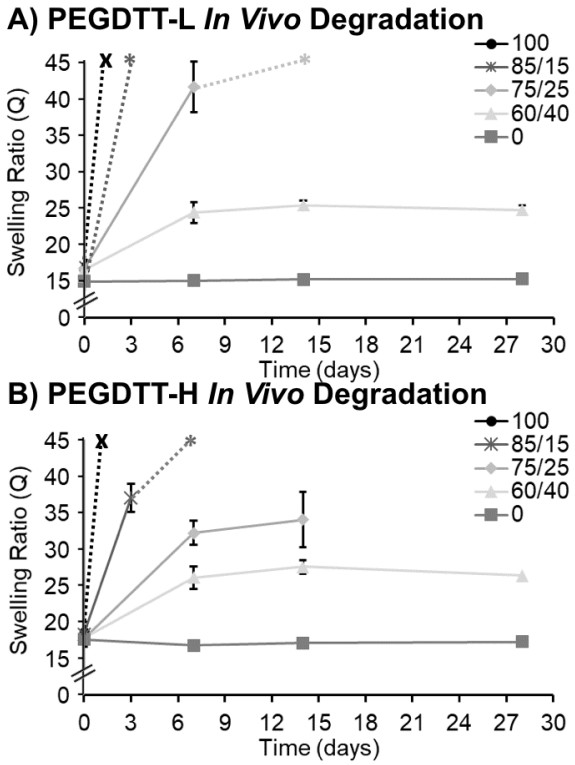

Figure 3.9. *In vivo* degradation monitored through swelling ratio of PEGDTT-L and PEGDTT-H of varying concentrations 85/15 (A), 75/25 (B), 60/40 (C), and 0 (D) fabricated with a similar molecular weight PEGDA was investigated before and after subcutatenous implantation in a rat model. [X]Denotes complete dissolution, [X]Denotes complete dissolution, (- - -) Dotted lines denote loss of mechanical integrity.

3.4. Conclusions

This study characterized the degradation profile of a hydrolytically degradable hydrogel, PEGDTT, to support its broad utility in biomedical applications. Degradation was tuned through the modulation of thio-β esters in the hydrogel composition. Initial hydrogel properties such as swelling ratio, compressive modulus, and scaffold gel fraction were systematically controlled independent of hydrolytic degradation rate. The *in vitro/in vivo* degradation correlation was established and a tunable system was identified to

modulate degradation profiles independent of matrix modulus. Finally, evaluation of the cellular response to the degradation products and bioactivity incorporation demonstrated high viability and good cell-material interactions. Overall, this work demonstrates the versatility of this degradable hydrogel platform for various applications such as stem cell carriers, delivery of therapeutics, and resorbable wound dressings.

CHAPTER IV

BACTERICIDAL ACTIVITY OF 3D-PRINTED HYDROGEL GAUZE LOADED WITH GALLIUM MALTOLATE

4.1. Introduction

The natural wound healing response to injury occurs in four different phases: hemostasis, inflammation, proliferation and remodeling. In chronic wounds, issues with infection, excessive inflammatory responses, biofilm development, and the inability of cells to respond appropriately to reparative chemotactic factors prevent the phases of wound healing from occurring.[149] Chronic wounds have complex colonizing bacteria with *Staphlococcus aureus* being the most prevalent in venous leg ulcers.[235] Although extensive research on infection control has been done, several debated issues still exist: critical wound colonization and the role of biofilm, antimicrobials, and antibiotics.[149] Attempts at infection control and reduction of inflammatory byproducts have been investigated through debridement. This process helps remove necrotic or infected tissue that slows down the wound healing process.[23] Other protective dressings thought to address infection include absorbent dressings, autolytic debridement dressings, and antimicrobial dressings.[23, 236, 237] There has been a large shift in antimicrobial investigation due to the development of antibiotic resistant bacteria.[238, 239] Zubair et al. investigated isolated bacteria from diabetic foot ulcer patients and found several classes of antibiotics susceptible to resistance.[240] The increasing development of resistance in several bacteria strains demonstrates the need for an improved system to control infection.

The ability of antimicrobials to be loaded into dressings and delivered topically helps reduce negative systemic effects. However, clinically available antimicrobial dressings such as iodine and silver have potential for severe negative outcomes. Iodine products are commonly used in wound care to reduce bacterial growth as it has been shown to prove effective against most micro-organisms and disrupt mature biofilms *in vitro*.[241] Dressings containing iodine, however; have been contraindicated for patients suffering from thyroid disorders, Grave's disease, and patients who are pregnant or lactating due to systemic absorption.[160, 161] Silver has been highly investigated as an antimicrobial because it has been shown to be effective against a broad range of micro-organisms.[151, 152] Silver is absorbed by sensitive strains of bacteria impairing cell walls, inhibiting respiration, and inactivating bacterial DNA and RNA.[153] However, it has been suggested that uncontrolled use of silver could result in bacteria developing resistance and reported incidents of allergic response has occurred.[151, 154] One of the main challenges is the ability to maintain high enough concentrations of silver to provide bactericidal effects without the development of dose or concentration dependent toxicity.[38]

Recently, gallium maltolate (GaM), a novel antimicrobial agent, has been shown to prevent bacterial growth and colonization.[167-169, 242] GaM is a coordination complex of gallium and maltol, which has an octonal:water partition coefficient of 0.41, illustrating its solubility in both water and lipids ideal for bacterial uptake.[165, 166] GaM has been found to significantly reduce the number of colony forming units (CFUs) of several different bacteria types often known to cause biofilm formation.[167-170] Gallium functions as a ferric iron mimic that has been used to control various microorganisms by taking advantage of

the iron dependence in bacterial growth.[166] The impact of GaM on cellular actions is unclear, but gallium has been shown to promote collagen synthesis, cell migration, and favorably modulate integrin expression which are all important aspects of wound healing.[174, 175] As a result, GaM has the potential to serve as an improved antimicrobial with reduced side effects and positively improve wound healing.

The aim of this study was to evaluate the efficacy of a 3D-printed hydrogel loaded with GaM on preventing bacterial infection of chronic wounds. Minimum inhibitory and bactericidal concentrations of GaM were determined to validate its use as an antimicrobial agent. Poly(ethylene glycol)-diacrylate (PEGDA) hydrogels were fabricated via emulsion templating and 3D-printed into a hydrogel gauze with hierarchical porosity. The ability to control hydrogel properties, emulsion variables, and scaffold geometry will allow for the development of a tunable dressing with potential to improve wound moisture balance. 3D-printed hydrogels were then characterized to determine the effect of this templated architecture on hydrogel swelling rate. It has been shown that appropriate fluid balance improves wound healing by preventing tissue dehydration and cell death, accelerating angiogenesis, increasing the breakdown of dead tissue, and enhancing the interaction of growth factors with target cells.[59] GaM-loaded hydrogels were characterized using UV-Vis to determine release profiles at two loading concentrations. Finally, *in vivo* analysis of GaM release, bactericidal effects, wound closure, and host response was evaluated to determine its use as an antimicrobial wound dressing. Overall, the goal of this work was to investigate GaM and its role in bacterial inhibition and demonstrate its therapeutic application in a topical wound dressing for wound management.

4.2. Materials and Methods

4.2.1. Materials

All chemicals were purchased from Sigma Aldrich (Milwaukee, WI) and used as received unless otherwise noted. Poly(ethylene glycol)-diacrylate (PEGDA) and lithium phenyl-2,4,6 trimethylbenzoylphosphinate (LAP) photoinitiator were synthesized as previously demonstrated.[56, 243] Trimethylolpropane ethoxylate triacrylate (TMPE, Mn= 912 Da), light mineral oil, and Kolliphor P188 surfactant was used in ink formulations.

4.2.2. Poly(ethylene glycol)-diacrylate Synthesis

PEGDA was synthesized according to a method adapted from Hahn, et al.[56] Briefly, acryloyl chloride was added dropwise to a solution of PEG 2 kDa, 3.4 kDa, 6 kDa, or 10 kDa diol and triethylamine (TEA) in dichloromethane (DCM) under nitrogen. The molar ratio of PEG, acryloyl chloride, and triethylamine was 1:2:4, respectively. After the addition of acryloyl chloride, the reaction was stirred for an additional 24 hours at room temperature. The resulting solution was then washed with 8 molar equivalents of 2 M potassium bicarbonate to remove acidic byproducts. The product was then precipitated in cold diethyl ether, filtered, and dried under vacuum.

4.2.3. Lithium phenyl-2,4,6 trimethylbenzoylphosphinate Synthesis

Lithium phenyl-2,4,6 trimethylbenzoylphosphinate (LAP) was synthesized according to a method adapted from Fairbanks, et al.[243] Briefly, dimethyl phenylphosphonite was reacted with 2,4,6-trimethylbenzoyl chloride via a Michaelis-Arbuzov reaction. Equimolar amounts (0.006 mol) of 2,4,6-trimethylbenzoyl chloride was added dropwise to dimethyl phenylphosponite stirring at room temperature under a

nitrogen blanket. The reaction mixture was stirred overnight and then a four-fold excess (0.024 mol) of lithium bromide in 2-butanone (6 wt%) was added to the reaction and heated to 50°C for 15 minutes. The precipitated solid was then cooled to room temperature, filtered via vacuum filtration, and washed 3 times with 2-butanone.

4.2.4. Hydrogel Slab Fabrication

Hydrogels slabs were (D = 8 mm, T = 1.5 mm) fabricated by making (10 wt%) precursor solutions of PEG(6K)DA in water. A photoinitiator solution (1 mg Irgacure 2959 per 0.01 ml 70% ethanol) was added at 1 vol% of precursor solution. Solutions were pipetted between 1.5 mm spaced plates and crosslinked by 6 min exposure to long wave UV light (Intelli Ray Shuttered UV Flood Light, Integrated Dispensing Solutions, Inc., 365 nm, 4 mW/cm2).

4.2.5. 3D-Printed Hydrogel Gauze Fabrication

Hydrocolloid inks were prepared using a FlackTek SpeedMixer DAC 150 FVZ-K. Prior to emulsification, PEGDA and water (25 w/v%) were mixed with Kolliphor P188 surfactant (10 w/v%), TMPE crosslinker (5 w/v%) and LAP photoinitiator (40% of total moles of acrylate groups) in the SpeedMixer cup. Once combined, light mineral oil was added to the aqueous, hydrogel solution in four additions and mixed at 2500 rpm for 2.5 minutes each, until a 75% weight fraction was achieved. Once emulsified a ceramic stir-bead (10 mm diameter and height) was added and mixed at 3500 rpm for 2.5 minutes in the speed mixer.

3D-printed hydrocolloids were fabricated utilizing a RepRap Prusa i3 with an open-source RAMPS v1.4 electronics set and external MOSFETs to control the UV cure

system. Hydrocolloids were loaded into a customized HYREL EMO-25 extruder equipped with a luer lock adapter and a 22 gauge blunted stainless steel needle (413 μm, 6.35 mm in length, Sigma Aldrich). The extruder was modified to print emulsion inks in a cure on dispense manner. Briefly, four 3-watt ultraviolet (UV) LEDs (365 nm, Mouser Electronics, Mansfield, TX) were mounted to a heat sink and affixed to the extruder syringe, approximately 50 mm above the nozzle tip. The MOSFETs are externally powered to accept up to 24 V which allows for precise tuning of the voltage driving the UV LED cure source and allowed for UV of 100 mW/cm^2. Cylindrical constructs (h = 4 mm, r = 10 mm) in OpenSCAD program, were exported as an STL file, and then imported into the "slicing" software, Slic3r version 1.2.9 with the following printing parameters: printing speed of 10 mm/s, nonprinting speed of 25 mm/s, layer thickness of 200 μm, rectilinear grid infill of 70%, extrusion width of 0.6 mm, one perimeter, and no top or bottom solid layers.

The removal of the mineral oil from printed constructs was required for accurate characterization. The constructs were first allowed to completely air dry to allow for bulk oil removal and thorough swelling in DCM. Samples were then soaked in a series of washes for 1 hour each in DCM, 50% v/v DCM/ethanol, ethanol, and 50% v/v ethanol/water. Finally, constructs were soaked overnight in water. After extraction and swelling in water overnight, constructs were frozen at -80°C and lyophilized.

4.2.6. Hydrogel Characterization

To measure swelling ratio, hydrogel slabs were swollen for 3 hours to reach equilibrium swelling and 8-mm discs were punched from hydrogel sheets. Specimens

were then dried under vacuum overnight to determine dry mass (W_d). 3D-printed specimen dry weights (W_d) were measured after cleaning and lyophilizing. Both hydrogel specimen types were then submerged in RO water and swollen weight (W_s) weight was measured at distinct time points. The swelling ratio (Q) was calculated:

$$Q = \frac{W_s}{W_d} \qquad [1]$$

4.2.7. Gallium Maltolate Loading

Hydrogel dressings (D = 10 mm, T = 1.5 mm) were loaded at two concentrations of gallium maltolate (Norac, Inc., Azusa, CA, USA): low (~2 mg/dressing) and high (~7 mg/dressing). To achieve these loading concentrations GaM was dissolved in DCM at 8 mg/ml and 30 mg/ml to achieve low and high concentrations, respectively. Dried hydrogel dressings were measured (W_{di}), placed into glass vials, and submerged in 2 mL of GaM solutions based on desired concentration. Hydrogels were swelled for 3 hours to reach equilibrium swelling to ensure full hydration in GaM solutions. GaM solutions were then extracted and air dried for 10 minutes prior to an overnight vacuum dry. Dried hydrogel samples were then weighed (W_{df}) to measure theoretical loaded GaM (M):

$$M = \frac{W_{di}}{W_{df}} \qquad [2]$$

4.2.8. Gallium Maltolate Release

GaM release was performed under two conditions to better predict *in vivo* release, submersion and Transwell® models. In the submersion models GaM loaded hydrogels were submersed in 2 mL of water and samples were extracted at distinct time points and 2 mL of water was replaced. In the Transwell® model, GaM loaded hydrogel samples

were prehydrated with 80 μl of RO water and placed into a 12 mm Transwell® permeable membrane insert in a 12 well plate. Wells were filled with 500 μl of water to fill up to the insert membrane interface. Releasate was collected at distinct time points and water was replaced.

To measure GaM concentrations a Cary 50 UV-Vis spectrophotometer (Agilent Technologies) recorded UV-Vis absorption spectra in the range of 200 to 400 nm. The data were collected with a scan speed of 300 nm/sec and 0.5 nm resolution. A calibration curve was generated for concentrations of GaM in water between 5 and 25 μM to create a standard curve. Collected GaM releasates were diluted to a theoretical concentration of 15-20 μM with water to prevent saturation.

4.2.9. Bacteria and Growth Conditions

Staphylococcus aureus (*S. aureus*; ATCC 29213) and methicillin-resistant *S. aureus (MRSA*; ATCC 43300) were cultured in brain heart infusion broth (BHIB; Beckton, Dickinson and Company, Sparks, MD, USA) for 24 h at 37 °C on a shaker plate at 250 rpm. Bacterial cells were pelleted by centrifugation at 3000 × *g* for 10 min and washed 3 times with phosphate-buffered saline (PBS; Thermo Fisher Scientific). The concentration of bacteria was determined spectrophotometrically (Smartspec 3000) at an optical density (OD) of 625 nm, and approximately 5×10^6 colony forming units (CFU) /ml were inoculated into Roswell Park Memorial Institute 1640 Medium (RPMI; Thermo Fisher Scientific). All RPMI 1640 media were supplemented with 5 mL sodium pyruvate (100 mM, Thermo Fisher Scientific) and 5 ml glutamax solution (200 mM, Thermo Fisher Scientific) per 500 ml RPMI 1640. RPMI was used as the control medium to assess the

effects of GaM on growth of *S. aureus* and MRSA. In all experiments, concentrations of bacteria were determined by 10-fold serial dilutions cultured in triplicate on brain heart infusion agar.

4.2.10. GaM Minimum Inhibitory Concentration

The MIC of GaM against *S. aureus* and MRSA was determined by identifying the lowest GaM concentration that prevented visible bacteria growth. Gallium maltolate was suspended in RPMI at a concentration of 8 mg/ml. All MIC tests were performed using 96-well plates. All dilutions were 2-fold dilutions starting at 4 mg/ml gallium maltolate and ending at 0.25 mg/ml. 3D-printed hydrogels samples loaded with GaM were evaluated by submersion of dressings in RPMI to create a final concentration of 8 mg/ml and releasate was evaluated at final concentration of 4 mg/ml. Wells containing RPMI medium with or without the Staphylococcus isolates were included as positive and negative control wells, respectively. Bacterial growth was measured by a change in turbidity of the OD at 625 nm utilizing a microplate reader (BioTek Synergy 2) at time zero and then at 24 hours after incubation at 37°C. After 24 hours of GaM exposure, bacterial concentrations were determined and reported as CFU/ml.

4.2.11. In Vivo *Splinted Wound Model*

All procedures were approved by the Texas A&M University Institutional Animal Care and Use Committee. Two month old C57BL/6 inbred mice were utilized to investigate bacterial inhibition and wound healing for a 3D-printed hydrogel dressing study. Mice were anesthetized with 3% isoflurane and injected with 0.3 mg/ml Buprenorphine at a dose of 0.1 mg/kg. Their backs were shaved and residual hair was

removed with two applications depilatory cream. The surgical area was then cleaned with chlorhexidine and isopropyl alcohol. One 8 mm biopsy punch was taken from the back and a silicone ring (10 mm OD and 6 mm ID, 12 mm OD and 10 mm ID) was glued to the skin and sutured (Quill Monoderm VLM-1009) for hydrogel slab and 3D-printed hydrogel dressing studies, respectively. Mice were inoculated with 30 μL of $3.3X10^4$ CFU/ml of *S. aureus* (ATCC 29213) to yield a concentration of 1000 CFU/wound.

GaM loaded 3D-printed hydrogel dressings (D = 10 mm, T = 1.5 mm) were added to the mouse wounds 24 hours after initial inoculation. GaM concentrations (Low – 2 mg and High – 7 mg) were chosen based on preliminary *in vivo* scouting studies and therapeutic range of *in vitro* MIC studies. 3D-printed hydrogel dressings loaded with GaM were sterilized via ethylene oxide sterilization. Treatment groups consisted of PBS, low, and high GaM loaded dressings. GaM loaded dressings were pre-hydrated with 80 μL of PBS prior to application and re-bandaging. Wounds were then bandaged with OpSite Flexifix bandages. Bandages and wound dressings were changed at 24 hours after initial application and then every 2 days for 12 days. At each time point bandages were removed, fresh dressings were applied, and animal weight was obtained according to AUP.

To quantify the *in vivo* GaM release, hydrogel dressings were collected at 48 hours post application and the GaM content remaining in the dressing was quantified using mass spectrometry as compared to the initial concentration in dressings. Briefly, GaM-loaded specimens (0 hour) were digested with nitric acid, hydrochloric acid, and hydrogen peroxide in a Milestone UltraWave microwave digester and then analyzed for GaM using a Spectro CirOS ICP-OES instrument. The initial GaM loading concentration of 4

specimens were reported as an average of quantified GaM mass. Hydrogel dressings (n=6) were removed from the wound after 48 hours and soaked in 70% ethanol. The liquid samples were then diluted with 1% nitric acid and the samples analyzed for GaM on a Perkin Elmer DRC 2 ICP-MS instrument. The GaM remaining in the dressing was reported as an average of GaM mass.

After 12 days, mice were euthanized, bandages and rings were carefully removed, and wound size was measured. Wounds were excised with 12 mm biopsy punches and split for analysis of bacterial growth and histology. Tissue excised for bacterial growth analysis was homogenized in 5 mL of PBS using a tissue homogenizer and diluted in PBS $1X10^2$, $1x10^3$, and $1X10^4$-fold. 100 μL of diluted samples were plated in luria broth (LB) agar plates and incubated at 37°C for 24 hours. Colonies were then counted to determine CFU/g of tissue. Tissues were processed for routine paraffin embedding, sectioned with a microtome (5 um-thick sections) and stained with hematoxylin and eosin (H&E). Samples were then scored based on criteria listed in **Table 4.1**.

Table 4.1. Ordinal scoring for histological analysis.

Score	Epithelial Coverage	Debris, Inflammatory Cells, Epithelial Hyperplasia, Vascular Buds	Bacteria, Foreign Material
0	0-10%	None	No
1	10-25%	Mild	Yes
2	25-50%	Moderate	
3	>50%	Marked	

4.2.12. Statistical Analysis

All statistical analyses were expressed as the mean ± standard deviation unless stated as standard error of the mean (SEM). Statistical analysis was performed utilizing a standard one-way ANOVA with Tukey's post-hoc analysis for multiple comparisons with variables greater than two. Statistical significance was accepted at $p < 0.05$ with a 95% confidence interval.

4.3. Results and Discussion

4.3.1. Hydrogel Characterization

Approaches to developing hydrogel inks with rheological properties suitable for 3D-printing has been investigated to improve print fidelity by incorporating additives to increase viscosity.[244, 245] Here, we demonstrate the ability to 3D-print a hydrogel hydrocolloid ink photocrosslinked via UV irradiation through a Cure-on-Dispense method, **Figure 4.1A**. Typical bulk hydrogel slabs are limited to scaffold geometries that can be cast into a mold. This oil-in-water emulsion exhibits viscosities for high fidelity printing and creates a dual porosity dressing with both macro- and micro-pores. Microporosity is formed upon the removal of the oil phase which can be tuned through emulsion parameters while the macroporosity is formed through 3D-printing, **Figure 4.1B**. The dual porosity of this 3D-printed construct allows for rapid water uptake reaching equilibrium swelling after 15 minutes compared to a hydrogel slab at 3 hours, **Figure 4.1C**. Additionally, the rapid swelling capabilities of these 3D-printed hydrogel dressings have potential for therapeutic delivery of an antimicrobial agent to create a multifaceted wound dressing design. **Figure 4.1D** demonstrates a more rapid release profile for 3D-

printed hydrogel dressings compared to traditional hydrogel slabs. However, both systems achieve near complete release after 24 hours. We identified that the accelerated swelling capacity of the 3D-printed dressing allows for rapid release that could reach the therapeutic concentration of an antimicrobial agent faster.

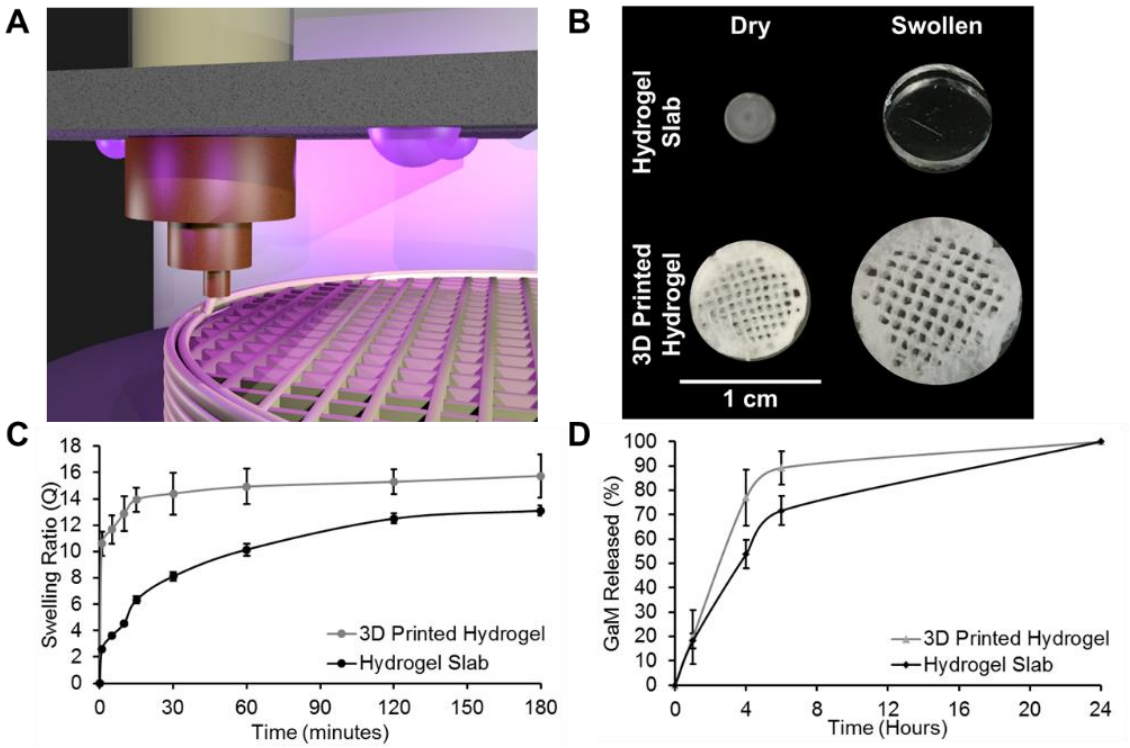

Figure 4.1. (A) Schematic representation of 3D-printed hydrocolloid inks via extrusion deposition printing with cure-on-dispense technology. (B) Comparison of dimensional changes upon hydration and dressing porosity of 3D-printed hydrogel. (C) Swelling ratio characterized over time to investigate swelling rate improvements of 3D-printed hydrogel. (D) 24 hour release profiles of GaM loaded hydrogel slabs and 3D-printed hydrogels.

4.3.2. In Vitro *Bacterial Inhbition Analysis*

Bacterial inhibition studies were performed to identify therapeutic ranges of soluble GaM for both *S. aureus* and MRSA. The minimum inhibitory concentrations (MIC) of *S. aureus* and MRSA were found to be 2 mg/ml and 1 mg/ml, respectively, **Figure 4.2A**. These reported concentrations had no visible growth of bacteria after 24 hours compared to the negative control. GaM MICs for *S. aureus* and MRSA were consistent with those reported previously by Baldoni et al.[169] Optical density (OD) was utilized to determine statistical changes in bacterial growth and confirmed the visual MIC assay. To quantify bacterial growth after 24 hour exposure to GaM, colony forming units (CFU) for a single concentration below the MIC and up to 4 mg/ml were counted for both *S. aureus* and MRSA. A concentration dose dependence was demonstrated by reduction in CFU/ml as demonstrated in **Figure 4.2B**. Concentrations below the MIC for both *S. aureus* and MRSA resulted in a significantly increased bacteria colony counts of ~5.3 x10 and 9.4 $x10^4$ CFU/ml, respectively. Although these concentrations do not illustrate a bactericidal effect, MICs are the gold standard for determining microbe susceptibility.[246] Additionally, it has been shown that concentrations of bacteria less than 10^5 CFU/g tissue allowed for wound healing to proceed normally.[247] These results demonstrate the utility of GaM in reducing bacteria activity with potential to inhibit bacterial load *in vivo* at concentrations above the MIC.

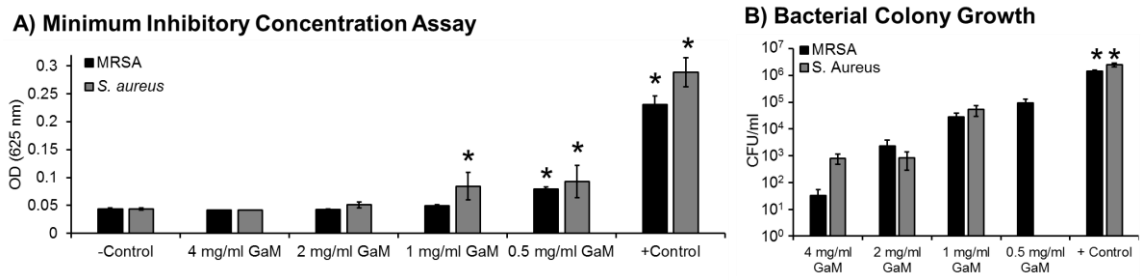

Figure 4.2. (A) Determination of minimum inhibitory concentration for gallium maltolate in MRSA and *S. aureus*. Minimum inhibitory concentration identified at 1 mg/ml and 2 mg/ml for MRSA and *S. aureus*, respectively. *indicates statistical differences with respect to negative control. ($p < 0.05$) (B) Bacterial colony growth after 24 hour exposure to GaM at concentrations at and above at the MIC. *indicates statistical differences with respect to positive control ($p < 0.05$).

4.3.3. Gallium Maltolate Loading and Release

Concentrations of GaM between 5 and 25 µM were measured utilizing UV-Vis spectroscopy to create a calibration curve, **Figure 4.3A**. A standard curve was then identified utilizing a linear trend line and unknown sample masses were then extrapolated, **Figure 4.3B and 4.3C.** GaM loaded dressings were identified as low GaM and high GaM with loaded GaM amounts quantified at 1.4 ± 0.4 mg and 7.05 ± 0.7 mg, respectively. GaM loaded dressings were fabricated with a low GaM (1.4 ± 0.4 mg) and a high GaM (7.05 ± 0.7 mg) concentration. *In vitro* release profiles of GaM from the dressings was investigated using two distinct release conditions, sink and diffusion methods, **Figure 4.4A and 4.4B**. First, a commonly utilized submersion method was investigated to create sink conditions to determine release rates. As expected, submersion release profiles demonstrated a burst release of greater than 95% after 1 hour, with concentrations below MICs after this time point, **Figure 4.4C and 4.4E**. Next, a diffusion release method was developed by placing 3D-printed hydrogel dressings into a Transwell® insert and

allowing diffusion of through a polyester insert membrane with 0.4 µm pores. Solutions were collected over 24 hours to approximate antimicrobial release from the tissue contacting surface of the dressing. High burst release, greater than 65%, was observed after 1 hour for both concentrations, **Figure 4.4D and 4.4F**. However, release concentrations were greater than the minimum inhibitory concentration for high GaM concentrations observed after 1 hour for *S. aureus* and 2 hours for MRSA. There was a minimal concentration dependent effect observed with low GaM loaded dressings, as they retained similar release profiles over the 24 hours. However, at this loading concentration, only the initial 1-hour time point resulted in concentrations meeting the MIC therapeutic range for MRSA.

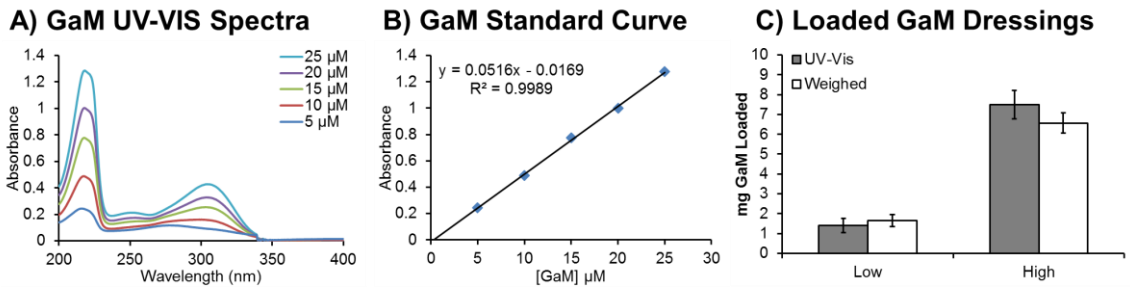

Figure 4.3. Gallium maltolate (GaM) concentration (A) calibration curve and resulting (B) standard curve at 217 nm. (C) Confirmation of theoretical loading via gravimetrical analysis was confirmed utilizing UV-Vis.

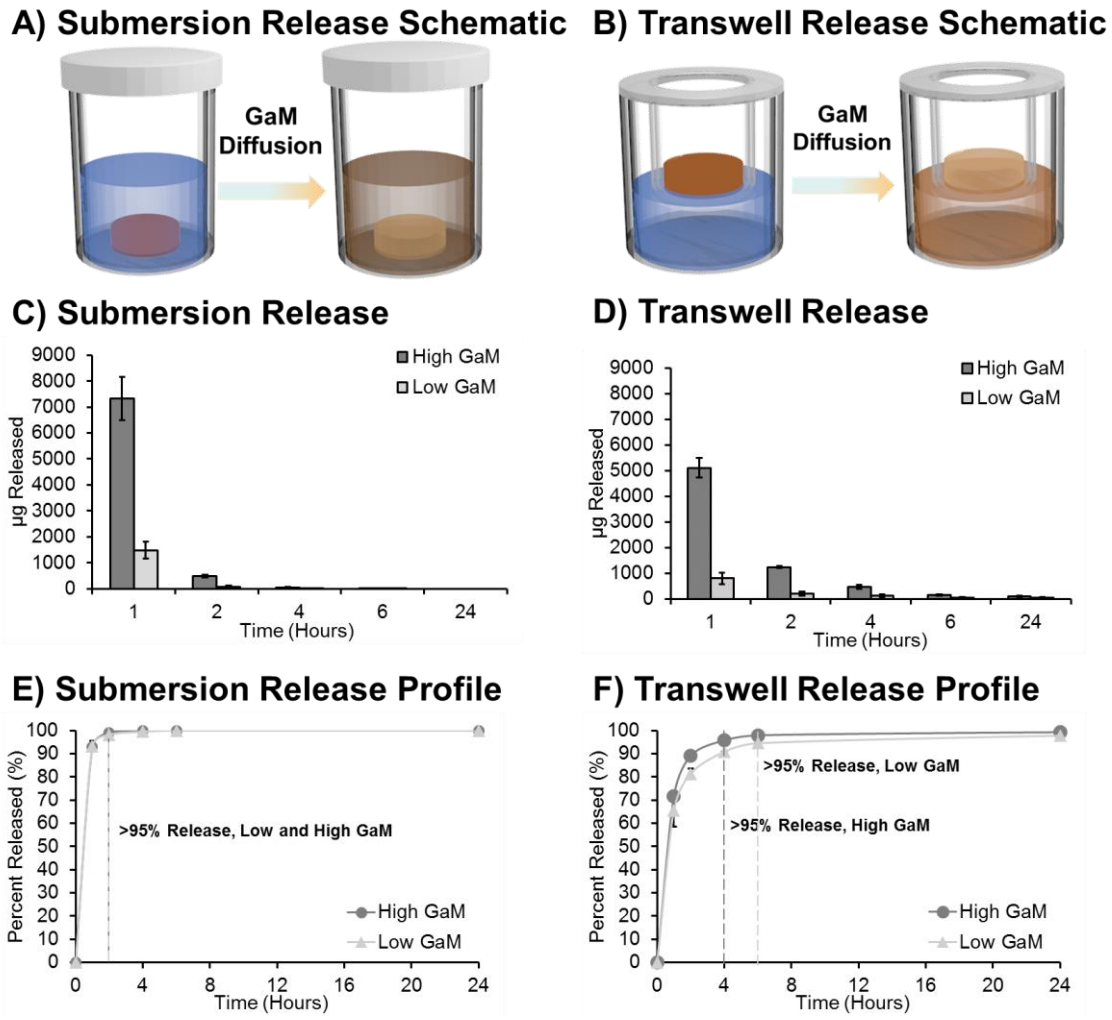

Figure 4.4. GaM hydrogel release schematic for 3D-printed hydrogel dressings in (A) Transwell® and (B) submersion model. *In vitro* GaM hydrogel release profiles from 3D-printed hydrogel dressing in (C and E) Transwell® and (D and F) submersion model.

To ensure that the GaM retained antimicrobial activity after loading into 3D-printed hydrogels, a modified MIC assay was performed to investigate bacterial growth in the presence of hydrogel releasates, **Figure 4.5B**. GaM was released from 3D-printed dressings by submersion in supplemented RPMI media at a concentration of 4 mg/ml, which is above the MIC for both MRSA and *S. aureus*. Optical density analysis confirmed

that bacteria growth was inhibited after 24 hours with densities matching negative controls. This demonstrated that GaM could be loaded into hydrogel dressings without effect on its bactericidal properties.

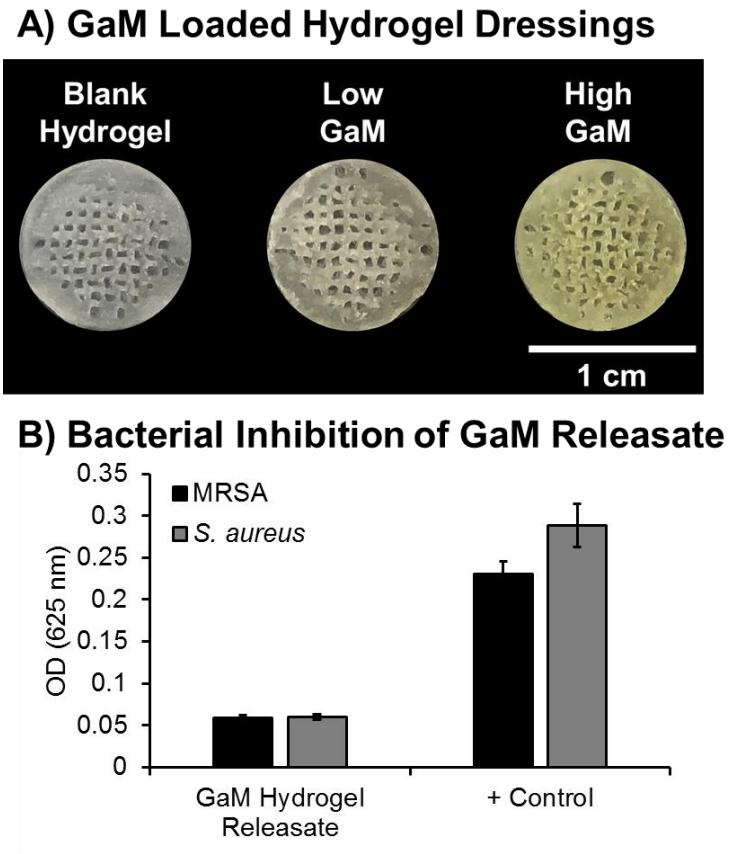

Figure 4.5. (A) GaM loaded hydrogel dressings with increasing GaM concentration. (B) Effect of GaM released from antimicrobial-loaded hydrogels on bacterial growth measured by changes in optical density.

4.3.4. In Vivo *Splinted Wound Analysis*

Splinted wound models were then investigated in a murine model to determine the effects of hydrogel dressing application on bacterial load and wound closure, **Figure 4.6A**. The addition of a wound dressing creates a barrier and helps reduce infection by mimicking the skin's primary structure.[39, 248] Additionally, the incorporation of GaM into 3D-printed gauze was applied to improve wound moisture balance while inhibiting bacterial growth. Dressing changes were performed every 48 hours to ensure GaM concentration was in the therapeutic range based on burst release profiles identified in *in vitro* studies. Mass spectrometry was performed to quantify initial (0 hour) and remaining (48 hour) GaM concentration in the dressings after initial application. Initial loading of GaM concentrations were determined to be 1597.7 ± 61.5 µg and 5089.4 ± 952.3 µg for the low and high GaM loaded dressings, respectively. Less than 3% of GaM remained after 48 hours with 6.3 ± 4.1 µg and 148.9 ± 116.2 µg remaining in the low and high dressings, respectively. Based on these findings, dressing changes were performed every 48 hours to ensure complete release and a therapeutic delivery for a total of 12 days. The use of these dressings as a carrier for GaM release resulted in significantly decreased bacterial growth, ~$2x10^6$ CFU/g tissue compared to PBS treated controls, ~$50x10^6$ CFU/g tissue, **Figure 4.6B**. There was no significant difference in wound closure of the untreated control and wounds treated with the GaM-loaded dressings with approximately 30% wound closure after 12 days, **Figure 4.6C**. Histological analysis determined no significant differences ($p > 0.05$) between the two GaM doses and the untreated control in terms of epithelial coverage, **Figure 4.6D**. This confirmation of wound closure via histological

characterization further supports wound dimensional analysis. Additionally, foreign material and debris at the wound site had no significant differences illustrating that there was no significant dressing left within the wound between dressing applications. Inflammatory responses identified for all compositions demonstrated on average between mild and moderate inflammatory cell accumulation and similar levels of vascular budding demonstrating comparable effects with all treatment types. Collectively, these findings indicate that GaM delivery resulted in reduced bacteria growth with no negative effects on wound healing.

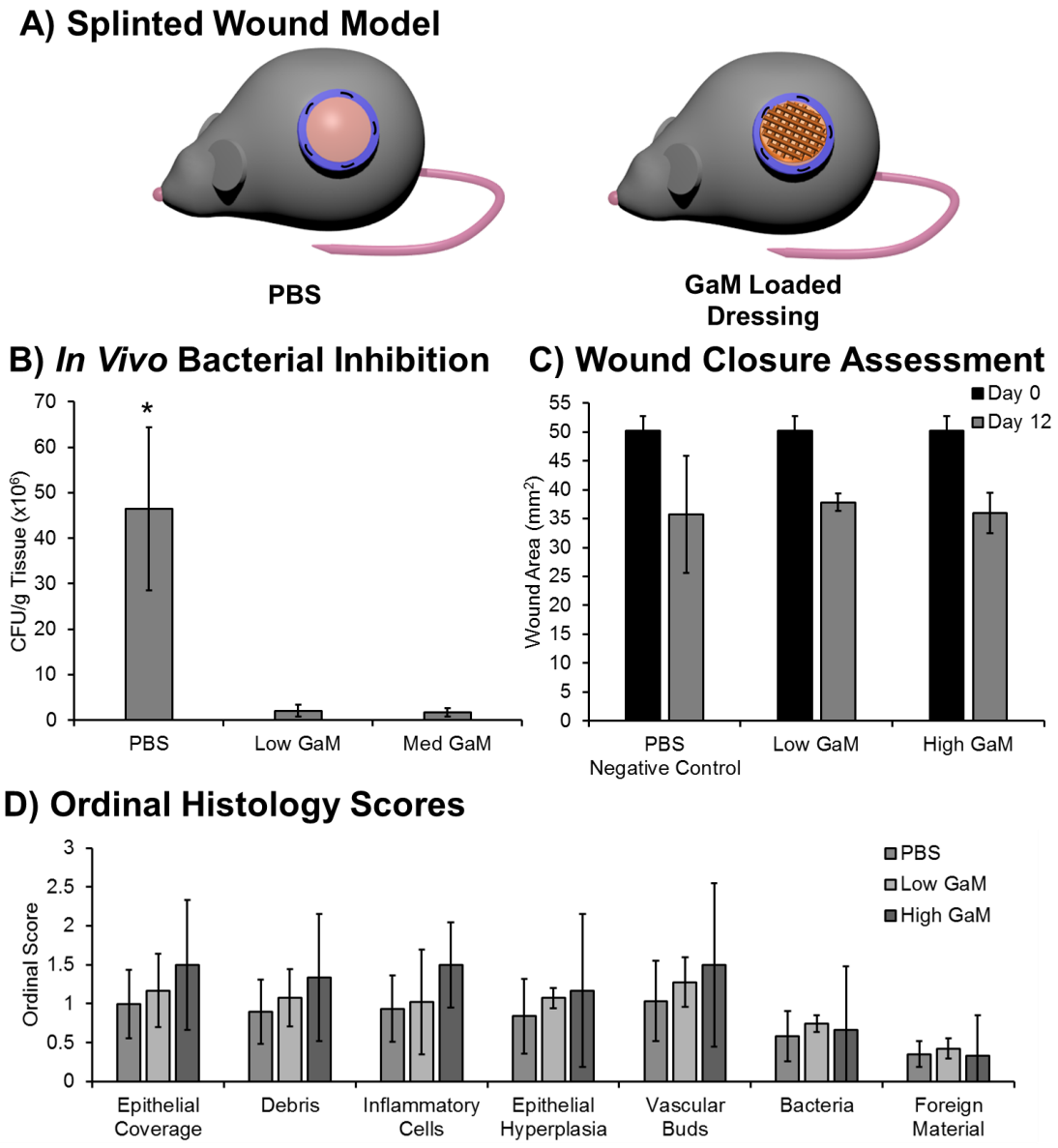

Figure 4.6. (A) Splinted murine wound model schematic with untreated control and applied 3D-printed dressing. Data represented as average ± SEM. B) *In vivo* bacterial inhibition determined by CFU/g of tissue for low and high GaM loaded hydrogel dressings. *indicates statistical differences between corresponding samples ($p < 0.05$). C) Wound closure assessment of all treatment groups at day 0 and day 12. D) Ordinal histology scores investigating vascularization, inflammatory response, and wound closure.

Current wound therapies aim to prevent wound recurrence and treatment failure through compression, infection maintenance, debridement, and appropriate dressing selection. Unfortunately, these therapies are often only able to control a single factor and inadequately fail to address the complex wound environment. We aimed to develop an improved wound dressing that demonstrates both wound moisture balance and infection control. Maintaining a moist wound environment has been shown to facilitate the wound healing process by preventing tissue dehydration and cell death, enhanced angiogenesis, improved breakdown of nectrotic tissue and fibrin, and initiating the interaction of chemotactic factors with target cells.[59] Clinically applied hydrogel dressings such as Granugel® and Aquaform®, have been shown to absorb 23-27% in highly exudative wounds but only allow for a marginal 3-5% hydration donation.[60] The increased water uptake and rapid swelling of our 3D-printed dressings demonstrate their ability to influence moisture balance in the wound environment to be applied dry for absorption control or applied hydrated for hydration donation.

Identifying predictive *in vitro* methods for transdermal release is important for evaluation of compound efficacy and safety. Currently utilized systems range in complexity ranging from diffusion cell models, organ-on-a-chip, and *in vitro* skin models.[249-252] Ng et al. demonstrates variability in a static franz diffusion cell system due to membrane barrier, sampling volume, sampling frequency, and sampling frequency.[253] Additionally, there has been extensive research investigating *ex vivo* animal and human models, however; several limitations exist due to ethical concerns, hair density, and thickness.[250] The use of a Transwell® assembly with electrospun fibers and co-cultured

human skin cells has been shown to mimic the fibrous extracellular matrix and be utilized as a model for full-thickness human skin.[254] Here, we utilize two release systems, submersion and Transwell®, to demonstrate the release of GaM from our hydrogel dressings. The low level sustained release demonstrated with the Transwell® system has potential for improved patient comfort and wound care. GaM has been shown that at low doses it can provide nearly complete pain relief with topical applications reducing inflammation.[172, 173] Additionally, gallium has been shown to promote collagen synthesis and cell migration that could be beneficial for improved wound closure and healing.[174, 175] We hypothesize that the demonstrated low level release has potential to improve *in vivo* wound healing response.

In chronic wounds, issues with infection with biofilm development, excessive inflammatory responses, and the inability of cells to respond appropriately to reparative chemotactic factors prevent the phases of wound healing from occurring.[149] Chronic wounds have complex colonizing bacteria with *Staphlococcus aureus* (*S. aureus)* being the most prevalent in venous leg ulcers.[235] In the late 1970s and early 1980s, the emergence of methicillin-resistant *Staphlococcus aureus* (MRSA) became an endemic in the United States.[255] This strain of *S. aureus* is resistant to all β-lactam antibiotics demonstrating the complications with traditional antibiotic therapies.[256] Antimicrobial resistance is rapidly developing issue which could result in increased patient outcomes of morbidity and mortality.[257] Gallium has the potential to overcome typical resistance mechanisms associated with antibiotics such as decreased cellular uptake due to permeability of the cellular envelope due to its ability to mimic Fe(III) pathways in bacteria.[258, 259] The

inability for Ga(III) to be reduced like Fe(III), interrupts the reduction and oxidation processes necessary for DNA and protein synthesis necessary for bacterial and mammalian cell proliferation.[173, 259, 260] Additionally, delivery of antimicrobials locally is the preferred delivery method to reduce systemic toxicity, increase efficacy, and to overcome problems associated with poor blood circulation in lower extremities commonly afflicting patients suffering from diabetes.[23] These studies demonstrate the a method to deliver GaM to target lower extremity chronic wounds to improve infection control and reduce complications with bacterial resistance.

The *in vivo* evaluation of GaM demonstrates improved infection control and comparable wound closure rates to that of the untreated control. Boateng et al. reports that foreign bodies introduced into the wound can cause chronic inflammatory responses and lead to wound healing complications.[23] Histological analysis of the wound site illustrates comparable wound healing in all treatment groups which demonstrates a reduction in foreign bodies during dressing changes. Additionally, our dressing design allows control over hydrogel chemistry to tailor the design to meet application specific needs. The use of a biodegradable hydrogel matrix would eliminate the concerns of residual foreign bodies within the wound bed during dressing changes. Concentrations of GaM selected were shown to be within the therapeutic range for bacterial inhibition *in vitro* and complete release was confirmed *in vivo.* Selected concentrations of GaM verified bacterial inhibition without off target effects that could negatively affect wound closure. In some studies, gallium-based compounds are utilized as anticancer treatments to induce apoptosis in cells; however, we demonstrate that the selected concentrations still resulted

in similar wound closure.[165, 172, 261, 262] The incorporation of GaM into this 3D-printed wound dressing provides an improved delivery method to topically deliver this antimicrobial agent to inhibit bacterial growth. These studies demonstrate the potential of therapeutic delivery of GaM from a self-tuning moisture balanced wound dressing. Current studies are investigating a method to sustain delivery of GaM within the therapeutic range to improve long term bacterial inhibition.

4.4. Conclusions

The aim of this study was to develop an improved wound dressing platform through incorporation of the novel antimicrobial agent, gallium maltolate, in a 3D-printed hydrogel gauze. The multi-layer porosity of this 3D-printed hydrogel dressing allowed for controlled moisture balance through rapid water uptake. Antimicrobial activity of GaM was characterized by identifying minimum bactericidal concentrations in *Staphylococcus aureus* and *Methicillin-resistant Staphylococcus aureus*. Release profiles of GaM loaded 3D-printed hydrogel dressings were identified using submersion and Transwell® release systems and retention of antimicrobial activity post release was confirmed. Additionally, the effects of GaM loaded hydrogel dressings on wound healing and antimicrobial activity were investigated *in vivo* using a murine splinted wound model. Mass spectrometry analysis was utilized to confirm complete delivery of therapeutic dosages were delivered prior to dressing change. Explanted wound tissue confirmed decreased bacteria levels and wound closure retention with the addition of the GaM loaded dressing. Overall, this work provides a versatile platform that can be used to provide a wound dressing matrix to support antimicrobial delivery and wound fluid balance in chronic wounds.

CHAPTER V

CONCLUSIONS

5.1. Summary

This work establishes several tunable platforms for the development of a poly(ethylene glycol)-based hydrogel wound dressing platform. These studies demonstrate the fabrication of hydrogel scaffolds with tunable moisture balance, the development of engineered proteins for integrin-mediated bioactivity, tunable biodegradation for an improved wound dressing, and the incorporation of an antimicrobial agent for bacterial inhibition. Collectively, the advancements made in this work aim to provide a platform for an improved wound dressing with tunable properties to address different wound environments.

Hydrogel microspheres were developed as a tunable, degradable hydrogel wound dressing for improved injectable delivery. These uniform hydrogel microspheres were fabricated using a dual fluidics setup to allow for an injectable, space filling dressing for irregular shaped wounds. Furthermore, additional fabrication techniques were investigated to improve scale-up and throughput. Additionally, a collagen mimetic, $eCol_{GFPGER}$ was developed to improve protein stability by increasing melting temperature while maintaining triple helix formation compared to $Scl2_{GFPGER.}$ Furthermore, steric hindrance of integrin binding sites were assessed by monitoring α1 I-domain binding and fibroblast adhesion was assessed to compare cellular adhesion and spreading.

To establish a resorbable hydrogel system to be used in wound dressings, the *in vitro* and *in vivo* biocompatibility and biodegradation of a PEG-based hydrogel with thio-β-esters was evaluated. Two different PEGDTT macromers were synthesized to achieve different hydrogel properties and examine the effect on the degradation profiles. PEGDTT macromers (PEGDTT-L and PEGDTT-H) and PEGDA controls were evaluated to confirm synthesis, functionalization, and molecular weights. Hydrogels fabricated with various ratios of PEGDTT:PEGDA (100:0, 85:15, 75:25, 60:40, and 0:100) were investigated to determine the effect of composition on swelling ratio, gel fraction, compressive modulus, and degradation profiles. The *in vitro* biocompatibility of human dermal fibroblasts (hDFs) exposed to the degradation products of 100% PEGDTT hydrogels exhibited high viability and no effect on cell proliferation after 24 and 72 hour exposure. Additionally, bioactivity was conferred into hydrogels and resulting cellular attachment and spreading were found to be similar in PEGDTT and PEGDA hydrogels. Finally, the *in vivo* degradation profile was established and PEGDTT compositions were found to degrade much more rapidly *in vivo* compared to the *in vitro* conditions.

Finally, the last chapter demonstrates the versatility of this hydrogel system with the fabrication of a 3D-printed hydrogel gauze loaded with gallium maltolate (GaM) as a wound dressing. The minimum inhibitory concentration (MIC) of GaM was identified in *Staphylococcus aureus* and *Methicillin-resistant Staphylococcus aureus* demonstrating the potential of GaM to inhibit bacterial growth. Development of this 3D-printed hydrogel exhibited rapid water uptake demonstrating its capability to be utilized as an antimicrobial carrier. 3D-printed hydrogel dressings were loaded with GaM and burst release profiles

were identified using Transwell® and submersion release systems over 24 hours. Mass spec analysis was utilized to confirm the full release after 48 hours in a murine model. Additionally, released GaM from hydrogel dressings was investigated in a modified MIC assay and exhibited bacterial inhibition similar to soluble GaM. These GaM loaded hydrogel dressings were evaluated in a murine splinted wound model and demonstrated decreased bacterial load while maintaining comparable wound closure.

In summary, this work highlights the potential of this biodegradable hydrogel system to serve as an improved dressing to increase wound healing through bioactivity incorporation, wound moisture balance, and conferred antimicrobial activity. The development of these technologies have not only created a tunable platform for wound healing scaffolds but also can be applied to various regenerative applications.

5.2. Significance of Work

There have been several advances in wound healing to improve healing capability, reduce amputations, and improve patient comfort and care. Recent wound dressing research has focused on scaffold design, vascularization, regulatory factors, and accurate *in vitro* models. Ideally wound dressings would initiate and manage wound healing in the following three ways: manage infection and wound fluid maintenance, encourage cellular interactions to promote healthy tissue formation, and degrade at an appropriate rate. Specifically, this work investigates a biodegradable hydrogel system to address the different aspects of wound healing. The combined technologies discussed in this work provides a foundation for the development of a tunable wound healing platform with potential for improved wound closure.

In Chapter 2, a collagen-mimetic injectable hydrogel microsphere wound dressing was investigated to space fill irregularly shaped wounds. The hydrogel microsphere platform improves upon current hydrogel geometries illustrating its ability to provide maximum dermal contact through sphere packing. Controlled modulation of cellular interactions through recombinantly expressed Scl2 proteins was further optimized by improving protein stability to develop $eCol_{GFPGER}$. Additionally, the tethering of the protein into the hydrogel matrix is facilitated through the use of PEG linkers that functionalize this protein utilizing amine-NHS chemistries. Modification of this Scl2 protein also resulted in a reduction of lysines in the protein backbone, and despite the steric hindrance from PEG-linkers this engineered design allows for improved cellular interactions with integrin binding sites. The ability to modify stability and integrin interactions of these Scl2 proteins illustrates an important advantage over traditional bioactive factors. As a result of these protein modifications, the incorporation of these Scl2 proteins into bioinert PEG-based hydrogels imparts bioactivity to provide potential for integrin-mediated cellular interactions and wound healing. Through the development of the scaffold design, moisture balance, and bioactivity incorporation this dressing has potential as a neotissue matrix to promote active wound healing.

In Chapter 3, the *in vivo* degradation profiles and biocompatibility of the hydrolytically degradable macromer, PEGDTT, was evaluated to support its use as a degradable matrix to support wound healing. Poly(ethylene glycol) hydrogels are widely used due to their ability to be easily modulated chemically, mechanically, and biologically; however, they have been shown to degrade slowly *in vivo* limiting its use for clinically

relevant applications. Although there has been successful modulation of PEG-based hydrogels utilizing other chemical modifications, these hydrogels cannot tune degradation rate independent of swelling ratio and modulus. By modulating the number of thio-β esters in the hydrogel composition, this platform displayed broadly tunable hydrolytic degradation while maintaining relatively constant hydrogel swelling ratio and modulus. Furthermore, to date there has been limited characterization of the *in vivo* degradation profile of these thio-β ester containing PEG hydrogels. The *in vitro-in vivo* degradation correlation was established and a tunable system was identified to modulate degradation profiles independent of matrix modulus. Finally, evaluation of the cellular response to the degradation products, *in vivo* host response, and bioactivity incorporation demonstrates the versatility of this platform for various applications and scaffold geometries such as stem cell carriers and fabrication of microspheres and 3D-printed dressings for wound healing.

In Chapter 4, antimicrobial loading and release from 3D-printed hydrogels was explored to investigate bacterial inhibition in contaminated wounds. This work, demonstrated the use of solid freeform fabrication to 3D-print hydrogel gauze with micro- and macro- porosity. The fabrication of this dual porosity scaffold led to rapid swelling rates and significant water uptake demonstrating its ability to provide improved wound fluid balance over traditional bulk hydrogels. The design of this dressing allows for dry or hydrated application illustrating its versatility to be used in different wound environments to absorb fluids in highly exudative wounds or provide moisture to dry necrotic tissues. Additionally, methods were developed to quantifiably determine minimum inhibitory

concentrations for GaM by investigating bacteria optical density, confirming results from traditional MIC assays. Dressing compositions were modulated at two doses to investigate dose dependence of GaM within the therapeutic range for bacterial inhibition. Furthermore, these studies investigated *in vivo* bacterial inhibition with the addition of GaM and demonstrated no inhibition of wound closure with the application of this hydrogel gauze. Although GaM has been investigated as a novel antimicrobial agent, these studies demonstrate for the first time its incorporation into a wound dressing for therapeutic applications and its response *in vivo*.

Overall, the methods developed in this work detail a tunable, biodegradable hydrogel wound dressing platform with improved regenerative capacity thorough wound fluid balance, bacterial inhibition, and bioactivity development. Methods to control scaffold geometries were investigated to develop a system that will provide wound dressings with control over wound fluid balance. Furthermore, the incorporation Scl2 proteins and gallium maltolate provide biological cues for improved cellular interactions and bacterial resistance, respectively. Cumulatively, each component of this wound healing platform provides explicit advantages for improved wound healing but independently these tunable systems can be utilized broadly for the development of technologies for various regenerative therapies.

5.3. Challenges and Future Directions

Detailed in this work is the development of a hydrogel wound dressing platform with tunable properties and imparted antimicrobial activity. Although we have demonstrated the incorporation of bioactivity utilizing collagen and $Scl2_{GFPGER}$, further

investigation must be done to ensure that the incorporation of bioactivity into the various scaffold constructs promotes active wound closure and healing. Additionally, further work must investigate the combinatorial effect of the incorporation of both bioactivity and antimicrobial incorporation to assess the independent and synergistic effects *in vivo.*

A primary focus of this work has been incorporating gallium maltolate (GaM) into our hydrogel platform to impart antimicrobial activity. Despite having demonstrated its minimum bactericidal concentration *in vitro* and exhibiting release within the therapeutic range there is still significant bacterial load observed *in vivo*. It has been noted in literature that there is a bacterial threshold ($>10^5$ CFU/g tissue) for wound infection which prevents normal wound healing.[247] To improve upon bacterial inhibition seen *in vivo* the development of a controlled release system of GaM such as PLGA microspheres could be utilized allow for sustained release within the therapeutic concentration range. Here, electrosprayed microspheres could be fabricated and release can be tuned through fabrication techniques or polymer composition. Fabrication parameters such as polymer concentration, solvent, and voltage are a few ways that microsphere size can be modulated.[263, 264] Smaller particles would provide a larger surface area to volume ratio which would correlate to faster release. In addition, release from these microspheres could be further tuned by modulating co-polymer concentrations of PLGA as widely demonstrated in literature.[265-268] Additionally, negative side effects were observed *in vivo* for dressings containing higher concentrations of GaM due to the high burst release. However, the sustained delivery at the targeted therapeutic range through the use of

microspheres has potential to overcome this limitation. Future studies investigating sustained release would need to balance GaM toxicity with therapeutic efficacy.

Development of a degradable polymer matrix for wound healing is one of the key requirements necessary for eliminating negative side effects, such as inflammation, due to residual dressing material left in the wound bed. We established a step-growth polymerization that tuned stoichiometric macromer ratios to get desired endgroup functionality. However; after further investigation of PEGDTT synthesis, it was discovered that there was a large distribution of heterogenous molecular weight species. Currently, we are investigating a two-step synthesis protocol to have improved control over stoichiometry and reaction products to develop monodisperse macromers. By controlling molecular weight through macromer synthesis we can better predict hydrogel degradation profiles and develop a tunable library of degradable PEGDTT macromers. This system has potential for use in several tissue engineering and regenerative medicine applications. The development of a library of tunable degradation profiles with various hydrogel properties (modulus and swelling ratio) could have a tremendous impact on the field. Additionally, preliminary work focused on the investigation of a simulated body fluid to predict *in vivo* degradation profiles in chronic wound environments. Initially, PEGDTT hydrogels degraded rapidly in this simulated body fluid and it was hypothesized that this solution over predicted *in vivo* degradation profiles. After comparison of the *in vitro* and *in vivo* degradation profiles it was noted that PBS did not accurately predict the *in vitro* degradation. Further investigation could be done to develop *in vitro* degradation conditions to identify a correlation between *in vivo* and *in vitro* degradation.

The incorporation of bioactivity utilizing Scl2 proteins has been investigated for their role in integrin mediated wound healing. We have established the tunability of these proteins to improve protein stability and modulate cell-material interactions. Through the development of this work, we observed batch variability due to production and isolation processes during protein expression. Current work being investigated includes protein monomer content, aggregation, protein stability, and cellular interactions. After confirmation of batch reproducibility, investigation of soluble protein loading and release from hydrogel scaffolds will be analyzed. *In vitro* assays such as CBQCA and BCA can be utilized to determine release rates and concentrations necessary for improved cellular interactions. Additionally, cell attachment, spreading, and proliferation on bioactive hydrogels of all geometries will then be assessed compared to a collagen control to assess cell-material interactions. Finally, murine and equine models could be used to evaluate this composite scaffold *in vivo.* Here, the evaluation of integrin binding utilizing histology and immunohistochemistry to evaluate wound vascularity, inflammatory cell infiltration, and granulation tissue formation could identify the integrin mediated effects. Investigation of the wound healing mechanisms due to Scl2 proteins can be utilized through investigation of wound cellular composition and wound transcriptional profile using flow cytometry and RNA-seq.

Lastly, each of these platforms have been established independently; however, in order to develop a functional wound dressing all of these components must be developed into a composite dressing and evaluated collectively. In addition to its antimicrobial activity, gallium maltolate has been shown to promote collagen synthesis and cell

migration, and favorably modulate integrin expression. The potential synergistic effect of GaM with Scl2 could not only allow for antimicrobial incorporation but also improve the active wound healing process by improving cellular interactions and resulting collagen synthesis. Equine distal wound models can be utilized to evaluate effect of integrin contribution and GaM contribution independently and synergistically to evaluate wound healing. Additionally, characterization of wound vascularity and inflammatory cell infiltration can be investigated through histological analysis. Finally, the incorporation of both an antimicrobial agent along with a bioactive protein serves to establish a novel biomaterial platform with multifaceted techniques for improved wound healing with bacterial inhibition.

Although additional studies and investigation is necessary to develop a combinatorial wound dressing for improved wound healing, the platforms established in this work illustrate independently, the ability to address the complex wound environment. First, a stable protein with improved cellular interactions to impart bioactivity with potential to improve cell-mediated wound closure was developed. Then a biodegradable hydrogel system that can be fabricated into various scaffold geometries to modulate wound fluid balance was established. Finally, gallium maltolate was incorporated into these hydrogel dressings and the antimicrobial properties in splinted wound models were demonstrated. In summary, this work provides technologies for improving wound healing through wound fluid maintenance, imparted bioactivity and antimicrobial activity, and tunable biodegradation.

REFERENCES

1. Frykberg, R.G. & Banks, J. Challenges in the treatment of chronic wounds. *Advances in wound care* **4**, 560-582 (2015).

2. Wu, S.C., Driver, V.R., Wrobel, J.S. & Armstrong, D.G. Foot ulcers in the diabetic patient, prevention and treatment. *Vascular health and risk management* **3**, 65 (2007).

3. Brownrigg, J., Apelqvist, J., Bakker, K., Schaper, N. & Hinchliffe, R. Evidence-based management of PAD & the diabetic foot. *European Journal of Vascular and Endovascular Surgery* **45**, 673-681 (2013).

4. Dickinson, L.E. & Gerecht, S. Engineered biopolymeric scaffolds for chronic wound healing. *Frontiers in Physiology* **7** (2016).

5. Singer, A.J. & Clark, R.A. Cutaneous wound healing. *New England journal of medicine* **341**, 738-746 (1999).

6. Huang, S. & Fu, X. Tissue-engineered skin: bottleneck or breakthrough. *Int J Burns Trauma* **1**, 1-10 (2011).

7. Sen, C.K. et al. Human Skin Wounds: A Major and Snowballing Threat to Public Health and the Economy. *Wound repair and regeneration : official publication of the Wound Healing Society [and] the European Tissue Repair Society* **17**, 763-771 (2009).

8. Guo, S.a. & DiPietro, L.A. Factors affecting wound healing. *Journal of dental research* **89**, 219-229 (2010).

9. Wound assessment: the patient and the wound. *Wound Essentials* **4**, 14-24 (2009).

10. Kearney, C.J. & Pandit, A. Special Collection: Closing the Gaps in Skin Wound Healing. *Tissue Engineering Part A* **22**, 401-402 (2016).

11. Radek, K.A., Ranzer, M.J. & DiPietro, L.A. Brewing complications: the effect of acute ethanol exposure on wound healing. *Journal of leukocyte biology* **86**, 1125-1134 (2009).

12. Martin, P. Wound healing--aiming for perfect skin regeneration. *Science* **276**, 75-81 (1997).

13. Kurkinen, M., Vaheri, A., Roberts, P. & Stenman, S. Sequential appearance of fibronectin and collagen in experimental granulation tissue. *Laboratory investigation; a journal of technical methods and pathology* **43**, 47-51 (1980).

14. Fukai, F., Suzuki, H., Suzuki, K., Tsugita, A. & Katayama, T. Rat plasma fibronectin contains two distinct chemotactic domains for fibroblastic cells. *Journal of Biological Chemistry* **266**, 8807-8813 (1991).

15. Grinnell, F., Feld, M. & Minter, D. Fibroblast adhesion to fibrinogen and fibrin substrata: requirement for cold-insoluble globulin (plasma fibronectin). *Cell* **19**, 517-525 (1980).

16. Diegelmann, R.F. & Evans, M.C. Wound healing: an overview of acute, fibrotic and delayed healing. *Front Biosci* **9**, 283-289 (2004).

17. Witte, M.B. & Barbul, A. General principles of wound healing. *Surgical Clinics of North America* **77**, 509-528 (1997).

18. Dovi, J.V., He, L.-K. & DiPietro, L.A. Accelerated wound closure in neutrophil-depleted mice. *Journal of leukocyte biology* **73**, 448-455 (2003).

19. DiPietro, L.A. Wound healing: the role of the macrophage and other immune cells. *Shock* **4**, 233-240 (1995).

20. DiPietro, L.A. & Polverini, P. Role of the macrophage in the positive and negative regulation of wound neovascularization. *Behring Institute Mitteilungen*, 238-247 (1993).

21. Dipietro, L.A., Reintjes, M.G., Low, Q.E., Levi, B. & Gamelli, R.L. Modulation of macrophage recruitment into wounds by monocyte chemoattractant protein-1. *Wound Repair and Regeneration* **9**, 28-33 (2001).

22. Falanga, V. in The Diabetic Foot 59-73 (Springer, 2002).

23. Boateng, J.S., Matthews, K.H., Stevens, H.N. & Eccleston, G.M. Wound healing dressings and drug delivery systems: a review. *Journal of pharmaceutical sciences* **97**, 2892-2923 (2008).

24. Gurtner, G.C., Werner, S., Barrandon, Y. & Longaker, M.T. Wound repair and regeneration. *Nature* **453**, 314-321 (2008).

25. Demidova-Rice, T.N., Hamblin, M.R. & Herman, I.M. Acute and impaired wound healing: pathophysiology and current methods for drug delivery, part 1: normal and chronic wounds: biology, causes, and approaches to care. *Advances in skin & wound care* **25**, 304 (2012).

26. Harding, K., Morris, H. & Patel, G. Science, medicine, and the future: healing chronic wounds. *BMJ: British Medical Journal* **324**, 160 (2002).

27. Barrick, B., Campbell, E.J. & Owen, C.A. Leukocyte proteinases in wound healing: roles in physiologic and pathologic processes. *Wound Repair and Regeneration* **7**, 410-422 (1999).

28. Hasan, A. et al. Dermal fibroblasts from venous ulcers are unresponsive to the action of transforming growth factor-β 11. *Journal of dermatological science* **16**, 59-66 (1997).

29. Stanley, A.C., Park, H.-Y., Phillips, T.J., Russakovsky, V. & Menzoian, J.O. Reduced growth of dermal fibroblasts from chronic venous ulcers can be stimulated with growth factors. *Journal of vascular surgery* **26**, 994-1001 (1997).

30. Higley, H., Ksander, G., Gerhardt, C. & Falanga, V. Extravasation of macromolecules and possible trapping of transforming growth factor-β in venous ulceration. *British journal of dermatology* **132**, 79-85 (1995).

31. Mast, B.A. & Schultz, G.S. Interactions of cytokines, growth factors, and proteases in acute and chronic wounds. *Wound Repair and Regeneration* **4**, 411-420 (1996).

32. James, G.A. et al. Biofilms in chronic wounds. *Wound Repair and regeneration* **16**, 37-44 (2008).

33. Robson, M.C. Wound infection: a failure of wound healing caused by an imbalance of bacteria. *Surgical Clinics* **77**, 637-650 (1997).

34. Tarnuzzer, R.W. & Schultz, G.S. Biochemical analysis of acute and chronic wound environments. *Wound Repair and Regeneration* **4**, 321-325 (1996).

35. Falanga, V. Wound healing and its impairment in the diabetic foot. *The Lancet* **366**, 1736-1743 (2005).

36. Zhong, S., Zhang, Y. & Lim, C. Tissue scaffolds for skin wound healing and dermal reconstruction. *Wiley Interdisciplinary Reviews: Nanomedicine and Nanobiotechnology* **2**, 510-525 (2010).

37. Naderi-Meshkin, H. et al. Critical Issues in Successful Production of Skin Substitutes for Wound Healing. *Cell Therapy and Regenerative Medicine Journal* **1**, 38-60 (2016).

38. Murphy, P.S. & Evans, G.R. Advances in wound healing: a review of current wound healing products. *Plastic surgery international* **2012** (2012).

39. Metcalfe, A.D. & Ferguson, M.W. Tissue engineering of replacement skin: the crossroads of biomaterials, wound healing, embryonic development, stem cells and regeneration. *Journal of the Royal Society Interface* **4**, 413-437 (2007).

40. Marston, W.A., Hanft, J., Norwood, P. & Pollak, R. The efficacy and safety of dermagraft in improving the healing of chronic diabetic foot ulcers results of a prospective randomized trial. *Diabetes Care* **26**, 1701-1705 (2003).

41. Chakrabarti, S.K., Bhattacharya, R. & Deb, K.D. Cell-based Wound Healing: Mechanisms and Treatments. *British Journal of Medicine and Medical Research* **11** (2016).

42. Hart, C.E., Loewen-Rodriguez, A. & Lessem, J. Dermagraft: use in the treatment of chronic wounds. *Advances in wound care* **1**, 138-141 (2012).

43. Hoffman, A.S. Hydrogels for biomedical applications. *Advanced drug delivery reviews* **64**, 18-23 (2012).

44. Peppas, N., Bures, P., Leobandung, W. & Ichikawa, H. Hydrogels in pharmaceutical formulations. *European journal of pharmaceutics and biopharmaceutics* **50**, 27-46 (2000).

45. Slaughter, B.V., Khurshid, S.S., Fisher, O.Z., Khademhosseini, A. & Peppas, N.A. Hydrogels in regenerative medicine. *Advanced materials* **21**, 3307-3329 (2009).

46. Zhu, J. Bioactive modification of poly(ethylene glycol) hydrogels for tissue engineering. *Biomaterials* **31**, 4639-4656 (2010).

47. Lee, K.Y. & Mooney, D.J. Hydrogels for tissue engineering. *Chemical reviews* **101**, 1869-1880 (2001).

48. Van Vlierberghe, S., Dubruel, P. & Schacht, E. Biopolymer-based hydrogels as scaffolds for tissue engineering applications: a review. *Biomacromolecules* **12**, 1387-1408 (2011).

49. Miller, T., Goude, M.C., McDevitt, T.C. & Temenoff, J.S. Molecular engineering of glycosaminoglycan chemistry for biomolecule delivery. *Acta Biomaterialia* **10**, 1705-1719 (2014).

50. Nicodemus, G.D. & Bryant, S.J. Cell encapsulation in biodegradable hydrogels for tissue engineering applications. *Tissue Engineering. Part B, Reviews* **14**, 149-165 (2008).

51. Burdick, J.A. & Anseth, K.S. Photoencapsulation of osteoblasts in injectable RGD-modified PEG hydrogels for bone tissue engineering. *Biomaterials* **23**, 4315-4323 (2002).

52. Schmedlen, R.H., Masters, K.S. & West, J.L. Photocrosslinkable polyvinyl alcohol hydrogels that can be modified with cell adhesion peptides for use in tissue engineering. *Biomaterials* **23**, 4325-4332 (2002).

53. Madden, L.R. et al. Proangiogenic scaffolds as functional templates for cardiac tissue engineering. *Proceedings of the National Academy of Sciences* **107**, 15211-15216 (2010).

54. Marshall, A.J. & Ratner, B.D. Quantitative characterization of sphere-templated porous biomaterials. *AIChE Journal* **51**, 1221-1232 (2005).

55. Gunn, J.W., Turner, S.D. & Mann, B.K. Adhesive and mechanical properties of hydrogels influence neurite extension. *Journal of Biomedical Materials Research Part A* **72A**, 91-97 (2005).

56. Hahn, M.S. et al. Photolithographic patterning of polyethylene glycol hydrogels. *Biomaterials* **27**, 2519-2524 (2006).

57. Kretlow, J.D. & Mikos, A.G. From material to tissue: Biomaterial development, scaffold fabrication, and tissue engineering. *AIChE Journal* **54**, 3048-3067 (2008).

58. Park, S., Lee, S. & Kim, W. Fabrication of hydrogel scaffolds using rapid prototyping for soft tissue engineering. *Macromol. Res.* **19**, 694-698 (2011).

59. Field, C.K. & Kerstein, M.D. Overview of wound healing in a moist environment. *The American journal of surgery* **167**, S2-S6 (1994).

60. Jones, A. & Vaughan, D. Hydrogel dressings in the management of a variety of wound types: A review. *Journal of Orthopaedic nursing* **9**, S1-S11 (2005).

61. Lewis, R., Whiting, P., ter Riet, G., O'Meara, S. & Glanville, J. A rapid and systematic review of the clinical effectiveness and cost-effectiveness of debriding agents in treating surgical wounds healing by secondary intention. (Core Research, 2001).

62. Parlato, M., Reichert, S., Barney, N. & Murphy, W.L. Poly (ethylene glycol) hydrogels with adaptable mechanical and degradation properties for use in biomedical applications. *Macromolecular bioscience* **14**, 687-698 (2014).

63. Zustiak, S.P. & Leach, J.B. Hydrolytically degradable poly (ethylene glycol) hydrogel scaffolds with tunable degradation and mechanical properties. *Biomacromolecules* **11**, 1348-1357 (2010).

64. Hudalla, G.A., Eng, T.S. & Murphy, W.L. An approach to modulate degradation and mesenchymal stem cell behavior in poly (ethylene glycol) networks. *Biomacromolecules* **9**, 842-849 (2008).

65. Benoit, D.S., Durney, A.R. & Anseth, K.S. Manipulations in hydrogel degradation behavior enhance osteoblast function and mineralized tissue formation. *Tissue engineering* **12**, 1663-1673 (2006).

66. Anderson, D.G. et al. A combinatorial library of photocrosslinkable and degradable materials. *Advanced Materials* **18**, 2614-2618 (2006).

67. Cereceres, S. et al. Chronic wound dressings based on collagen-mimetic proteins. *Advances in wound care* **4**, 444-456 (2015).

68. Safranski, D.L. et al. Effect of poly (ethylene glycol) diacrylate concentration on network properties and in vivo response of poly (β-amino ester) networks. *Journal of Biomedical Materials Research Part A* **96**, 320-329 (2011).

69. Brey, D.M., Erickson, I. & Burdick, J.A. Influence of macromer molecular weight and chemistry on poly (β-amino ester) network properties and initial cell interactions. *Journal of Biomedical Materials Research Part A* **85**, 731-741 (2008).

70. Biswal, D., Wattamwar, P.P., Dziubla, T.D. & Hilt, J.Z. A single-step polymerization method for poly (β-amino ester) biodegradable hydrogels. *Polymer* **52**, 5985-5992 (2011).

71. Zaquen, N., Wenn, B., Ranieri, K., Vandenbergh, J. & Junkers, T. Facile design of degradable poly (β-thioester) s with tunable structure and functionality. *Journal of Polymer Science Part A: Polymer Chemistry* **52**, 178-187 (2014).

72. Qiu, Y. et al. PEG-based hydrogels with tunable degradation characteristics to control delivery of marrow stromal cells for tendon overuse injuries. *Acta biomaterialia* **7**, 959-966 (2011).

73. van de Wetering, P., Metters, A.T., Schoenmakers, R.G. & Hubbell, J.A. Poly(ethylene glycol) hydrogels formed by conjugate addition with controllable swelling, degradation, and release of pharmaceutically active proteins. *Journal of Controlled Release* **102**, 619-627 (2005).

74. Hao, Y. & Lin, C.C. Degradable thiol-acrylate hydrogels as tunable matrices for three-dimensional hepatic culture. *Journal of Biomedical Materials Research Part A* **102**, 3813-3827 (2014).

75. Jongpaiboonkit, L. et al. An adaptable hydrogel array format for 3-dimensional cell culture and analysis. *Biomaterials* **29**, 3346-3356 (2008).

76. King, W.J., Jongpaiboonkit, L. & Murphy, W.L. Influence of FGF2 and PEG hydrogel matrix properties on hMSC viability and spreading. *Journal of biomedical materials research Part A* **93**, 1110-1123 (2010).

77. Jongpaiboonkit, L., King, W.J. & Murphy, W.L. Screening for 3D environments that support human mesenchymal stem cell viability using hydrogel arrays. *Tissue Engineering Part A* **15**, 343-353 (2008).

78. Xu, S. et al. Generation of monodisperse particles by using microfluidics: control over size, shape, and composition. *Angewandte Chemie* **117**, 734-738 (2005).

79. Jeong, B., Bae, Y.H. & Kim, S.W. Thermoreversible gelation of PEG− PLGA− PEG triblock copolymer aqueous solutions. *Macromolecules* **32**, 7064-7069 (1999).

80. Ibusuki, S., Fujii, Y., Iwamoto, Y. & Matsuda, T. Tissue-engineered cartilage using an injectable and in situ gelable thermoresponsive gelatin: fabrication and in vitro performance. *Tissue Engineering* **9**, 371-384 (2003).

81. Yeh, J. et al. Micromolding of shape-controlled, harvestable cell-laden hydrogels. *Biomaterials* **27**, 5391-5398 (2006).

82. Liu, V.A. & Bhatia, S.N. Three-dimensional photopatterning of hydrogels containing living cells. *Biomedical microdevices* **4**, 257-266 (2002).

83. Dendukuri, D., Pregibon, D.C., Collins, J., Hatton, T.A. & Doyle, P.S. Continuous-flow lithography for high-throughput microparticle synthesis. *Nature materials* **5**, 365 (2006).

84. Reis, C.P., Ribeiro, A.J., Neufeld, R.J. & Veiga, F. Alginate microparticles as novel carrier for oral insulin delivery. *Biotechnology and bioengineering* **96**, 977-989 (2007).

85. Chen, J., Park, H. & Park, K. Synthesis of superporous hydrogels: hydrogels with fast swelling and superabsorbent properties. *Journal of Biomedical Materials Research: An Official Journal of The Society for Biomaterials, The Japanese Society for Biomaterials, and the Australian Society for Biomaterials* **44**, 53-62 (1999).

86. Zhu, W. et al. 3D printing of functional biomaterials for tissue engineering. *Current opinion in biotechnology* **40**, 103-112 (2016).

87. Billiet, T., Vandenhaute, M., Schelfhout, J., Van Vlierberghe, S. & Dubruel, P. A review of trends and limitations in hydrogel-rapid prototyping for tissue engineering. *Biomaterials* **33**, 6020-6041 (2012).

88. Dhandayuthapani, B., Yoshida, Y., Maekawa, T. & Kumar, D.S. Polymeric scaffolds in tissue engineering application: a review. *International Journal of Polymer Science* **2011** (2011).

89. Parlato, M., Johnson, A., Hudalla, G.A. & Murphy, W.L. Adaptable poly (ethylene glycol) microspheres capable of mixed-mode degradation. *Acta biomaterialia* **9**, 9270-9280 (2013).

90. Khurshid, M.F., Hussain, T., Masood, R. & Hussain, N. Development and evaluation of a controlled drug delivery wound dressing based on polymeric porous microspheres. *Journal of Industrial Textiles*, 1528083715612231 (2015).

91. Midha, K., Nagpal, M. & Arora, S. Microspheres: A recent update. *International Journal of Recent Scientific Research* **Vol. 6**, pp.5859-5867 (2015).

92. Hong, S., Hsu, H.-J., Kaunas, R. & Kameoka, J. Collagen microsphere production on a chip. *Lab on a Chip* **12**, 3277-3280 (2012).

93. Zeng, Y. et al. Preformed gelatin microcryogels as injectable cell carriers for enhanced skin wound healing. *Acta biomaterialia* **25**, 291-303 (2015).

94. Tan, H. & Marra, K.G. Injectable, biodegradable hydrogels for tissue engineering applications. *Materials* **3**, 1746-1767 (2010).

95. Yu, L. & Ding, J. Injectable hydrogels as unique biomedical materials. *Chemical Society Reviews* **37**, 1473-1481 (2008).

96. Yusof, N.L.B.M., Lim, L.Y. & Khor, E. Preparation and characterization of chitin beads as a wound dressing precursor. *Journal of Biomedical Materials Research Part A* **54**, 59-68 (2001).

97. Annabi, N. et al. Controlling the porosity and microarchitecture of hydrogels for tissue engineering. *Tissue Engineering Part B: Reviews* **16**, 371-383 (2010).

98. Chen, J. & Park, K. Synthesis and characterization of superporous hydrogel composites. *Journal of Controlled Release* **65**, 73-82 (2000).

99. Huh, K.M., Baek, N. & Park, K. Enhanced swelling rate of poly (ethylene glycol)-grafted superporous hydrogels. *Journal of bioactive and compatible polymers* **20**, 231-243 (2005).

100. Bedel, N.S., Tezcan, M., Ceylan, O., Gurdag, G. & Cicek, H. Effects of pore morphology and size on antimicrobial activity of chitosan/poly (ethylene glycol) diacrylate macromer semi-IPN hydrogels. *Journal of Applied Polymer Science* **132** (2015).

101. Zellander, A., Kadakia-Bhasin, A., Mahksous, M. & Cho, M. Mechanical Diversity of Porous Poly (Ethylene Glycol) Diacrylate. *Adv. Biomed. Eng. Res.* **1**, 9 (2013).

102. Sannino, A. et al. Synthesis and characterization of macroporous poly (ethylene glycol)-based hydrogels for tissue engineering application. *Journal of Biomedical Materials Research Part A* **79**, 229-236 (2006).

103. Keskar, V., Gandhi, M., Gemeinhart, E.J. & Gemeinhart, R.A. Initial evaluation of vascular ingrowth into superporous hydrogels. *Journal of tissue engineering and regenerative medicine* **3**, 486-490 (2009).

104. Alge, D.L. & Anseth, K.S. Bioactive hydrogels: Lighting the way. *Nature materials* **12**, 950 (2013).

105. Hynes, R.O. The extracellular matrix: not just pretty fibrils. *Science* **326**, 1216-1219 (2009).

106. Bennett, N.T. & Schultz, G.S. Growth factors and wound healing: Part II. Role in normal and chronic wound healing. *The American Journal of Surgery* **166**, 74-81 (1993).

107. Chen, W.J., Rogers, A.A. & Lydon, M.J. Characterization of biologic properties of wound fluid collected during early stages of wound healing. *Journal of Investigative Dermatology* **99**, 559-564 (1992).

108. Nanney, L.B. & King Jr, L.E. in The molecular and cellular biology of wound repair 171-194 (Springer, 1988).

109. Rappolee, D.A., Mark, D., Banda, M.J. & Werb, Z. Wound macrophages express TGF-a and other growth factors in vivo: analysis by mRNA phenotyping. *Science* **241**, 708-712 (1988).

110. Werner, S. et al. Large induction of keratinocyte growth factor expression in the dermis during wound healing. *Proceedings of the National Academy of Sciences* **89**, 6896-6900 (1992).

111. Abraham, J.A. & Klagsbrun, M. in The molecular and cellular biology of wound repair 195-248 (Springer, 1988).

112. Eriksson, A., Siegbahn, A., Westermark, B., Heldin, C. & Claesson-Welsh, L. PDGF alpha-and beta-receptors activate unique and common signal transduction pathways. *The EMBO journal* **11**, 543 (1992).

113. Marikovsky, M. et al. Appearance of heparin-binding EGF-like growth factor in wound fluid as a response to injury. *Proceedings of the National Academy of Sciences* **90**, 3889-3893 (1993).

114. Brown, L.F. et al. Expression of vascular permeability factor (vascular endothelial growth factor) by epidermal keratinocytes during wound healing. *The Journal of experimental medicine* **176**, 1375-1379 (1992).

115. Werner, S. & Grose, R. Regulation of wound healing by growth factors and cytokines. *Physiological reviews* **83**, 835-870 (2003).

116. Steed, D.L. The role of growth factors in wound healing. *Surgical Clinics* **77**, 575-586 (1997).

117. Lai, H.-J. et al. Tailored design of electrospun composite nanofibers with staged release of multiple angiogenic growth factors for chronic wound healing. *Acta biomaterialia* **10**, 4156-4166 (2014).

118. Xie, Z. et al. Dual growth factor releasing multi-functional nanofibers for wound healing. *Acta biomaterialia* **9**, 9351-9359 (2013).

119. Andreopoulos, F.M. & Persaud, I. Delivery of basic fibroblast growth factor (bFGF) from photoresponsive hydrogel scaffolds. *Biomaterials* **27**, 2468-2476 (2006).

120. Yamamoto, M., Ikada, Y. & Tabata, Y. Controlled release of growth factors based on biodegradation of gelatin hydrogel. *Journal of Biomaterials Science, Polymer Edition* **12**, 77-88 (2001).

121. Babensee, J.E., McIntire, L.V. & Mikos, A.G. Growth factor delivery for tissue engineering. *Pharmaceutical research* **17**, 497-504 (2000).

122. Silva, E. & Mooney, D. Spatiotemporal control of vascular endothelial growth factor delivery from injectable hydrogels enhances angiogenesis. *Journal of Thrombosis and Haemostasis* **5**, 590-598 (2007).

123. Abair, T.D. et al. Functional analysis of the cytoplasmic domain of the integrin α1 subunit in endothelial cells. *Blood* **112**, 3242-3254 (2008).

124. Shi, M. et al. Enhancing integrin alpha1 inserted (I) domain affinity to ligand potentiates integrin alpha1beta1-mediated down-regulation of collagen synthesis. *The Journal of biological chemistry* **287**, 35139-35152 (2012).

125. Teige, I. et al. Induced keratinocyte hyper-proliferation in α2β1 integrin transgenic mice results in systemic immune cell activation. *International immunopharmacology* **10**, 107-114 (2010).

126. Zhang, Z.-G. et al. Interactions of primary fibroblasts and keratinocytes with extracellular matrix proteins: contribution of α2β1 integrin. *Journal of cell science* **119**, 1886-1895 (2006).

127. Senger, D.R. et al. The α 1 β 1 and α 2 β 1 integrins provide critical support for vascular endothelial growth factor signaling, endothelial cell migration, and tumor angiogenesis. *The American journal of pathology* **160**, 195-204 (2002).

128. Zweers, M.C. et al. Integrin α2β1 is required for regulation of murine wound angiogenesis but is dispensable for reepithelialization. *Journal of Investigative Dermatology* **127**, 467-478 (2007).

129. Pozzi, A., Wary, K.K., Giancotti, F.G. & Gardner, H.A. Integrin α1β1 mediates a unique collagen-dependent proliferation pathway in vivo. *The Journal of cell biology* **142**, 587-594 (1998).

130. Adams, J.C. & Watt, F.M. Expression of beta 1, beta 3, beta 4, and beta 5 integrins by human epidermal keratinocytes and non-differentiating keratinocytes. *The Journal of Cell Biology* **115**, 829-841 (1991).

131. Sebra, R.P., Masters, K.S., Bowman, C.N. & Anseth, K.S. Surface grafted antibodies: controlled architecture permits enhanced antigen detection. *Langmuir* **21**, 10907-10911 (2005).

132. West, J.L. & Hubbell, J.A. Polymeric biomaterials with degradation sites for proteases involved in cell migration. *Macromolecules* **32**, 241-244 (1999).

133. Mann, B.K., Gobin, A.S., Tsai, A.T., Schmedlen, R.H. & West, J.L. Smooth muscle cell growth in photopolymerized hydrogels with cell adhesive and proteolytically degradable domains: synthetic ECM analogs for tissue engineering. *Biomaterials* **22**, 3045-3051 (2001).

134. Lutolf, M. & Hubbell, J. Synthesis and physicochemical characterization of end-linked poly (ethylene glycol)-co-peptide hydrogels formed by Michael-type addition. *Biomacromolecules* **4**, 713-722 (2003).

135. Seliktar, D., Zisch, A., Lutolf, M., Wrana, J. & Hubbell, J. MMP-2 sensitive, VEGF-bearing bioactive hydrogels for promotion of vascular healing. *Journal of Biomedical Materials Research Part A* **68**, 704-716 (2004).

136. Aimetti, A.A., Machen, A.J. & Anseth, K.S. Poly (ethylene glycol) hydrogels formed by thiol-ene photopolymerization for enzyme-responsive protein delivery. *Biomaterials* **30**, 6048-6054 (2009).

137. DeForest, C.A., Polizzotti, B.D. & Anseth, K.S. Sequential click reactions for synthesizing and patterning three-dimensional cell microenvironments. *Nature materials* **8**, 659 (2009).

138. Miller, J.S. et al. Bioactive hydrogels made from step-growth derived PEG–peptide macromers. *Biomaterials* **31**, 3736-3743 (2010).

139. An, B., Kaplan, D.L. & Brodsky, B. Engineered recombinant bacterial collagen as an alternative collagen-based biomaterial for tissue engineering. *Protein engineering and other bio-synthetic routes for bio-based materials: Current uses and potential applications*, 33 (2007).

140. Ramshaw, J.A. Biomedical applications of collagens. *Journal of Biomedical Materials Research Part B: Applied Biomaterials* (2015).

141. Xu, Y., Keene, D.R., Bujnicki, J.M., Höök, M. & Lukomski, S. Streptococcal Scl1 and Scl2 proteins form collagen-like triple helices. *Journal of Biological Chemistry* **277**, 27312-27318 (2002).

142. Fu, X., Li, X., Cheng, B., Chen, W. & Sheng, Z. Engineered growth factors and cutaneous wound healing: success and possible questions in the past 10 years. *Wound repair and regeneration* **13**, 122-130 (2005).

143. Koivisto, L., Heino, J., Häkkinen, L. & Larjava, H. Integrins in wound healing. *Advances in wound care* **3**, 762-783 (2014).

144. Hynes, R.O. Integrins: versatility, modulation, and signaling in cell adhesion. *Cell* **69**, 11-25 (1992).

145. Humtsoe, J.O. et al. A streptococcal collagen-like protein interacts with the α2β1 integrin and induces intracellular signaling. *Journal of Biological Chemistry* **280**, 13848-13857 (2005).

146. Seo, N. et al. An engineered α1 integrin-binding collagenous sequence. *Journal of Biological Chemistry* **285**, 31046-31054 (2010).

147. An, B., Lin, Y.-S. & Brodsky, B. Collagen interactions: Drug design and delivery. *Advanced Drug Delivery Reviews* **97**, 69-84 (2016).

148. Cosgriff-Hernandez, E. et al. Bioactive hydrogels based on designer collagens. *Acta biomaterialia* **6**, 3969-3977 (2010).

149. Siddiqui, A.R. & Bernstein, J.M. Chronic wound infection: Facts and controversies. *Clinics in Dermatology* **28**, 519-526 (2010).

150. Kingsley, A. The wound infection continuum and its application to clinical practice. *Ostomy/wound management* **49**, 1-7 (2003).

151. Percival, S., Bowler, P. & Russell, D. Bacterial resistance to silver in wound care. *Journal of hospital infection* **60**, 1-7 (2005).

152. Atiyeh, B.S., Costagliola, M., Hayek, S.N. & Dibo, S.A. Effect of silver on burn wound infection control and healing: review of the literature. *burns* **33**, 139-148 (2007).

153. Lansdown, A.B. A review of the use of silver in wound care: facts and fallacies. *British journal of nursing* **13** (2004).

154. Lo, S.F., Hayter, M., Chang, C.J., Hu, W.Y. & Lee, L.L. A systematic review of silver-releasing dressings in the management of infected chronic wounds. *Journal of clinical nursing* **17**, 1973-1985 (2008).

155. Khundkar, R., Malic, C. & Burge, T. Use of Acticoat™ dressings in burns: what is the evidence? *Burns* **36**, 751-758 (2010).

156. Liedberg, H. & Lundeberg, T. Assessment of silver-coated urinary catheter toxicity by cell culture. *Urological research* **17**, 359-360 (1989).

157. Lam, P., Chan, E., Ho, W. & Liew, C. In vitro cytotoxicity testing of a nanocrystalline silver dressing (Acticoat) on cultured keratinocytes. *British journal of biomedical science* **61**, 125-127 (2004).

158. Leaper, D.J. & Durani, P. Topical antimicrobial therapy of chronic wounds healing by secondary intention using iodine products. *International Wound Journal* **5**, 361-368 (2008).

159. Thorn, R., Austin, A., Greenman, J., Wilkins, J. & Davis, P. In vitro comparison of antimicrobial activity of iodine and silver dressings against biofilms. *Journal of wound care* **18**, 343-346 (2009).

160. Morgan, J.P., Haug, R.H. & Kosman, J.W. Antimicrobial skin preparations for the maxillofacial region. *Journal of oral and maxillofacial surgery* **54**, 89-94 (1996).

161. Cooper, R.A. Iodine revisited. *International wound journal* **4**, 124-137 (2007).

162. Wang, L. et al. Hypochlorous acid as a potential wound care agent. *Journal of burns and wounds* **6**, 65-79 (2007).

163. Robson, M.C. et al. Hypochlorous acid as a potential wound care agent. *J Burns Wounds* **6**, 80-90 (2007).

164. Lineaweaver, W., Howard, R., Soucy, D. & et al. Topical antimicrobial toxicity. *Archives of Surgery* **120**, 267-270 (1985).

165. Bernstein, L.R., Tanner, T., Godfrey, C. & Noll, B. Chemistry and pharmacokinetics of gallium maltolate, a compound with high oral gallium bioavailability. *Metal-Based Drugs* **7**, 33 (2000).

166. Martens, R.J. et al. Pharmacokinetics of gallium maltolate after intragastric administration in neonatal foals. *American journal of veterinary research* **68**, 1041-1044 (2007).

167. Harrington, J., Martens, R., Cohen, N. & Bernstein, L. Antimicrobial activity of gallium against virulent Rhodococcus equiin vitro and in vivo. *Journal of veterinary pharmacology and therapeutics* **29**, 121-127 (2006).

168. Coleman, M. et al. In vitro antimicrobial activity of gallium maltolate against virulent Rhodococcus equi. *Veterinary microbiology* **146**, 175-178 (2010).

169. Baldoni, D., Steinhuber, A., Zimmerli, W. & Trampuz, A. In vitro activity of gallium maltolate against Staphylococci in logarithmic, stationary, and biofilm growth phases: comparison of conventional and calorimetric susceptibility testing methods. *Antimicrobial agents and chemotherapy* **54**, 157-163 (2010).

170. Arnold, C.E. et al. Antimicrobial activity of gallium maltolate against Staphylococcus aureus and methicillin-resistant S. aureus and Staphylococcus pseudintermedius: an in vitro study. *Veterinary microbiology* **155**, 389-394 (2012).

171. Martens, R. et al. Gallium maltolate: safety in neonatal foals following multiple enteral administrations. *Journal of veterinary pharmacology and therapeutics* **33**, 208-212 (2010).

172. Bernstein, L.R. in Encyclopedia of Metalloproteins 823-835 (Springer, 2013).

173. Bernstein, L.R. Mechanisms of therapeutic activity for gallium. *Pharmacological reviews* **50**, 665-682 (1998).

174. Goncalves, J. et al. Gallium nitrate accelerates partial thickness wound repair and alters keratinocyte integrin expression to favor a motile phenotype. *Journal of Surgical Research* **103**, 134-140 (2002).

175. Bockman, R.S., Guidon, P.T., Pan, L.C., Salvatori, R. & Kawaguchi, A. Gallium nitrate increases type I collagen and fibronectin mRNA and collagen protein levels in bone and fibroblast cells. *Journal of cellular biochemistry* **52**, 396-403 (1993).

176. Boulton, A. The Global Burden of Diabetic Foot Disease. *Diabetic Microvascular Complications Today* **1**, 23-25 (2008).

177. Edwards, J. & Stapley, S. Debridement of diabetic foot ulcers. *Cochrane Database Syst Rev*, CD003556 (2010).

178. Prevention, C.f.D.C.a. National Diabetes Fact Sheet: National estimates and general informaiton on diabetes and pre-diabetes in the United States, 2011. *US Department of Health and Human Service, Centers for Disease Control and Prevention* (2011).

179. Mansbridge, J., Liu, K., Patch, R., Symons, K. & Pinney, E. Three-dimensional fibroblast culture implant for the treatment of diabetic foot ulcers: Metabolic activity and therapeutic range. *Tissue Engineering* **4**, 403-414 (1998).

180. Brodsky, B. & Persikov, A.V. Molecular structure of the collagen triple helix. *Advances in protein chemistry* **70**, 301-339 (2005).

181. Han, R. et al. Assessment of prokaryotic collagen-like sequences derived from streptococcal Scl1 and Scl2 proteins as a source of recombinant GXY polymers. *Applied microbiology and biotechnology* **72**, 109-115 (2006).

182. FDA Federal Register. *Department of Health and Human Services* **72**, 1581-1619 (2007).

183. Yu, Z. et al. Noncollagenous region of the streptococcal collagen-like protein is a trimerization domain that supports refolding of adjacent homologous and heterologous collagenous domains. *Protein science : a publication of the Protein Society* **19**, 775-785 (2010).

184. Yu, Z., Brodsky, B. & Inouye, M. Dissecting a bacterial collagen domain from Streptococcus pyogenes: sequence and length-dependent variations in triple helix

stability and folding. *The Journal of biological chemistry* **286**, 18960-18968 (2011).

185. Yoshizumi, A. et al. Self-association of streptococcus pyogenes collagen-like constructs into higher order structures. *Protein science : a publication of the Protein Society* **18**, 1241-1251 (2009).

186. Seo, N. et al. An engineered alpha1 integrin-binding collagenous sequence. *The Journal of biological chemistry* **285**, 31046-31054 (2010).

187. Peng, Y.Y. et al. A Streptococcus pyogenes derived collagen-like protein as a non-cytotoxic and non-immunogenic cross-linkable biomaterial. *Biomaterials* **31**, 2755-2761 (2010).

188. Peng, Y.Y. et al. Towards scalable production of a collagen-like protein from Streptococcus pyogenes for biomedical applications. *Microbial cell factories* **11**, 146 (2012).

189. Mohs, A. et al. Mechanism of stabilization of a bacterial collagen triple helix in the absence of hydroxyproline. *The Journal of biological chemistry* **282**, 29757-29765 (2007).

190. Hoe, N.P., Lukomska, E., Musser, J.M. & Lukomski, S. Characterization of the immune response to collagen-like proteins Scl1 and Scl2 of serotype M1 and M28 group A Streptococcus. *FEMS microbiology letters* **277**, 142-149 (2007).

191. Browning, M.B. et al. Multilayer vascular grafts based on collagen-mimetic hydrogels. *Acta Biomaterialia* **8**, 1010-1021 (2012).

192. Biomaterials, S.f., Vol. 2013 (2011).

193. Persikov, A.V., Ramshaw, J.A. & Brodsky, B. Prediction of collagen stability from amino acid sequence. *The Journal of biological chemistry* **280**, 19343-19349 (2005).

194. Peng, Y.Y., Stoichevska, V., Schacht, K., Werkmeister, J.A. & Ramshaw, J.A. Engineering multiple biological functional motifs into a blank collagen-like protein template from Streptococcus pyogenes. *Journal of biomedical materials research. Part A* (2013).

195. Pozzi, A., Wary, K.K., Giancotti, F.G. & Gardner, H.A. Integrin alpha1beta1 mediates a unique collagen-dependent proliferation pathway in vivo. *J Cell Biol* **142**, 587-594 (1998).

196. Gardner, H., Broberg, A., Pozzi, A., Laato, M. & Heino, J. Absence of integrin alpha1beta1 in the mouse causes loss of feedback regulation of collagen synthesis in normal and wounded dermis. *J Cell Sci* **112 (Pt 3)**, 263-272 (1999).

197. Emsley, J., Knight, C.G., Farndale, R.W., Barnes, M.J. & Liddington, R.C. Structural basis of collagen recognition by integrin alpha2beta1. *Cell* **101**, 47-56 (2000).

198. Knight, C.G. et al. The collagen-binding A-domains of integrins alpha(1)beta(1) and alpha(2)beta(1) recognize the same specific amino acid sequence, GFOGER, in native (triple-helical) collagens. *The Journal of biological chemistry* **275**, 35-40 (2000).

199. Senger, D.R. et al. The alpha(1)beta(1) and alpha(2)beta(1) integrins provide critical support for vascular endothelial growth factor signaling, endothelial cell migration, and tumor angiogenesis. *Am J Pathol* **160**, 195-204 (2002).

200. Emsley, J., Knight, C.G., Farndale, R.W. & Barnes, M.J. Structure of the integrin alpha2beta1-binding collagen peptide. *Journal of molecular biology* **335**, 1019-1028 (2004).

201. Grenache, D.G. et al. Wound healing in the alpha2beta1 integrin-deficient mouse: altered keratinocyte biology and dysregulated matrix metalloproteinase expression. *The Journal of investigative dermatology* **127**, 455-466 (2007).

202. Parks, W.C. What is the alpha2beta1 integrin doing in the epidermis? *The Journal of investigative dermatology* **127**, 264-266 (2007).

203. Zweers, M.C. et al. Integrin alpha2beta1 is required for regulation of murine wound angiogenesis but is dispensable for reepithelialization. *The Journal of investigative dermatology* **127**, 467-478 (2007).

204. Teige, I. et al. Induced keratinocyte hyper-proliferation in alpha2beta1 integrin transgenic mice results in systemic immune cell activation. *Int Immunopharmacol* **10**, 107-114 (2010).

205. Browning, M.B., Russell, B., Rivera, J., Hook, M. & Cosgriff-Hernandez, E.M. Bioactive hydrogels with enhanced initial and sustained cell interactions. *Biomacromolecules* **14**, 2225-2233 (2013).

206. Franco, C., Price, J. & West, J. Development and optimization of a dual-photoinitiator, emulsion-based technique for rapid generation of cell-laden hydrogel microspheres. *Acta biomaterialia* **7**, 3267-3276 (2011).

207. Christopher, G.F. & Anna, S.L. Microfluidic methods for generating continuous droplet streams. *J. Phys. D: Appl. Phys.* **40**, R319-R336 (2007).

208. Young, C., Rozario, K., Serra, C., Poole-Warren, L. & Martens, P. Poly(vinyl alcohol)-heparin biosynthetic microspheres produced by microfluidics and ultraviolet photopolymerisation. *Biomicrofluidics* **7**, 1-13 (2013).

209. Gokmen, M.T., Van Camp, W., Colver, P.J., Bon, S.A.F. & Du Prez, F.E. Fabrication of porous "clickable" polymer beads and rods through generation of high internal phase emulsion (HIPE) droplets in a simple microfluidic device. *Macromolecules* **42**, 9289-9294 (2009).

210. An, B. et al. The influence of specific binding of collagen-silk chimeras to silk biomaterials on hMSC behavior. *Biomaterials* **34**, 402-412 (2013).

211. Rich, R.L. et al. Trench-shaped binding sites promote multiple classes of interactions between collagen and the adherence receptors, alpha(1)beta(1) integrin and Staphylococcus aureus cna MSCRAMM. *The Journal of biological chemistry* **274**, 24906-24913 (1999).

212. Leikina, E., Mertts, M.V., Kuznetsova, N. & Leikin, S. Type I collagen is thermally unstable at body temperature. *PNAS* **99**, 1314–1318 (2001).

213. Peppas, N.A., Hilt, J.Z., Khademhosseini, A. & Langer, R. Hydrogels in biology and medicine: from molecular principles to bionanotechnology. *Advanced materials* **18**, 1345-1360 (2006).

214. Censi, R. et al. A Printable Photopolymerizable Thermosensitive p (HPMAm-lactate)-PEG Hydrogel for Tissue Engineering. *Advanced Functional Materials* **21**, 1833-1842 (2011).

215. DeFail, A.J., Chu, C.R., Izzo, N. & Marra, K.G. Controlled release of bioactive TGF-β1 from microspheres embedded within biodegradable hydrogels. *Biomaterials* **27**, 1579-1585 (2006).

216. Browning, M., Cereceres, S., Luong, P. & Cosgriff-Hernandez, E. Determination of the in vivo degradation mechanism of PEGDA hydrogels. *Journal of Biomedical Materials Research Part A* **102**, 4244-4251 (2014).

217. Browning, M., Wilems, T., Hahn, M. & Cosgriff-Hernandez, E. Compositional control of poly (ethylene glycol) hydrogel modulus independent of mesh size. *Journal of Biomedical Materials Research Part A* **98**, 268-273 (2011).

218. Hubbell, J.A. Bioactive biomaterials. *Current Opinion in Biotechnology* **10**, 123-129 (1999).

219. Kharkar, P.M., Kiick, K.L. & Kloxin, A.M. Designing degradable hydrogels for orthogonal control of cell microenvironments. *Chemical Society Reviews* **42**, 7335-7372 (2013).

220. Metters, A.T., Anseth, K.S. & Bowman, C.N. Fundamental studies of a novel, biodegradable PEG-b-PLA hydrogel. *Polymer* **41**, 3993-4004 (2000).

221. Lutolf, M. et al. Synthetic matrix metalloproteinase-sensitive hydrogels for the conduction of tissue regeneration: engineering cell-invasion characteristics. *Proceedings of the National Academy of Sciences* **100**, 5413-5418 (2003).

222. Franssen, O., Vos, O.P. & Hennink, W.E. Delayed release of a model protein from enzymatically-degrading dextran hydrogels. *Journal of Controlled Release* **44**, 237-245 (1997).

223. Brandl, F.P., Seitz, A.K., Teßmar, J.K., Blunk, T. & Göpferich, A.M. Enzymatically degradable poly (ethylene glycol) based hydrogels for adipose tissue engineering. *Biomaterials* **31**, 3957-3966 (2010).

224. Yeung, T. et al. Effects of substrate stiffness on cell morphology, cytoskeletal structure, and adhesion. *Cytoskeleton* **60**, 24-34 (2005).

225. Engler, A.J., Sen, S., Sweeney, H.L. & Discher, D.E. Matrix elasticity directs stem cell lineage specification. *Cell* **126**, 677-689 (2006).

226. Wen, J.H. et al. Interplay of matrix stiffness and protein tethering in stem cell differentiation. *Nature materials* **13**, 979 (2014).

227. Peyton, S.R. & Putnam, A.J. Extracellular matrix rigidity governs smooth muscle cell motility in a biphasic fashion. *Journal of cellular physiology* **204**, 198-209 (2005).

228. Anseth, K.S., Bowman, C.N. & Brannon-Peppas, L. Mechanical properties of hydrogels and their experimental determination. *Biomaterials* **17**, 1647-1657 (1996).

229. Metters, A. & Hubbell, J. Network formation and degradation behavior of hydrogels formed by Michael-type addition reactions. *Biomacromolecules* **6**, 290-301 (2005).

230. Browning, M.B. & Cosgriff-Hernandez, E. Development of a biostable replacement for PEGDA hydrogels. *Biomacromolecules* **13**, 779-786 (2012).

231. Li, Q. et al. Biodegradable and photocrosslinkable polyphosphoester hydrogel. *Biomaterials* **27**, 1027-1034 (2006).

232. Lo, C.-M., Wang, H.-B., Dembo, M. & Wang, Y.-l. Cell movement is guided by the rigidity of the substrate. *Biophysical journal* **79**, 144-152 (2000).

233. DeForest, C.A. & Anseth, K.S. Advances in bioactive hydrogels to probe and direct cell fate. *Annual review of chemical and biomolecular engineering* **3**, 421-444 (2012).

234. Suggs, L.J. et al. In vitro and in vivo degradation of poly (propylene fumarate-co-ethylene glycol) hydrogels. *Journal of Biomedical Materials Research: An Official Journal of The Society for Biomaterials, The Japanese Society for Biomaterials, and the Australian Society for Biomaterials* **42**, 312-320 (1998).

235. Gjødsbøl, K. et al. Multiple bacterial species reside in chronic wounds: a longitudinal study. *International wound journal* **3**, 225-231 (2006).

236. Falabella, A.F. Debridement and wound bed preparation. *Dermatologic therapy* **19**, 317-325 (2006).

237. Seaman, S. Dressing selection in chronic wound management. *Journal of the American Podiatric Medical Association* **92**, 24-33 (2002).

238. Andersson, D.I. Persistence of antibiotic resistant bacteria. *Current opinion in microbiology* **6**, 452-456 (2003).

239. Hancock, R. & Patrzykat, A. Clinical development of cationic antimicrobial peptides: from natural to novel antibiotics. *Current drug targets-Infectious disorders* **2**, 79-83 (2002).

240. Zubair, M., Malik, A. & Ahmad, J. Clinico-microbiological study and antimicrobial drug resistance profile of diabetic foot infections in North India. *The Foot* **21**, 6-14 (2011).

241. BSc, R.M.S.T., BSc, A.J.A., PhD, J.G., J.P.G. Wilkins MA , F. & P.J. Davis PhD, C., FIBiol In vitro comparison of antimicrobial activity of iodine and silver dressings against biofilms. *Journal of Wound Care* **18**, 343-346 (2009).

242. DeLeon, K. et al. Gallium maltolate treatment eradicates Pseudomonas aeruginosa infection in thermally injured mice. *Antimicrobial agents and chemotherapy* **53**, 1331-1337 (2009).

243. Fairbanks, B.D., Schwartz, M.P., Bowman, C.N. & Anseth, K.S. Photoinitiated polymerization of PEG-diacrylate with lithium phenyl-2, 4, 6-trimethylbenzoylphosphinate: polymerization rate and cytocompatibility. *Biomaterials* **30**, 6702-6707 (2009).

244. Schütz, K. et al. Three-dimensional plotting of a cell-laden alginate/methylcellulose blend: towards biofabrication of tissue engineering constructs with clinically relevant dimensions. *Journal of tissue engineering and regenerative medicine* **11**, 1574-1587 (2017).

245. Xavier, J.R. et al. Bioactive nanoengineered hydrogels for bone tissue engineering: a growth-factor-free approach. *ACS nano* **9**, 3109-3118 (2015).

246. Andrews, J.M. Determination of minimum inhibitory concentrations. *Journal of antimicrobial Chemotherapy* **48**, 5-16 (2001).

247. Robson, M.C., Mannari, R.J., Smith, P.D. & Payne, W.G. Maintenance of wound bacterial balance. *The American journal of surgery* **178**, 399-402 (1999).

248. Hanna, J.R. & Giacopelli, J.A. A review of wound healing and wound dressing products. *The Journal of Foot and Ankle Surgery* **36**, 2-14 (1997).

249. Friend, D.R. In vitro skin permeation techniques. *Journal of Controlled Release* **18**, 235-248 (1992).

250. Flaten, G.E. et al. In vitro skin models as a tool in optimization of drug formulation. *European Journal of Pharmaceutical Sciences* **75**, 10-24 (2015).

251. Planz, V., Lehr, C.-M. & Windbergs, M. In vitro models for evaluating safety and efficacy of novel technologies for skin drug delivery. *Journal of Controlled Release* **242**, 89-104 (2016).

252. Amrutiya, N., Bajaj, A. & Madan, M. Development of microsponges for topical delivery of mupirocin. *AAPS PharmSciTech* **10**, 402-409 (2009).

253. Ng, S.-F., Rouse, J.J., Sanderson, F.D., Meidan, V. & Eccleston, G.M. Validation of a static Franz diffusion cell system for in vitro permeation studies. *Aaps Pharmscitech* **11**, 1432-1441 (2010).

254. Planz, V. et al. Three-dimensional hierarchical cultivation of human skin cells on bio-adaptive hybrid fibers. *Integrative Biology* **8**, 775-784 (2016).

255. Thompson, R.L., Cabezudo, I. & Wenzel, R.P. Epidemiology of nosocomial infections caused by methicillin-resistant Staphylococcus aureus. *Annals of Internal Medicine* **97**, 309-317 (1982).

256. Gosbell, I.B. Methicillin-resistant Staphylococcus aureus. *American journal of clinical dermatology* **5**, 239-259 (2004).

257. Aryee, A. & Price, N. Antimicrobial stewardship–can we afford to do without it? *British journal of clinical pharmacology* **79**, 173-181 (2015).

258. Alvarez-Ortega, C., Wiegand, I., Olivares, J., Hancock, R.E. & Martínez, J.L. The intrinsic resistome of Pseudomonas aeruginosa to β-lactams. *Virulence* **2**, 144-146 (2011).

259. Kelson, A.B., Carnevali, M. & Truong-Le, V. Gallium-based anti-infectives: targeting microbial iron-uptake mechanisms. *Current opinion in pharmacology* **13**, 707-716 (2013).

260. Rangel-Vega, A., Bernstein, L.R., Mandujano Tinoco, E.-A., García-Contreras, S.-J. & García-Contreras, R. Drug repurposing as an alternative for the treatment of recalcitrant bacterial infections. *Frontiers in microbiology* **6**, 282 (2015).

261. Chua, M., Bernstein, L.R., Li, R. & So, S.K. Gallium maltolate is a promising chemotherapeutic agent for the treatment of hepatocellular carcinoma. *Anticancer research* **26**, 1739-1743 (2006).

262. Bernstein, L.R., van der Hoeven, J.J. & Boer, R.O. Hepatocellular carcinoma detection by gallium scan and subsequent treatment by gallium maltolate: rationale and case study. *Anti-Cancer Agents in Medicinal Chemistry (Formerly Current Medicinal Chemistry-Anti-Cancer Agents)* **11**, 585-590 (2011).

263. Borselli, C. et al. Bioactivation of collagen matrices through sustained VEGF release from PLGA microspheres. *Journal of Biomedical Materials Research Part A* **92**, 94-102 (2010).

264. Xu, Q., Chin, S.E., Wang, C.-H. & Pack, D.W. Mechanism of drug release from double-walled PDLLA (PLGA) microspheres. *Biomaterials* **34**, 3902-3911 (2013).

265. Lu, L., Garcia, C.A. & Mikos, A.G. In vitro degradation of thin poly (DL-lactic-co-glycolic acid) films. *Journal of Biomedical Materials Research: An Official Journal of The Society for Biomaterials, The Japanese Society for Biomaterials, and The Australian Society for Biomaterials* **46**, 236-244 (1999).

266. Lu, L. et al. In vitro and in vivo degradation of porous poly (DL-lactic-co-glycolic acid) foams. *Biomaterials* **21**, 1837-1845 (2000).

267. Makadia, H.K. & Siegel, S.J. Poly lactic-co-glycolic acid (PLGA) as biodegradable controlled drug delivery carrier. *Polymers* **3**, 1377-1397 (2011).

268. Shin, H.J. et al. Electrospun PLGA nanofiber scaffolds for articular cartilage reconstruction: mechanical stability, degradation and cellular responses under mechanical stimulation in vitro. *Journal of Biomaterials Science, Polymer Edition* **17**, 103-119 (2006).